No. 3/2018

HIDRAULICA

HYDRAULICS-PNEUMATICS-TRIBOLOGY-ECOLOGY-SENSORICS-MECHATRONICS

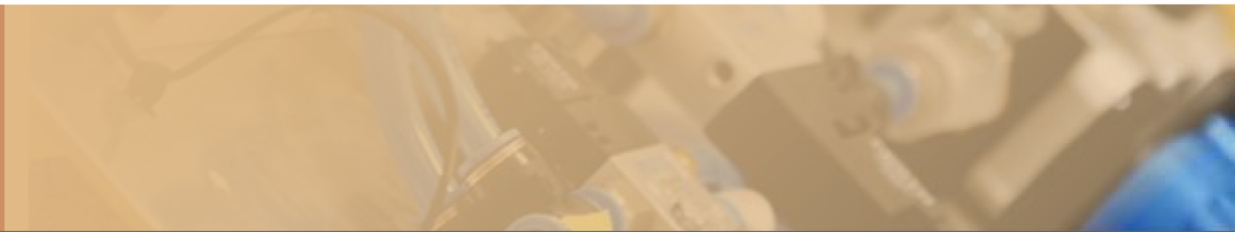

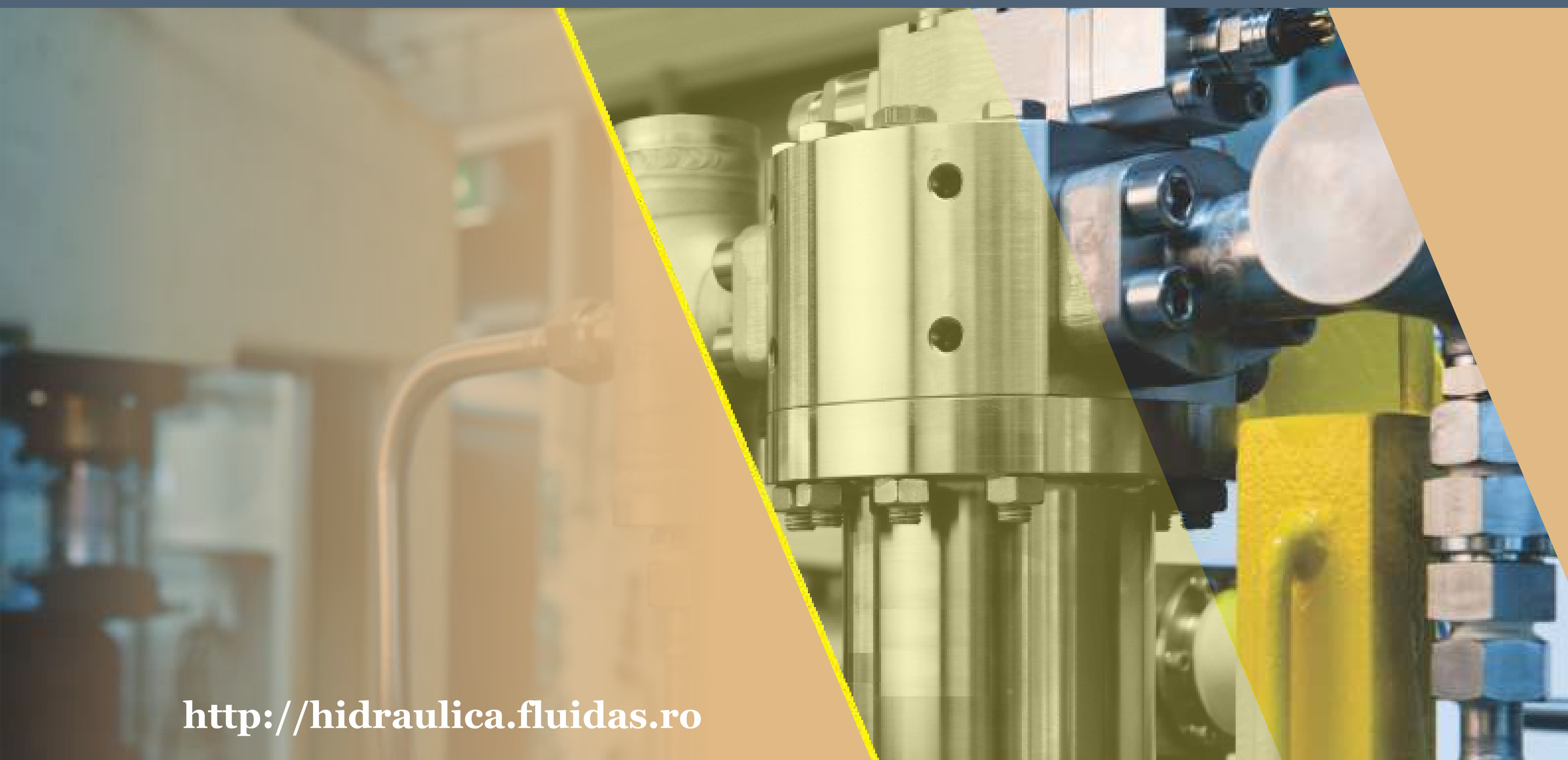

ISSN 1453 - 7303
ISSN-L 1453 - 7303

CONTENTS

BOARD

Published by:
Hydraulics and Pneumatics Research Institute, Bucharest-Romania
Address: 14 Cuţitul de Argint, district 4, Bucharest, 040558, Romania
Phone: +40 21 336 39 91; Fax: +40 21 337 30 40; e-Mail: ihp@fluidas.ro; Web: www.ihp.ro
with support from:
National Professional Association of Hydraulics and Pneumatics in Romania - FLUIDAS
e-Mail: fluidas@fluidas.ro; Web: www.fluidas.ro

HIDRAULICA Magazine is indexed by international databases

ISSN 1453 – 7303; ISSN – L 1453 – 7303

EDITORIAL

Trends in 2018

Ph.D.Eng. Petrin DRUMEA
MANAGING EDITOR

For some time, my younger colleagues keep repeating their questions whether hydraulics is still an area of interest and if so which would be the topics of the future. The answer to the first question is prompt and without much justification, maybe except the one that it is not possible to eliminate a type of drive which along with pneumatic, electric and mechanical drives underlies any kind of transmission or movement in the technics.
For the second question things get complicated, because there are many possible answers, which differ according to the specialists' interests, their field of activity, the trends in the related fields and, many times, even according to the general directions of development in science, technics, technology and new materials.

However, besides general stuff, which is most often unnecessary, I also have some practical answers. First of all, it should be made clear that most of the trends of the last decades have turned over time into "milestones in the development of the field", which will most likely happen to today's trends, as well.

Current trends fit into several directions, of which the most important ones are related to reducing energy losses, increasing functional performance and reducing production costs by using new technologies and new materials. Specifically, I believe that the following topics will be of great interest in the coming years.

1- Reducing energy losses by developing solutions by which the hydraulic energy produced gets very close to the energy consumed in each phase of the operating cycle of a machine.
2– Increasing the performance of hydraulic equipment by using new technologies and intelligent materials.
3- Developing new types of equipment with new features.
4- Discovering working fluids that can be used in systems with high fluctuations in temperature or extreme climatic conditions.
5- Embedding hydraulic or pneumatic systems in clean, renewable energy production equipment, both for power functions and for control and automation functions.
6- Digitalization of hydraulic systems.
7- Switching to series production of digital hydraulic equipment and systems.
8- Increasing reliability of hydraulic equipment and systems by careful control of heating, vibration and friction.

Operating Equations of a Rotating Machine that Drives Fluids

Drd. **Almaslamani Ammar FADHIL**[1], Prof. Dr. Eng. **Nicolae BĂRAN**[1]

[1] Politehnica University of Bucharest, n_baran_fimm@yahoo.com

Abstract: *The paper contains originality elements regarding both the constructive solution of the rotating machine and its functional equations. There are theoretical aspects regarding the fluid handling with this new type of rotating machine with profiled rotors. The end of the paper presents the operating equations and the advantages of using this new type of rotating machine.*

Keywords: *Rotating machine, profiled rotors, operating equations*

1. Introduction

By its content, the paper aims to present a new type of rotating machine with profiled rotors that can be practically used in several versions:
- As a working machine (pump, fan and blower); in this case the fluid pressure at discharge (p_2) is higher than at suction (p_1).
- As a force machine (steam engine or combustion gases, hydrostatic motor); in this case $p_1 > p_2$.
The use of rotating working machines is focused on two directions [1]:
a) Transportation of fluids from one place to another;
b) Increasing fluid pressure to generate the necessary forces for different hydraulic drives.
The constructive solution presented in this paper refers only to a).
Rotating working machines have the following advantages [2]:
• Transfers the received engines torque to the shaft with minimal losses in potential fluid pressure; these machines do not have alternate rectilinear motion, there are no valves;
• It has a higher reliability in operation; do not require maintenance over a relatively long period of time;
• Certain constructive solutions can carry fluids with impurities, rheological fluids.
The paper reveals new theoretical aspects regarding the fluid circulation with a new type of rotating machine with profiled rotors, its performances were validated by experimental researches.
It is stated that there are fundamental equations of the operation of hydraulic and thermal machines but it should not be confused with the operating equations.

2. Presentation of the rotating machine with profiled rotors

2.1 The sketch and operation principle of the rotating machine

In the paper, the term "machine" is used in the sense that it can be used as a fan, a low pressure compressor and a pump for pumping pure liquids or suspensions.
The sketch of the rotating machine and the operating principle are shown in Figure 1. The machine (fig.1) has two identical profiled rotors (2, 5) of a special shape which rotate with the same speed within a case (1, 4).

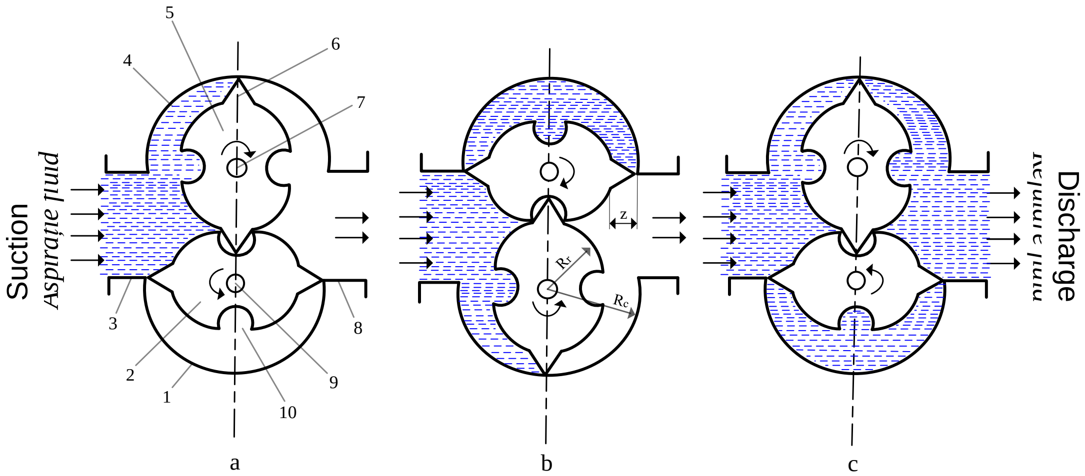

Fig. 1. The rotors position after a 90° rotation
1- lower case; 2- lower rotor; 3- suction chamber; 4- upper case; 5- upper rotor; 6- rotating piston; 7- driven shaft; 8- discharge chamber; 9- driving shaft; 10- cavity in which the upper rotor piston enters

The aspirated fluid (fig. 1. a) is transported to the discharge and after a 90° rotation of both rotors, the situation in Figure 1. b and in Figure 1. c is reached.
The synchronization of the rotation of the two rotors (2 and 5) is ensured by two gears of the same division diameter mounted outside the machine.
In Figure 1, the two rotors have the same radius (R_r), the cylindrical case has the radius (R_c), and the triangular-shaped rotating piston has the height (z). From figure (1) one can see that:

$$R_c = R_r + z[m] \tag{1}$$

2.2 The calculation of the rotating machine circulated fluid flow rate

It is noted with V_u (figure 1) the volume between the rotating pistons, the side surface of the case and the side surface of the lower rotor (2) of length l. On a 360 ° rotation of the shaft (9) two such volumes will be transported from suction to discharge:

$$2 \cdot V_u = 2\left(\frac{\pi R_c^2}{2} - \frac{\pi R_r^2}{2}\right) \cdot l \tag{2}$$

Replacing the relation (1) in (2) one can obtain:

$$V_u = \pi l z \cdot (z + 2R_r) \; [m^3 / rot] \tag{3}$$

The volumetric flow rate of the fluid displaced by the machine will be:

$$\dot{V} = \pi l z \cdot (z + 2R_r) \upsilon \left[m^3 / s\right] \tag{4}$$

in which υ - the rotation speed of the machine [rot / s]
replacing:

$$\upsilon = \frac{n}{60} \tag{5}$$

where n is the machine speed [rpm].
From the relation (4) one can obtain:

$$\dot{V} = \pi l z \cdot (z + 2R_r) \frac{n}{60} \left[m^3 / s\right] \tag{6}$$

Since the working machine has two identical rotors, the fluid flow of the machine will be:

$$\dot{V}_m = 2\dot{V} = \pi lz \cdot (z + 2R_r)\frac{n}{60}\left[m^3/s\right] \quad (7)$$

From the relation (7) one can observe that for a constructive solution given by l, z, R_r, the volumetric flow of the fluid varies linearly with the machine speed.
This rotating machine was built and tested in the laboratory of the Department of Thermotechnics, Engines, Heat & Refrigeration Equipment of POLITEHNICA University of Bucharest [3] [4].
If in relation (7) the following are introduced:
l = 0.05 m; z = 0.03 m; R_r = 0.05 m
n = 100, 200, 300, 400, 500 rpm, the data in Table 1 are obtained.

Table 1: Values of $\dot{V}_m$ = f (n)

n [rot/min]	100	200	300	400	500
$\dot{V} \cdot 10^{-3}$ [m³/s]	2.04	4.08	6.12	8.16	10.2

Based on the data in Table 1, the diagram in Figure 2 was constructed.

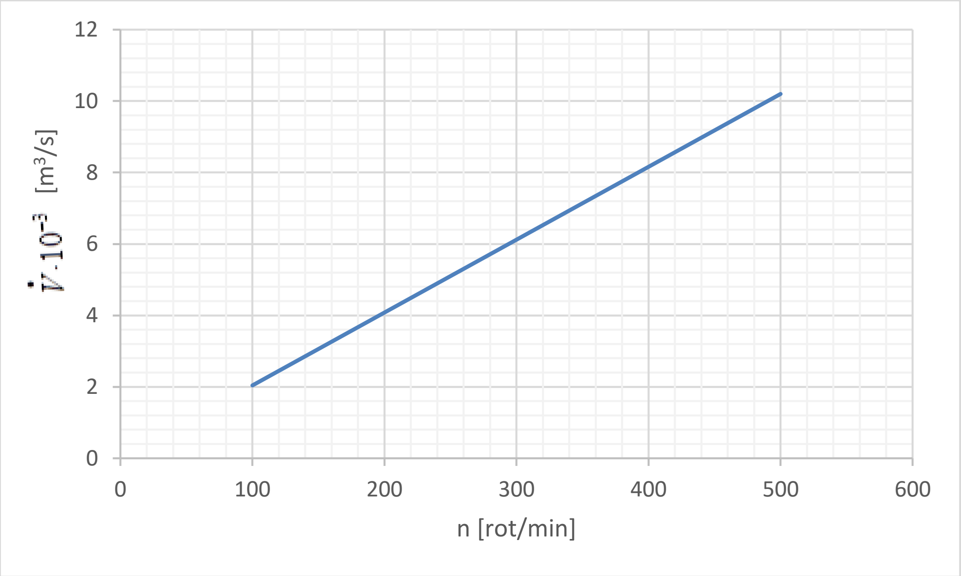

Fig. 2. The function $\dot{V}_m$ = f (n)

From graph 2 one can observe that the function $\dot{V}_m$ = f (n) is a linear function.

For a given constructive solution, from relation (7) it is observed that $\dot{V}_m = ct \cdot n\left[m^3/s\right]$, relation in which n is "given input", and $\dot{V}_m$ is "output date".

2.3 Calculating the theoretical power of the rotating machine

It is known from the literature [5] [6] [7] that the theoretical power to drive a rotating working machine is given by the relation:

$$P_m = \dot{V}_m \cdot \Delta p \left[W\right] \quad (8)$$

in which:
$\dot{V}_m$ - the volumetric flow rate [m³ / s]
Δp- machine pressure increase between suction and discharge [N / m²]
With relation (7), relation (8) becomes:

$$P_m = \pi lz \cdot (z + 2R_r)\frac{n}{60} \cdot \Delta p \quad (9)$$

Its value can be replaced as [8] [9]:

$$\Delta p = \rho_{H_2O} \cdot g \cdot H \left[N / m^2 \right] \tag{10}$$

where H is the pumping height [mH_2O]:

$$P_m = \pi l z \cdot \left(z + 2R_r \right) \frac{n}{60} \cdot \rho_{H_2O} \cdot g \cdot H \tag{11}$$

or:

$$P_m = \dot{V}_m \cdot \rho_{H_2O} \cdot g \cdot H = \dot{V} \cdot \Delta p \left[W \right] \tag{12}$$

For H = 2 m;

$$\Delta p = 10^3 \cdot 9.81 \cdot 2 = 19620 \, N / m^2 \tag{13}$$

$$P_m = \dot{V}_m \cdot \Delta p = 2.04 \cdot 10^{-3} \cdot 19620 = 40.20 \, W \tag{14}$$

Using the relations (10) and (12) for the same machine solution, the data in Table 2 are shown.

Table 2: Values of P_m =f(n), P_m =($\dot{V}$),P_m=f(H)

n [rot/min]	$\dot{V} \cdot 10^{-3}$ [m³/s]	H [m]	Δp [N/m²]	P_m [W]
100	2.04	2	19.620	40.20
200	4.08	4	39.240	160.09
300	6.12	6	58.860	360.22
400	8.16	8	78.480	640.39
500	10.2	10	98.100	1000.62

Based on the data in Table 2, the graphs were represented graphically:
P_m = f (n) in Figure 3;
P_m = f ($\dot{V}$) in Figure 4;
P_m = f (H) in Figure 5.

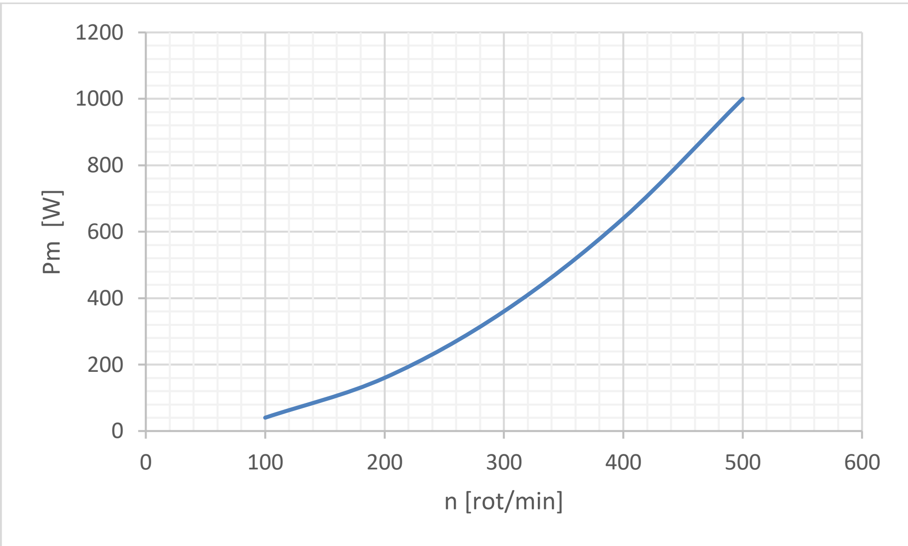

Fig. 3. The function P_m =f(n)

From Figure 3 one can observe that the function P_m =f(n) is not linear.

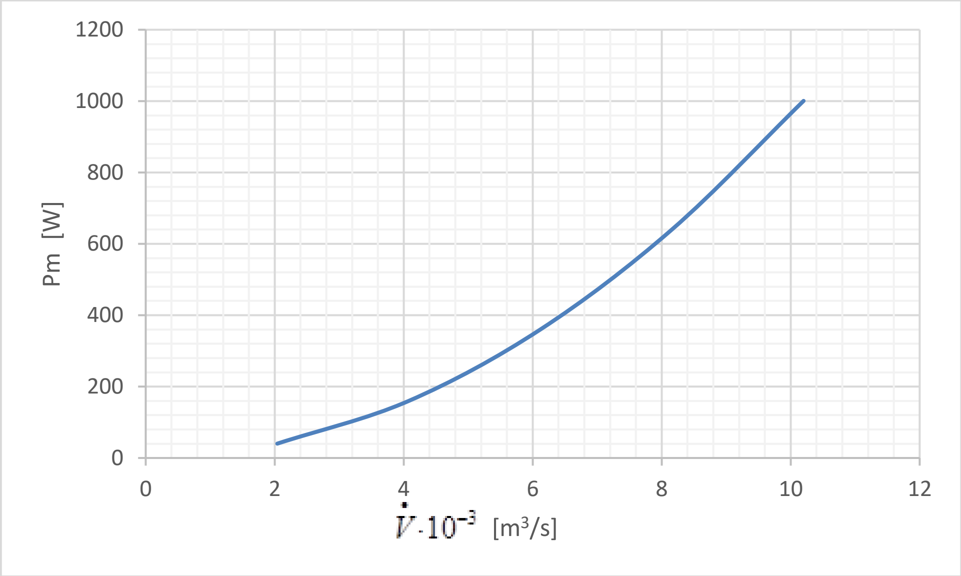

Fig. 4. The function $P_m = f(\dot{V})$

From Figure 4 one can observe that the function $P_m = f(\dot{V})$ is not linear.

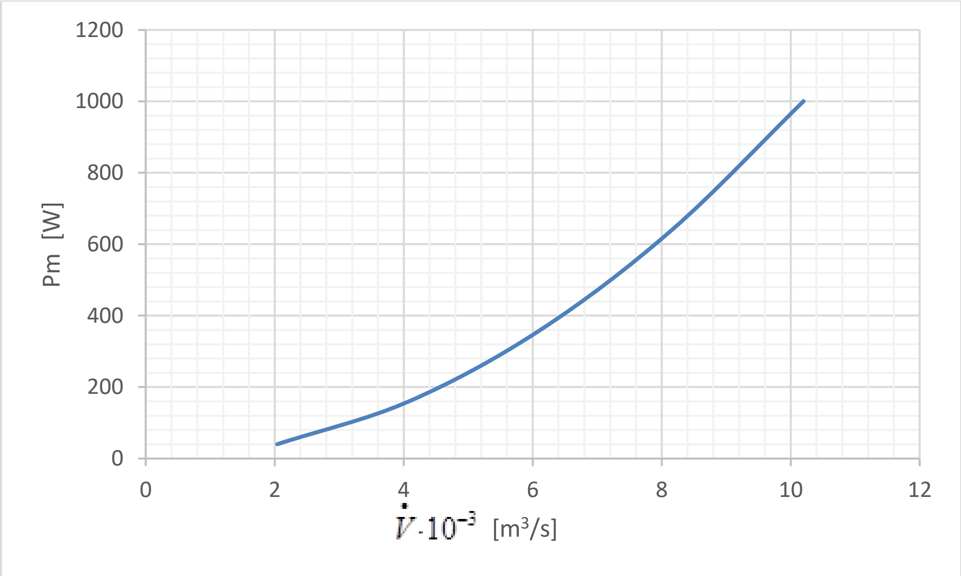

Fig. 5. The function $P_m = f(H)$

From Figure 5 one can observe that the function $P_m = f(H)$ is not linear.
Increasing pumping height (H) will obviously increase the theoretical power required to drive the rotating machine.

3. Operation equations

3.1. Definitions, operation equations of technical installations

In technique there are many operating equations, for example for [10] [11] [12]:
a) Electric transformers;
b) Power transmission lines;
c) Synchronous electric machines;
d) Bipolar transistors;

e) Three-phase asynchronous machines, etc.
The operating equations are the equations linking the inputs to the installations with the outputs of the installations. The operating equations must be equal to the number of unknowns.
From the above equation categories (a ... e) the paper refers briefly to class a).
To determine the operating equations of the single-phase transformer is considered as an iron-free transformer (Figure 6).

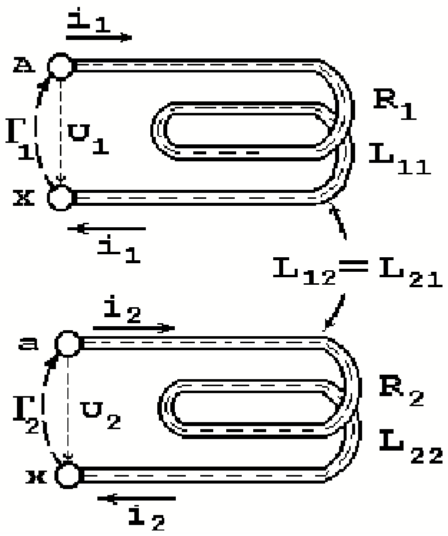

Fig. 6. Electric transformer with magnetic coupling without iron core

To establish the voltages equations, Kirchhoff's second theorem is applied to the contours Γ_1 and Γ_2; R_1 and R_2 are the resistors of the two windings (primary + secondary) and L_{11} and L_{22} are the inductances.
The mutual inductance between the two windings fulfils the condition: L_{12}. u_2 is the voltage at the secondary winding terminals. Under these conditions, the voltage equations for the two circuits are [10]:

$$u_1 = R_{1i1} + \frac{d}{dt}\left(L_{11i1} + L_{12i2}\right) \quad (15)$$

$$u_2 = R_{2i2} + \frac{d}{dt}\left(L_{11i2} + L_{21i1}\right) \quad (16)$$

These equations contain three unknowns: i_1, i_2, u_2, because the other sizes are known. To determine the unknown, the third equation for the voltage u_2 is written according to the impedance load parameters:

$$u_2 = R_{i_2} + L\frac{di_2}{dt} + \frac{1}{C}\int_0^t i_2\, dt \quad (17)$$

The three equations (15), (16), (17) describe the operation of the transformer in any mode; there is a closed system of 3 equations with 3 unknowns. It is noted that these three equations link the input quantities R_1, R_2, i_1, L_{11}, L_{22} to the output i_2, u_2.

3.2. Analysis of the operating equations of the rotating machine for fluid flow

It is considered that the machine architecture is specified, i.e. the sizes: l, z, R_r, R_c are known. It is formed a system of two equations:
- The first equation specifies the volumetric flow rate of the rotating machine;
- The second equation determines the theoretical driving power of the machine.

$$\dot{V} = \pi lz \cdot \left(z + 2R_r\right)\frac{n}{30}\left[m^3 / s\right] \quad (18)$$

$$P = \dot{V} \cdot \Delta p = \dot{V}\left(p_2 - p_1\right) = \pi lz \cdot \left(z + 2R_r\right) \cdot \frac{n}{30}\left(p_2 - p_1\right)\left[W\right] \quad (19)$$

In this system of two equations the following are known: l, z, R_r, n, p_1. The unknowns are: $\dot{V}$ and p_2. So this system, for a given constructive solution, links the input sizes: n, p_1, and the outputs and p_2.
There are three cases: I, II, III.
I) l, z, R_r, n known and $\dot{V}$ [m^3 / s] results.
The calculation relation was previously stated:

$$\dot{V} = \pi lz \cdot \left(z + 2R_r\right)\frac{n}{30}\left[m^3 / s\right]$$

and the function $\dot{V}_m$ = f (n) is represented in figure 2.

For these operating equation, the sizes l, z, R_r [m], n [rot / min] are input quantities and $\dot{V}$ [m^3 / s] is the output of the rotating machine. Changing the speed (n) leads to the change in volumetric flow rate ($\dot{V}$). The change of the rotation speed of the rotating machine is made by changing the speed of the asynchronous electric motor which can be done in 3 ways:
- Frequency variation (f_1) of the supply voltage;
- Changing the number of pairs of poles (p);
- Changing the slip (s).
The calculation relation is [13]:

$$n_2 = n_1(1-s) = \frac{f_1}{p}(1-s) \quad (20)$$

In the experimental investigations carried out, f_1 was modified, therefore n_2 was modified.
II) The known input sizes are: p_1, H and n and from the relation:

$$p_2 = p_1 + \Delta p = p_1 + \rho_{H_2O} \cdot g \cdot H \left[N / m^2\right]$$

the values of p_2 results.
Some data (H, n) of Table 2 are resumed, and the values of p_2 with the relation (20) results (shown in Table 3).

n [rot/min]	100	200	300	400	500
H [m H_2O]	2	4	6	8	10
Δp[N/m^2]	19.620	39.240	58.860	78.480	98.100
p_1 [N/m^2]	101325	101325	101325	101325	101325
p_2 [N/m^2]	120945	140565	160185	179805	199425

Based on the data in Table 3, the function: p_2 = f (H) is graphically represented in Figure 7.

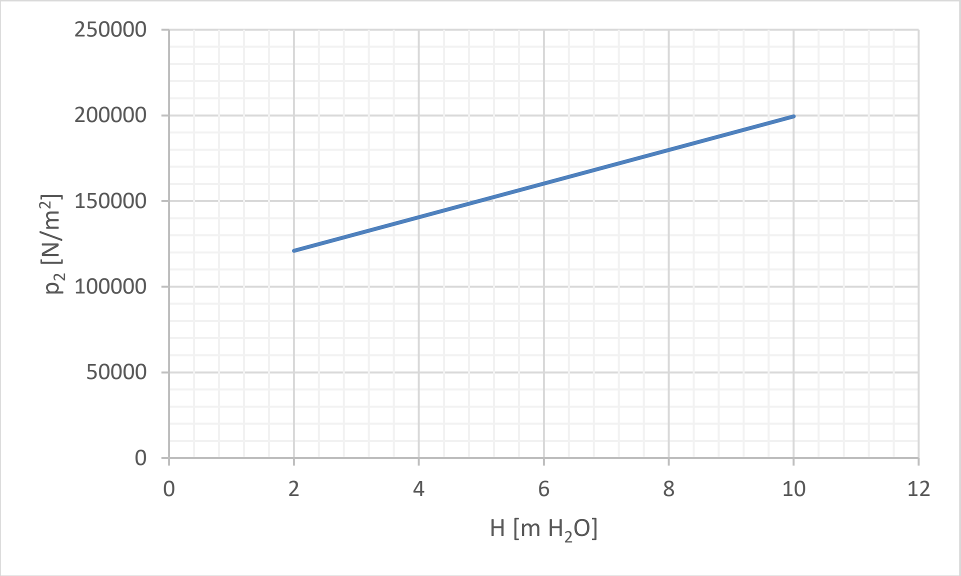

Fig. 7. The function: $p_2 = f(H)$

In case II, as input data: n and H and as output data p_2 is obtained.
The relation (19) can be written:

$$p_2 = p_1 + \frac{30 \cdot P}{\pi l z \cdot (z + 2R_r) \cdot n} \tag{21}$$

For a constructive solution with the sizes l, z, R_r and p1, considered constant:

$$p_2 = ct + ct\frac{P}{n} \tag{22}$$

From this relation one can observe that:
a) For a constant speed (n = ct) the pressure of the discharge fluid increases linearly with the power (P) supplied by the driving motor;
b) If P is maintained constant and the machine speed increases, the discharge pressure value (p_2) will decrease.
III) In the equation system (18 + 19) P is considered as unknown instead of $\dot{V}$, thus:

$$P = \pi l z (z + 2R_r)\frac{n}{30}\Delta p \tag{23}$$

By replacing: l = 0.05 m, z = 0.03 m, R_r = 0.05 m, one can obtain:

$$P = 2.04 \cdot 10^{-5} \cdot n (p_2 - p_1) \tag{24}$$

If n = 100 rpm and $\Delta p = 2 \cdot 10^5\ N/m^2$:

$$P = 2.04 \cdot 10^{-5} \cdot 100 \cdot 2 \cdot 10^5 = 408\ W$$

If n = 100, 200, 300, 400, 500 rpm, with the relation (24) the data in Table 4 is obtained.

Table 4: Values of P =f(n) for $\Delta p = 2 \cdot 10^5\ N/m^2$

n [rot/min]	100	200	300	400	500
Δp[N/m²]	$2 \cdot 10^5$	$2 \cdot 10^5$	$2 \cdot 10^5$	$2 \cdot 10^5$	$2 \cdot 10^5$
P [W]	408	816	1224	1632	2040

Performing the calculations for $\Delta p = 4, 6, 8, 10 \cdot 10^5\ N/m^2$ the graphs in Figure 8 is obtained.

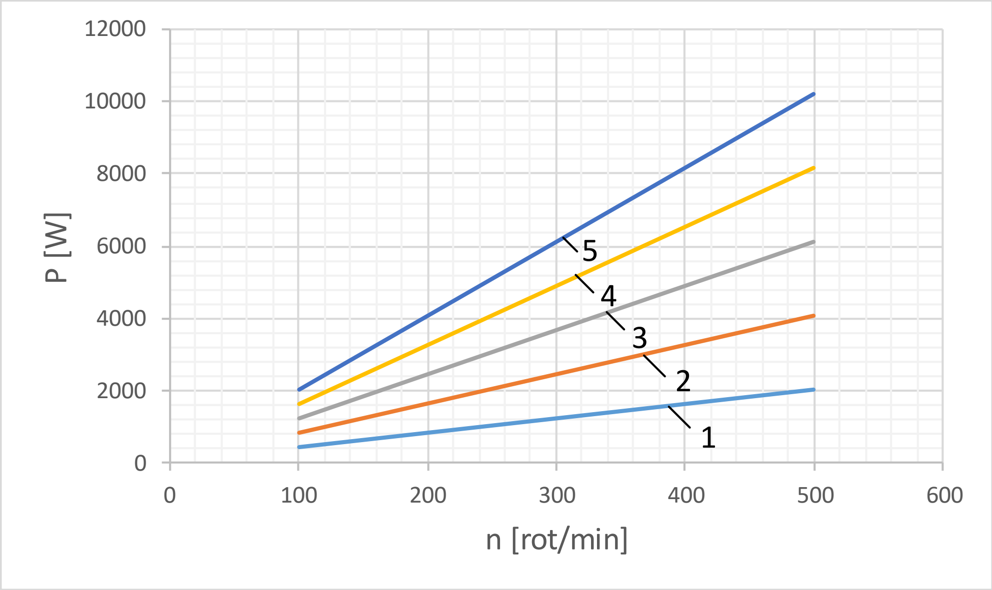

Fig. 8. The function: P = f (n) for different values of Δp
1 - $\Delta p = 2 \cdot 10^5\ N/m^2$, 2 - $\Delta p = 4 \cdot 10^5\ N/m^2$, 3 - $\Delta p = 6 \cdot 10^5\ N/m^2$, 4 - $\Delta p = 8 \cdot 10^5\ N/m^2$,
5 - $\Delta p = 10 \cdot 10^5\ N/m^2$

From Figure 8 one can notice that the shapes of the graphs are linear if Δp is constant.
Following the analysis of the operating equations of the rotating machine, the data presented in Table 5 were obtained.

Table 5: The link between the input and the output for the rotating machine

	Input data	The operation equation	Output data	Graphical representation
I	l, z, R_r [m], n [rot/min]	$\dot{V} = \pi l z \cdot (z + 2R_r)\frac{n}{30}\left[m^3/s\right]$	$\dot{V}\left[m^3/s\right]$	Fig. 2
II	p_1 [N/m²], H [m H_2O]	$p_2 = p_1 + \Delta p = p_1 + \rho_{H_2O} \cdot g \cdot H\left[N/m^2\right]$	$p_2\left[N/m^2\right]$	Fig. 7
III	L, z, R_r [m], n [rot/min], Δp [N/m²]	$P = 2.04 \cdot 10^{-5} \cdot n(\Delta p)$	P [W]	Fig. 8

Other forms of connection can be established between the different input and output sizes, such as P = f ($\dot{V}$), but the essential ones are shown in Table 5 [14] [15].

4. Conclusions

Rotating working machines has the following advantages:
a) Transforms the received motor torque on the shaft with minimal losses into potential pressure of the fluid;
b) These machines can carry fluids with impurities, rheological fluids and, in general, polyphase fluids;
c) It has increased reliability in operation; do not require maintenance over a relatively long period of time.
d) The above operating equations link the input sizes of the plant or process to the outputs one of the installation;
e) With this equation one can quickly determine the influence of the input quantities on the output quantities or vice versa;
f) This paper provides an important amount of specialized knowledge in the field of rotating volumetric machines with profiled rotors, machines for the transport of polyphase fluids.

References

[1] Arghirescu, Cristea, and Diana Cristina Arghirescu. *Analiza regimurilor pompelor și motoarelor volumice*. Editura AGIR, București 2010.
[2] Băran, N., P. Rădureanu, ș.a.. Colecția „Bazele Termodinamicii Tehnice”, vol. III, „Termodinamică Tehnică”. București, Editura POLITEHNICA PRESS, 2010.
[3] Băran, N., D. Despina, D. Besnea, and A. Motorga. „Theoretical and experimental researches regarding the performances of a new type of rotating machine with profiled rotors.” Paper presented at the 3rd International Conference on Mechanical and Electrical Tehnology ICMET 2011, Dalian, China, August 26-27, 2011.
[4] Băran, N., D. Despina, D. Besnea, and A. Detzortzis. „Theoretical and experimental researches regarding the performance of a new type of rotating machine with profiled rotors.” *Advanced Materials Research*, Trans tech Publications, Switzerland, vol. 488-489 (2012): 1757-1761.
[5] Hassel, Egon P. *Technical Thermodynamics*. University Rostock, Germany, Inst. Technical Thermodynamics, 2010.
[6] Bar-Meir, Genick. *Basics of fluid mechanics*. North Washtenaw Ave Chicago, IL, 2013.
[7] Turcan, Constantin, and Nicolae Ganea. *Pompe volumice pentru lichide*. București, Editura Tehnică, 1987.
[8] Burchiu, V., L. L. Gheorghiu, and Al. Dudău. *Ghidul utilizatorului de pompe*. București, Editura ATLAS PRESS, 2006.
[9] Georgescu, A., and S. Georgescu. *Hidraulica rețelelor de conducte și mașini hidraulice*. București, Editura PRINTECH, 2007.
[10] Craiu, Ovidiu, and Tiberiu Tudorache. *Mașini și acționări electrice*. București, Editura POLITEHNICA PRESS, 2015.
[11] Ghiță, Constantin. *Mașini și acționări electrice*. București, Editura I.C.P.E., 1997.
[12] Tăbăcaru, Teodor. *Mașini electrice și acționări*. Editura Universității din Petroșani, 2009.
[13] Hawas, Malik N.. *Influența viscozității fluidului asupra performanțelor mașinilor rotative cu rotoare profilate*. Teză de doctorat, Universitatea POLITEHNICA din București, 2016.
[14] Hawas, M., N. Băran, and A. Detzortzis. „Influence of the rotor architecture and of the speed on the volumetric efficiency of a new type of rotating volumetric machine.” *Advanced Materials Research*, Trans Tech Publication, Switzerland, vol. 905 (2014): 487-491.
[15] Detzortzis, A., N. Băran, and M. Hawas. „Influence of the profiled rotor design on the performance of rotating machines.” Paper presented at the National Conference of Thermodynamics with International Participation NACOT 2013 „Present and Future in Thermodynamics”, Constanța, Romania, May 30 - June 01, 2013.

ISSN 1453 – 7303 **"HIDRAULICA" (No. 3/2018)**
Magazine *of Hydraulics, Pneumatics, Tribology, Ecology, Sensorics, Mechatronics*

The Influence of Corrosion and Temperature Variation on the Minimum Safety Factor of a 3D Hexagonal Toroid with Regular Hexagonal Cross-Section Used in Manufacturing of LPG Storage Tanks

Assoc. Prof. PhD. Eng. **Mihai ŢĂLU**[1], Assoc. Prof. PhD. Eng. **Ștefan ŢĂLU**[2,*]

[1] University of Craiova, Faculty of Mechanics, Department of Applied Mechanics and Civil Engineering, Calea București Street, no. 107, 200512 Craiova, Dolj county, Romania. E-mail: mihai_talu@yahoo.com

[2] Technical University of Cluj-Napoca, The Directorate of Research, Development and Innovation Management (DMCDI), Constantin Daicoviciu Street, no. 15, Cluj-Napoca, 400020, Cluj county, Romania. Corresponding author* e-mail: stefan_ta@yahoo.com

Abstract: *In this paper we investigate the minimum safety factor (SF) values of a three-dimensional (3D) hexagonal toroid with regular hexagonal cross-section used in manufacturing of LPG storage tanks from the automotive industry. A design strategy was proposed to determine SF according to manufacturing objectives due to the influence of corrosion and temperature variation. Numerical simulations were carried out to determine the surfaces or curves for which the SF has the minimum values and the corresponding variation laws were computed by polynomial interpolation. We coupled numerical simulations of a 3D model (done in the AutoCAD Autodesk 2017 software, which was imported for analysis to SolidWorks 2017 software) with numerical limit analysis to calculate confidence intervals of the safety factor. The results of analyzed cases advocate the need for implementing a reliability improvement program of toroidal LPG fuel tanks.*

Keywords: *3D hexagonal toroidal LPG fuel tank, automotive industry, industrial engineering design, optimization methods, safety factor*

1. Introduction

The dynamics of storage fuel tanks markets, technology, and competition have brought changes in design driven innovation strategy that have potential to create a competitive advantage [1-6].
During the last few decades the evolution of the storage fuel tanks industry can be characterized by the convergence of technologies and designs to create new products in terms of adaptations, differentiation and quality [7-11].
Numerous contributions to the storage fuel tanks literature have investigated various models (based on material, capacity, and vehicle type) with different prices to satisfy the demands of the competitive market [12-15].
The manufacturers of storage fuel tanks, make use of new materials, to keep costs low, while bolstering safety, and increasing reliability in various environmental conditions [16-19].
3D CAD modelling of prototypes of storage fuel tanks used in automotive industry is a strategic resource to get better products in terms of structure, service life and durability and to avoid expensive tests equipment and expensive tests [21-32].
There are various softwares with virtual computer aided engineering tools specialized for storage fuel tank design, analysis, and evaluation, which performs calculations in accordance with national standards [33-40].
In the manufacturing of fuel tank various materials such as plastic, steel, and aluminum are used to satisfy the general structural design and certification rules [41].
Current storage fuel tanks industry trends show that the basic methods of protection of materials (like use of corrosion-resistant materials and application of surface coatings) have largely remained the same, the advanced approaches and techniques adopted can create appropriate protection systems with high reliability and performance [42, 43].
Many different methods have been developed in the technical literature to compute the safety factor (or factor of safety) (SF or FOS), ranging from simplified approaches to more sophisticated methods and advanced numerical procedures. These methods are based on several considerations, such as the accuracy of predictions on the imposed loads, strength, wear estimates and rigor in results interpretive research. Such methods allow us to calculate confidence

intervals of the SF due to uncertainty and exploitation conditions, data errors, and model structural inadequacies [43].
In our research, the minimum safety factor (SF) of a three-dimensional (3D) hexagonal toroid with regular hexagonal cross-section used in manufacturing of LPG storage tanks was determined due to the influence of corrosion and temperature variation. The obtained results provide a new insight into the design decisions are made during the early design stages in the storage fuel tanks development process.

2. Design methodology

In our previous studies [14, 44, 45], an optimal design of a 3D hexagonal toroid with regular hexagonal cross-section was performed.

2.1 Basic geometry of the parametric 3D model

Let's consider the parametric 3D model generated by revolving of a closed generating curve C_G (a hexagon with rounded corners) along a closed guiding curve C_D (a hexagon with rounded corners) as shown in figure 1 [14].

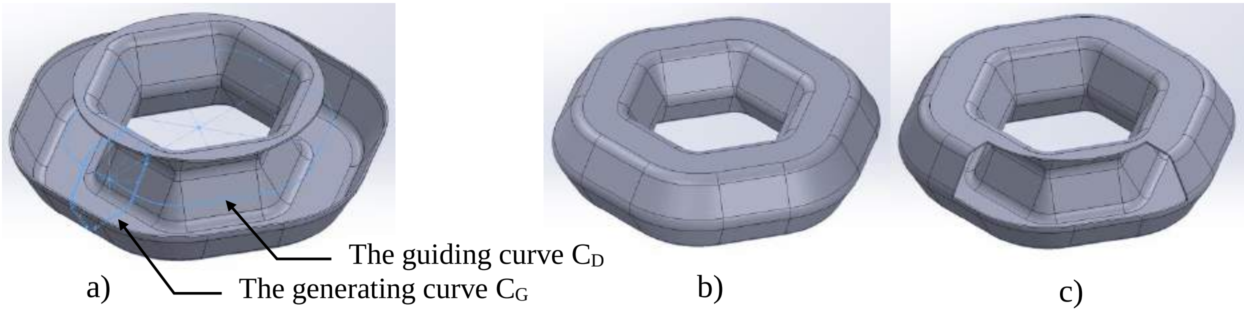

Fig. 1. The axonometric representation of the parametric 3D solid model

The following parameters were applied as input parameters to the 3D parametric model (figure 1): a) a closed generating curve C_G (a hexagon with a side value L = 175 mm, with rounded corners, radius R = 50 mm), and b) the guiding curve C_D (a hexagon with a side value L = 430 mm, with rounded corners, radius R = 180 mm).

2.2 Numerical analysis of the parametric 3D model

Based on the physical model, the modeling was done in the AutoCAD Autodesk 2017 software [39] and the numerical analysis was performed with SolidWorks 2017 software [40] with the Static, Thermal and Design Study modules. The design data used were:

- the tank material is AISI 4340 steel;
- the maximum hydraulic test pressure: p_{max} = 30 bar;
- the working temperature between the limits: T = -30 ^{0}C up to T = 60 ^{0}C;
- supporting surfaces located on the inferior side;
- the duration of the tank exploitation: n_a = 16 years;
- the corrosion rate of the material: v_c = 0.07 mm/years.

Let's compute for parametric 3D model the safety factor (SF) relative to a limit state of resistance using the following formula [43]:

$$SF = \sigma_k / \sigma_{max} \geq 1 \tag{1}$$

where: - σ_k, the effort limit taken into account;
- σ_{max}, the maximum effective effort of the cover material.

In addition, the minimum value of the SF that must exceed a prescribed allowable value [43]:

$$SF_{min} \geq SF_{adm} \tag{2}$$

In this case, the maximum effective effort of the cover material corresponds to the Von Mises effort, and the the effort limit taken into account is the admissible value of the traction stress of the material.

It can be seen that due to the geometry of the cover material, the boundary conditions, or the intensity of application or distribution of different loads occurring during exploitation, the safety factor has different values on the surface of the envelope, with values ranging from 2.1 to 273.18. Graphical representations for cases with various values of SF are given in fig. 2.

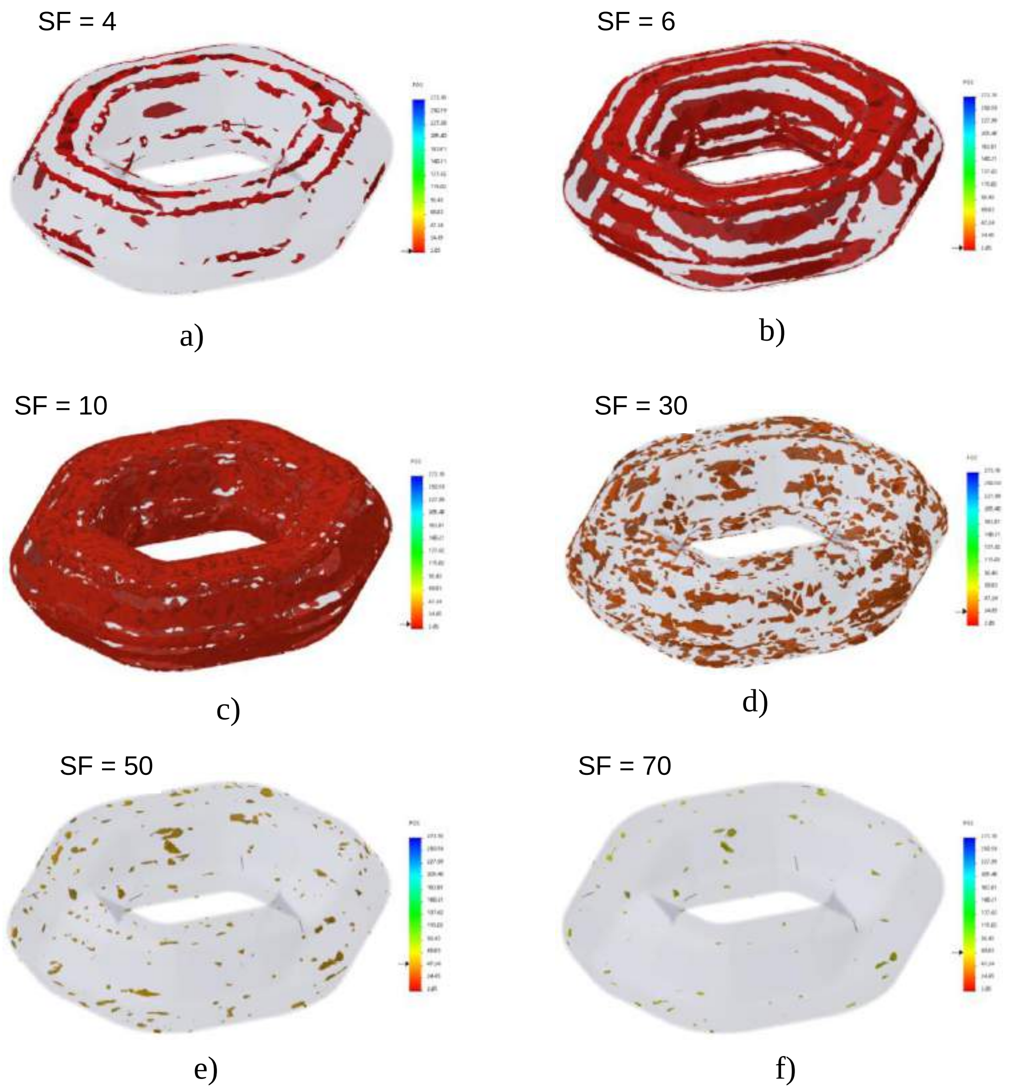

Fig. 2. Different isometric views of the parametric 3D model with the corresponding values of SF

Numerical calculations were performed for: mesh standard type, solid mesh with quality high, automatic transition, Jacobian in 16 points, element size 10 mm, tolerance 1 mm, number of nodes 130215, number of elements 68415, maximum aspect ratio 26.30, number of degrees freedom 346152.

Table 1: The minimum safety factor

SF_{min} [-]	T [^{o}C]									
n_a [years]	-30 ^{0}C	-20 ^{0}C	-10 ^{0}C	0 ^{0}C	10 ^{0}C	20 ^{0}C	30 ^{0}C	40 ^{0}C	50 ^{0}C	60 ^{0}C
0	1.791	1.896	2.012	2.14	2.263	2.399	2.351	2.467	2.563	2.493
1	1.751	1.83	1.917	2.011	2.115	2.229	2.355	2.494	2.486	2.497
2	1.715	1.795	1.82	1.977	2.082	2.198	2.326	2.469	2.522	2.453
3	1.692	1.769	1.853	1.945	2.046	2.156	2.279	2.415	2.372	2.398
4	1.649	1.775	1.838	1.925	2.021	2.126	2.241	2.368	2.365	2.372
5	1.652	1.727	1.808	1.898	1.996	2.104	2.223	2.337	2.418	2.34

6	1.657	1.731	1.813	1.901	1.998	2.105	2.185	2.259	2.337	2.313
7	1.594	1.663	1.738	1.819	1.908	2.005	2.112	2.23	2.324	2.354
8	1.538	1.605	1.679	1.759	1.843	1.921	2.005	2.094	2.19	2.223
9	1.541	1.607	1.68	1.79	1.845	1.939	2.003	2.07	2.14	2.212
10	1.470	1.544	1.625	1.713	1.812	1.92	2.041	2.175	2.203	2.241
11	1.489	1.586	1.654	1.728	1.808	1.895	1.99	2.094	2.208	2.231
12	1.508	1.579	1.656	1.74	1.831	1.931	2.039	2.158	2.219	2.158
13	1.41	1.465	1.525	1.589	1.658	1.734	1.815	1.905	2.002	2.109
14	1.397	1.453	1.513	1.577	1.647	1.724	1.807	1.898	1.997	2.107
15	1.359	1.409	1.464	1.524	1.588	1.658	1.733	1.815	1.904	2.002
16	1.425	1.452	1.508	1.569	1.634	1.705	1.781	1.864	1.953	2.051

The graphs of 3D surfaces (by type surf and fire) corresponding to the variation of minimum SF for SF_{min} (n_a, T), taking into account the results from Table 1, are graphically shown in fig. 3.

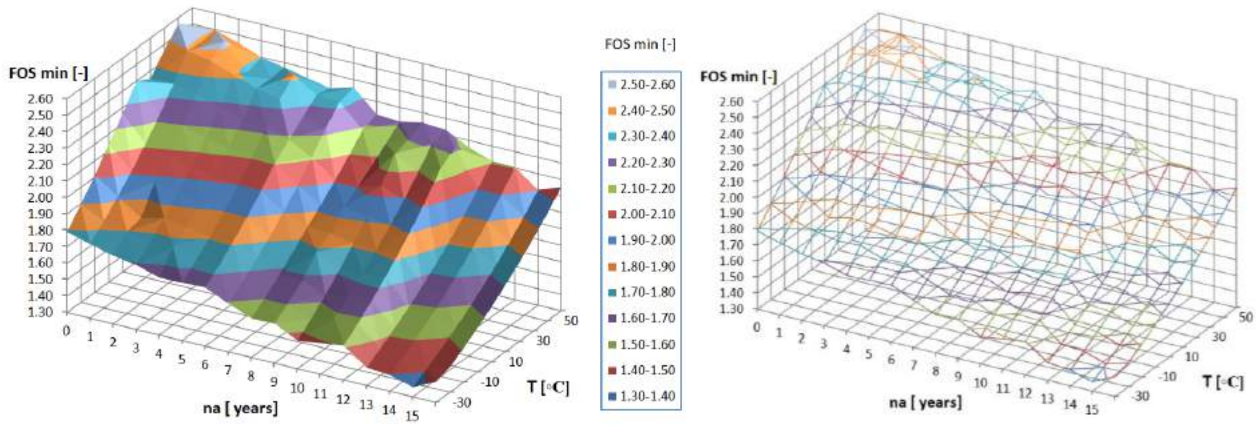

a) b)

Fig. 3. The 3D graphs SF_{min} (n_a, T): a) surf type; b) fire type

The graphs of the isothermal coefficient variation curves, SF_{min} (n_a, T = ct), are graphically shown in fig. 4.

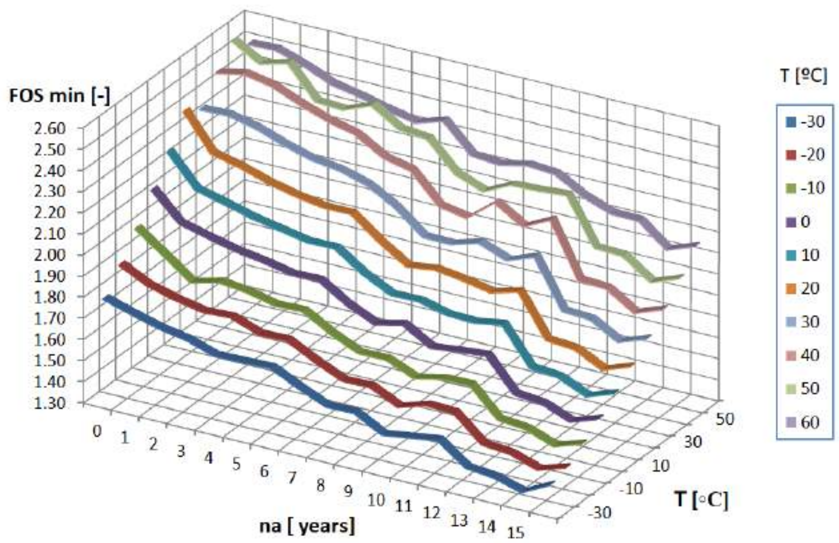

Fig. 4. The 3D graphs of the isothermal coefficient variation curves, SF_{min} (n_a, T = ct)

The graphs and laws of the variance of resulting SF_{min} (n_a, T = ct), calculated through a polynomial interpolation using Microsoft Excel 2017 are shown in fig. 5.

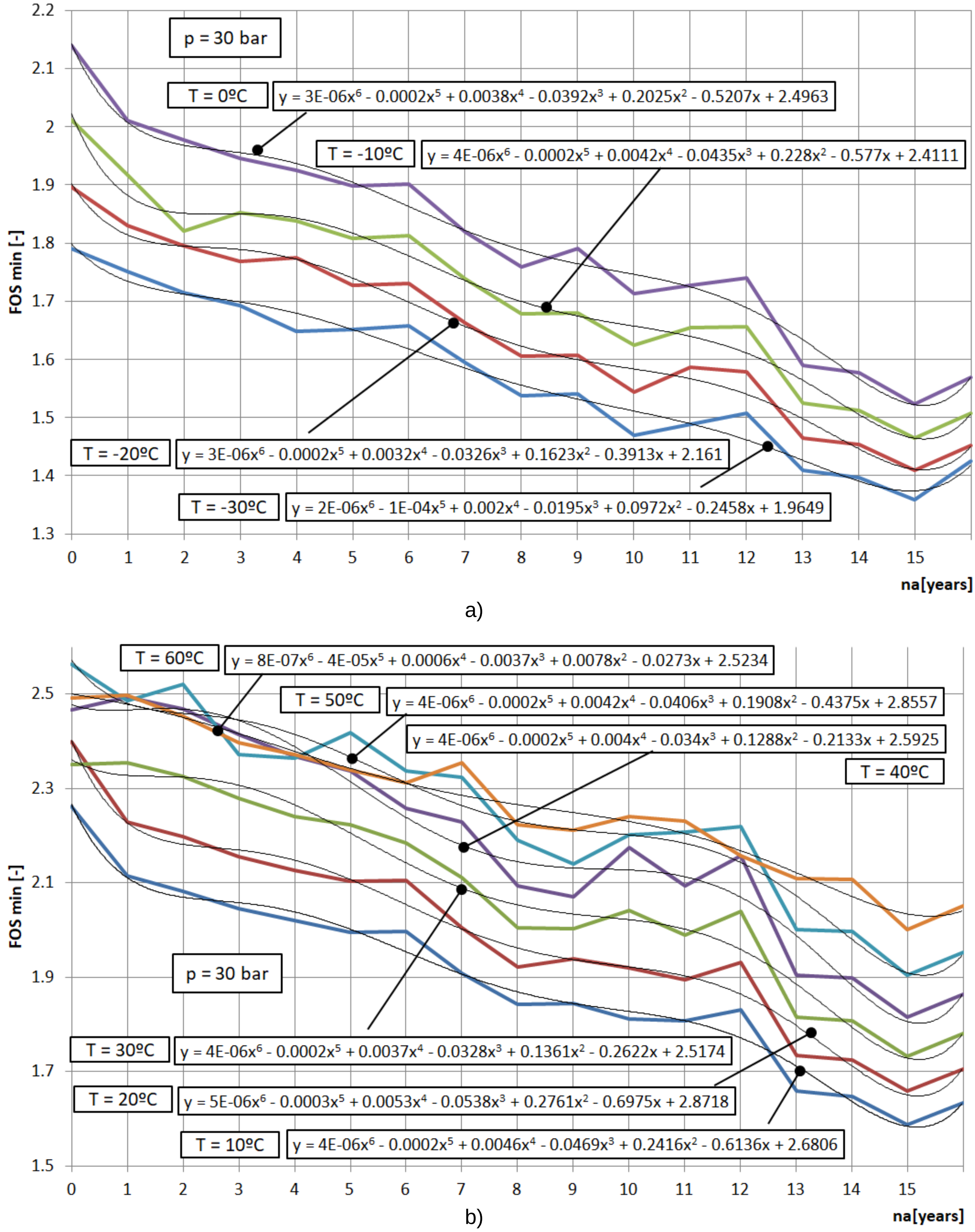

Fig. 5. The 2D graphs and laws of the variance of resulting SF_{min} (n_a, T = ct)

The graphs of the isothermal coefficient variation curves, SF_{min} (n_a = ct, T), are graphically shown in fig. 6.

The graphs and laws of the variance of resulting SF_{min} (n_a = ct, T), calculated through a polynomial interpolation using Microsoft Excel 2017 are shown in fig. 6.

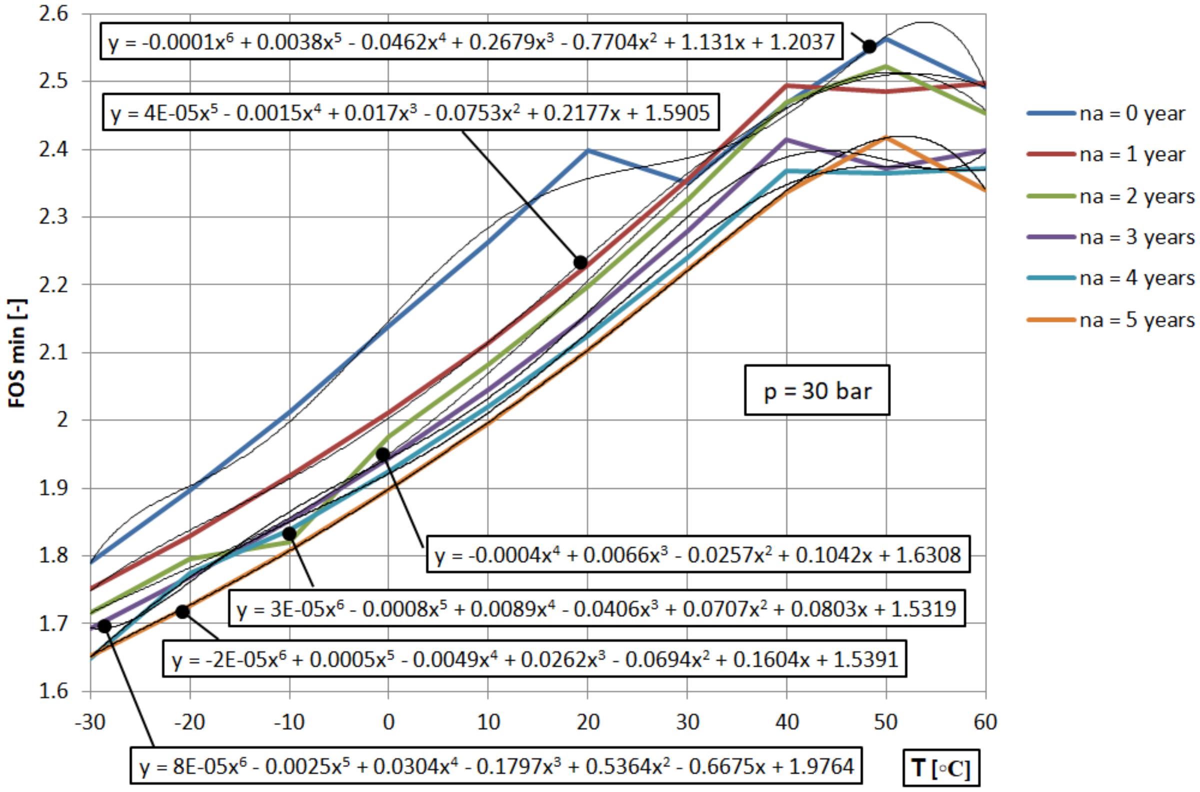

a)

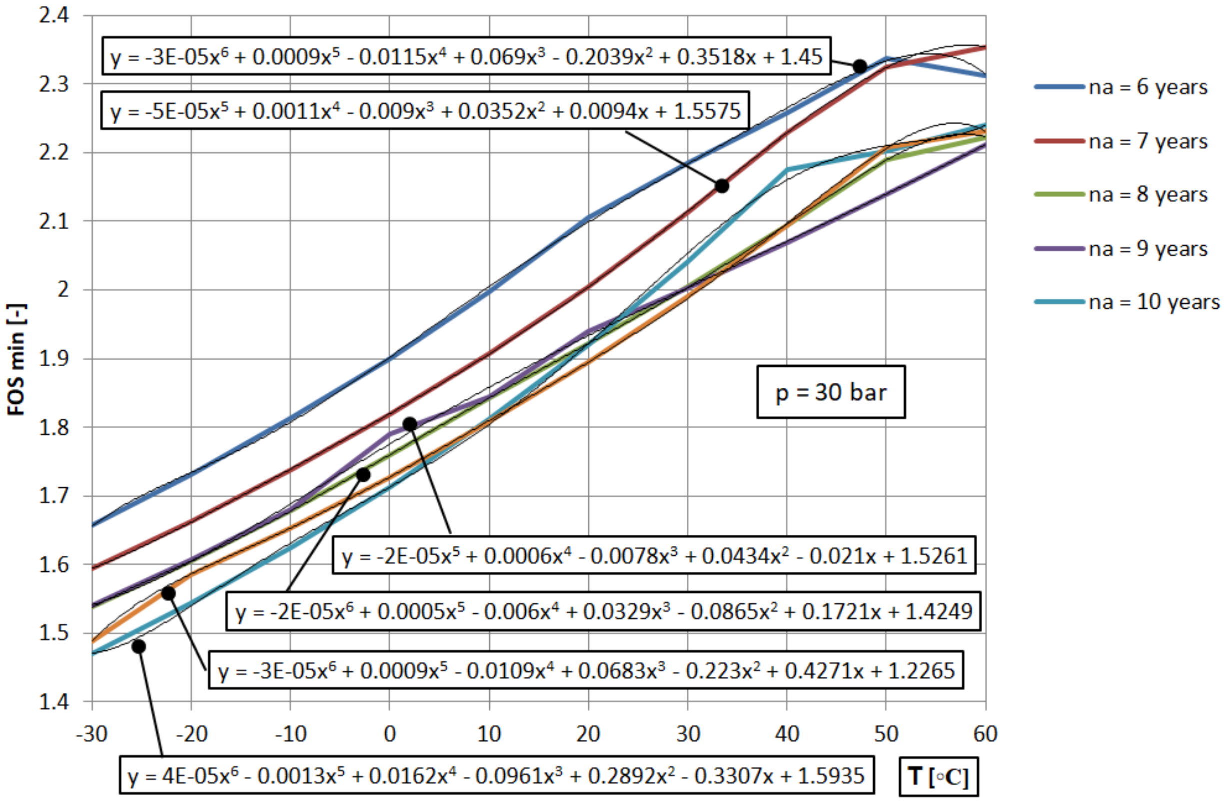

b)

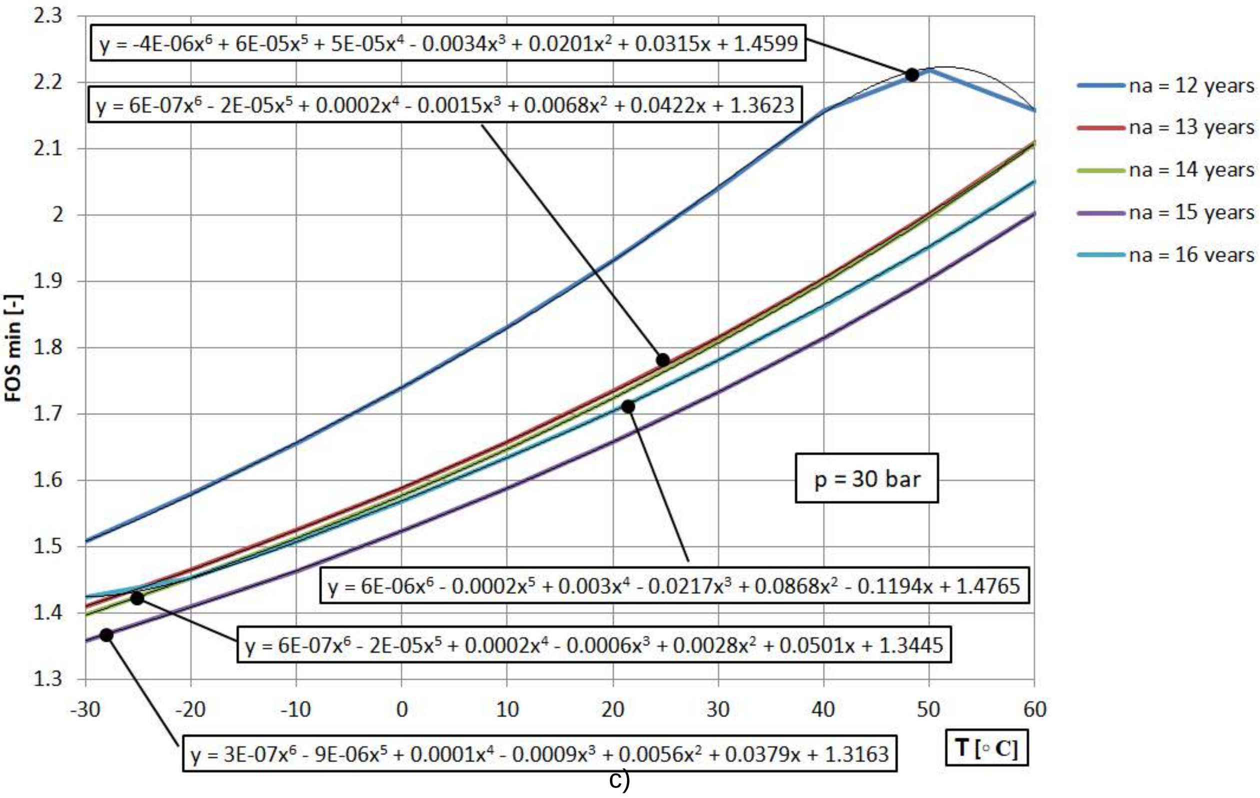

c)

Fig. 6. The 2D graphs and laws of the variance of resulting SF_{min} (n_a = ct, T)

The computed percentage decrease of minimum SF (for n_a = 0 years), considering the simultaneous influence of corrosion and temperature, is given in Table 2 and fig. 7.

Table 2: The percentage decrease of minimum safety factor

Δ SF_{min} [%]	T [°C]									
n_a [years]	-30 °C	-20 °C	-10 °C	0 °C	10 °C	20 °C	30 °C	40 °C	50 °C	60 °C
1	-2.23	-3.48	-4.72	-6.02	-6.53	-7.08	0.17	1.09	-3.00	0.16
2	-4.24	-5.32	-9.54	-7.61	-7.99	-8.37	-1.06	0.08	-1.59	-1.60
3	-5.52	-6.69	-7.90	-9.11	-9.58	-10.12	-3.06	-2.10	-7.45	-3.81
4	-7.92	-6.38	-8.64	-10.04	-10.69	-11.37	-4.67	-4.01	-7.72	-4.85
5	-7.76	-8.91	-10.13	-11.30	-11.79	-12.29	-5.44	-5.26	-5.65	-6.13
6	-7.48	-8.70	-9.89	-11.16	-11.71	-12.25	-7.06	-8.43	-8.81	-7.22
7	-10.99	-12.28	-13.61	-15.00	-15.68	-16.42	-10.16	-9.60	-9.32	-5.57
8	-14.12	-15.34	-16.55	-17.80	-18.55	-19.92	-14.71	-15.11	-14.55	-10.83
9	-17.92	-18.56	-19.23	-19.95	-19.92	-19.96	-13.18	-11.83	-14.04	-10.10
10	-17.92	-18.56	-19.23	-19.95	-19.92	-19.96	-13.18	-11.83	-14.04	-10.10
11	-16.86	-16.35	-17.79	-19.25	-20.10	-21.00	-15.35	-15.11	-13.85	-10.50
12	-15.80	-16.71	-17.69	-18.69	-19.08	-19.50	-13.27	-12.52	-13.42	-13.43
13	-21.27	-22.73	-24.20	-25.74	-26.73	-27.71	-22.79	-22.78	-21.88	-15.40
14	-21.99	-23.36	-24.80	-26.30	-27.22	-28.13	-23.13	-23.06	-22.08	-15.48
15	-24.12	-25.68	-27.23	-28.78	-29.82	-30.88	-26.28	-26.42	-25.71	-19.69
16	-20.43	-23.41	-25.04	-26.68	-27.79	-28.92	-24.24	-24.44	-23.80	-17.72

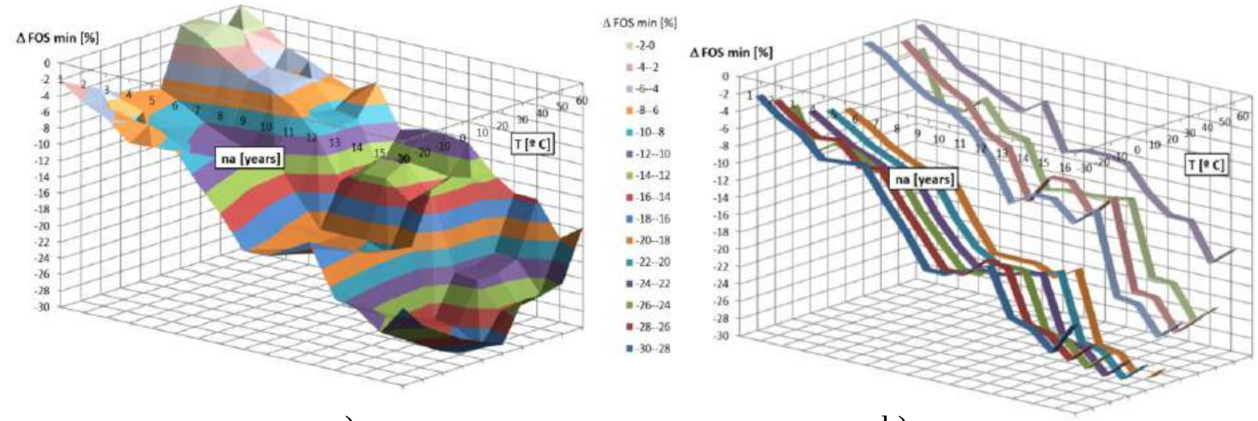

a) b)

Fig. 7. The 3D graphs of Δ SF_{min} (n_a, T): a) surf type; b) fire type

A direct determination of SF_{min} (n_a, T) is shown in fig. 8.

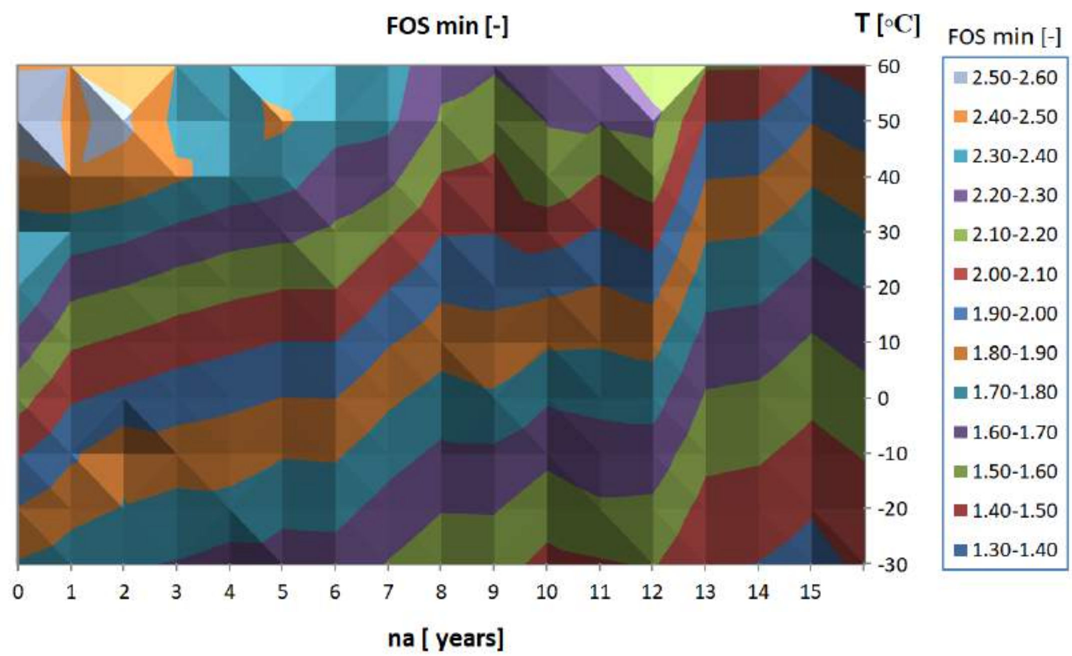

Fig. 8. The 2D graph of SF_{min} (n_a, T)

3. Discussion

Following the SF analysis and the resulting graphs for the parametric 3D model structure through the method of finite elements it has been found that:
- the graphical and analytical results of the mathematical dependencies determined by the laws of variation, allow for the determination of minimum SF considering the simultaneous influence of the corrosion and temperature;
- the laws of variation determined are important predictive tools for the minimum SF computed for a limit state of efforts;
- the percentage of decrease of the minimum SF is higher at the negative operating temperatures, increasing with the increase of the exploitation period (fig. 7).
- the graphs of the isothermal coefficient variation curves, as a result of the influence of a single parameter, keeping the constant value of the other parameter are graphically plotted: a) SF_{min} (n_a, T = ct), shown in fig. 4, and b) SF_{min} (n_a = ct, T), shown in fig. 6.

4. Conclusions

The proposed method is applicable in the design phase of a 3D hexagonal toroid with regular hexagonal cross-section used in manufacturing of LPG storage tanks from the automotive industry.

Conflict of Interest: The authors declare that they have no conflict of interest.

References

[1] Ghiţă, C. Mirela, Anton C. Micu, Mihai Ţălu and Ştefan Ţălu. "Shape optimization of a thoroidal methane gas tank for automotive industry." *Annals of Faculty of Engineering Hunedoara - International Journal of Engineering, Hunedoara, Romania*, Tome X, Fascicule 3 (2012): 295-297.
[2] Ghiţă, C. Mirela, Anton C. Micu, Mihai Ţălu and Ştefan Ţălu. "Shape optimization of vehicle's methane gas tank." *Annals of Faculty of Engineering Hunedoara - International Journal of Engineering, Hunedoara, Romania*, Tome X, Fascicule 3 (2012): 259-266.
[3] Ghiţă, C. Mirela, Anton C. Micu, Mihai Ţălu and Ştefan Ţălu. "3D modelling of a gas tank with reversed end up covers for automotive industry.", *Annals of Faculty of Engineering Hunedoara - International Journal of Engineering, Hunedoara*, *Romania*, Tome XI, Fascicule 3 (2013): 195-200.
[4] Ghiţă, C. Mirela, Anton C. Micu, Mihai Ţălu, Ştefan Ţălu and Ema I. Adam. "Computer-Aided Design of a classical cylinder gas tank for the automotive industry." *Annals of Faculty of Engineering Hunedoara - International Journal of Engineering, Hunedoara*, *Romania*, Tome XI, Fascicule 4 (2013): 59-64.
[5] Ghiţă, C. Mirela, Anton C. Micu, Mihai Ţălu and Ştefan Ţălu. "3D modelling of a shrink fitted concave ended cylindrical tank for automotive industry." *Acta Technica Corviniensis – Bulletin of Engineering, Hunedoara, Romania*, Tome VI, Fascicule 4 (2013): 87-92.
[6] Ghiţă, C. Mirela, Ştefan C. Ghiță, Ştefan Ţălu and Simona Rotaru, "Optimal design of cylindrical rings used for the shrinkage of vehicle tanks for compressed natural gas." *Annals of Faculty of Engineering Hunedoara - International Journal of Engineering, Hunedoara*, Tome XII, Fascicule 3 (2014): 243-250.
[7] Bică, Marin, Mihai Ţălu and Ştefan Ţălu. "Optimal shapes of the cylindrical pressurized fuel tanks." *Magazine of Hydraulics, Pneumatics, Tribology, Ecology, Sensorics, Mechatronics (HIDRAULICA)*, no. 4 (December 2017): 6-17.
[8] Ţălu, Ştefan and Mihai Ţălu. "The influence of deviation from circularity on the stress of a pressurized fuel cylindrical tank." *Magazine of Hydraulics, Pneumatics, Tribology, Ecology, Sensorics, Mechatronics (HIDRAULICA)*, no. 4 (December 2017): 34-45.
[9] Vintilă, Daniela, Mihai Ţălu and Ştefan Ţălu. "The CAD analyses of a torospheric head cover of a pressurized cylindrical fuel tank after the crash test." *Magazine of Hydraulics, Pneumatics, Tribology, Ecology, Sensorics, Mechatronics (HIDRAULICA)*, no. 4 (December 2017): 57-66.
[10] Ţălu, Mihai. "The influence of the corrosion and temperature on the Von Mises stress in the lateral cover of a pressurized fuel tank." *Magazine of Hydraulics, Pneumatics, Tribology, Ecology, Sensorics, Mechatronics (HIDRAULICA)*, no. 4 (December 2017): 89-97.
[11] Ţălu, Mihai and Ştefan Ţălu. "Analysis of temperature resistance of pressurized cylindrical fuel tanks." *Magazine of Hydraulics, Pneumatics, Tribology, Ecology, Sensorics, Mechatronics (HIDRAULICA)*, no. 1 (March 2018): 6-15.
[12] Ţălu, Mihai and Ştefan Ţălu. "Design and optimization of pressurized toroidal LPG fuel tanks with variable section." *Magazine of Hydraulics, Pneumatics, Tribology, Ecology, Sensorics, Mechatronics (HIDRAULICA)*, no. 1 (March 2018): 32-41.
[13] Ţălu, Ştefan and Mihai Ţălu. "Algorithm for optimal design of pressurized toroidal LPG fuel tanks with constant section described by imposed algebraic plane curves." *Magazine of Hydraulics, Pneumatics, Tribology, Ecology, Sensorics, Mechatronics (HIDRAULICA)*, no. 2 (June 2018): 14-21.
[14] Ţălu, Mihai and Ştefan Ţălu. "The optimal CAD design of a 3D hexagonal toroid with regular hexagonal cross-section used in manufacturing of LPG storage tanks." *Magazine of Hydraulics, Pneumatics, Tribology, Ecology, Sensorics, Mechatronics (HIDRAULICA)*, no. 2 (June 2018): 49-56.
[15] Ţălu, Mihai and Ştefan Ţălu. "3D geometrical solutions for toroidal LPG fuel tanks used in automotive industry." *Advances in Intelligent Systems Research,* vol. 151 (2018): 189-193. DOI: 10.2991/cmsa-18.2018.44.
[16] Ţălu, Ştefan and Mihai Ţălu. "Constructive CAD variants of toroidal LPG fuel tanks used in automotive Industry." *Advances in Intelligent Systems Research,* vol. 159 (2018): 27-30. DOI: 10.2991/mmsa-18.2018.7.
[17] Ţălu, Ştefan and Mihai Ţălu. "The Influence of corrosion on the vibration modes of a pressurized fuel tank used in automotive industry." *DEStech Transactions on Materials Science and Engineering,* (2018): 1-6. DOI: 10.12783/dtmse/icmsa2018/20560.

[18] Ţălu, Mihai and Ştefan Ţălu. “Optimal engineering design of a pressurized paralepipedic fuel tank.“ *Annals of Faculty of Engineering Hunedoara - International Journal of Engineering, Hunedoara, Romania*, Tome XVI, Fascicule 2 (2018): 193-200.
[19] Malviya, Rupesh Kumar and Muhamed Rushaid. "Consequence analysis of LPG storage tank." Materials today, vol. 5, issue 2 (2018): 4359-4367. DOI: 10.1016/j.matpr.2017.12.003.
[20] Ţălu, Ştefan. *Limbajul de programare AutoLISP. Teorie şi aplicaţii. (AutoLISP programming language. Theory and applications)*. Cluj-Napoca, Risoprint Publishing house, 2001.
[21] Țălu, Mihai. *Calculul pierderilor de presiune distribuite în conducte hidraulice. (Calculation of distributed pressure loss in hydraulic pipelines).* Craiova, Universitaria Publishing house, 2016.
[22] Ţălu, Mihai. *Mecanica fluidelor. Curgeri laminare monodimensionale. (Fluid mechanics. The monodimensional laminar flow).* Craiova, Universitaria Publishing house, 2016.
[23] Țălu, Mihai. *Pierderi de presiune hidraulică în conducte tehnice cu secțiune inelară. Calcul numeric și analiză C.F.D. (Hydraulic pressure loss in technical piping with annular section. Numerical calculation and C.F.D.)*, Craiova, Universitaria Publishing house, 2016.
[24] Ţălu, Ştefan. *Geometrie descriptivă. (Descriptive geometry)*, Cluj-Napoca, Risoprint Publishing house, 2010.
[25] Valencia, Garcia. *Geometría descriptiva, paso a paso*. Primera edición, Bogotá, Colombia, D.C, editorial Ecoe Ediciones, 2009.
[26] Florescu-Gligore, Adrian, Magdalena Orban and Ştefan Ţălu. *Cotarea în proiectarea constructivă şi tehnologică. (Dimensioning in technological and constructive engineering graphics).* Cluj-Napoca, Lithography of The Technical University of Cluj-Napoca, 1998.
[27] Florescu-Gligore, Adrian, Ştefan Ţălu and Dan Noveanu. *Reprezentarea şi vizualizarea formelor geometrice în desenul industrial. (Representation and visualization of geometric shapes in industrial drawing).* Cluj-Napoca, U. T. Pres Publishing house, 2006.
[28] Racocea, Cristina and Ştefan Ţălu. *Reprezentarea formelor geometrice tehnice în axonometrie. (The axonometric representation of technical geometric shapes).* Cluj-Napoca, Napoca Star Publishing house, 2011.
[29] Ţălu, Ştefan and Cristina Racocea. *Reprezentări axonometrice cu aplicaţii în tehnică. (Axonometric representations with applications in technique).* Cluj-Napoca, MEGA Publishing house, 2007.
[30] Ţălu, Ştefan and Mihai Ţălu. “CAD generating of 3D supershapes in different coordinate systems.“ *Annals of Faculty of Engineering Hunedoara - International Journal of Engineering, Hunedoara, Romania*, Tome VIII, Fascicule 3 (2010): 215-219.
[31] Ţălu, Ştefan and Mihai Ţălu. “A CAD study on generating of 2D supershapes in different coordinate systems.“ *Annals of Faculty of Engineering Hunedoara - International Journal of Engineering, Hunedoara, Romania*, Tome VIII, Fascicule 3 (2010): 201-203.
[32] Niţulescu, Theodor and Ştefan Ţălu. *Aplicaţii ale geometriei descriptive şi graficii asistate de calculator în desenul industrial. (Applications of descriptive geometry and computer aided design in engineering graphics).* Cluj-Napoca, Risoprint Publishing house, 2001.
[33] Ţălu, Ştefan. *Grafică tehnică asistată de calculator. (Computer assisted technical graphics)*. Cluj-Napoca, Victor Melenti Publishing house, 2001.
[34] Ţălu, Ştefan. *Reprezentări grafice asistate de calculator. (Computer assisted graphical representations).* Cluj-Napoca, Osama Publishing house, 2001.
[35] Ţălu, Ştefan. *AutoCAD 2005*. Cluj-Napoca, Risoprint Publishing house, 2005.
[36] Ţălu, Ştefan and Mihai Ţălu. *AutoCAD 2006. Proiectare tridimensională. (AutoCAD 2006. Three-dimensional designing)*. Cluj-Napoca, MEGA Publishing house, 2007.
[37] Ţălu, Ştefan. *AutoCAD 2017*. Cluj-Napoca, Napoca Star Publishing house, 2017.
[38] Nedelcu, Dorian. *Proiectare și simulare numerică cu SolidWorks*. *(Digital Prototyping and Numerical Simulation with SolidWorks)*. Timişoara, Eurostampa Publishing house, 2011.
[39] *** Autodesk AutoCAD 2017 software.
[40] *** SolidWorks 2017 software.
[41] *** Certification tests of LPG and CNG. http://vzlutest.cz/en/certification-tests-of-lpg-and-cng-c3.html.
[42] Ţălu, Ştefan. *Micro and nanoscale characterization of three dimensional surfaces. Basics and applications*. Napoca Star Publishing House, Cluj-Napoca, Romania, 2015.
[43] Bîrleanu, Corina and Ştefan Ţălu. *Organe de maşini. Proiectare şi reprezentare grafică asistată de calculator. (Machine elements. Designing and computer assisted graphical representations).* Cluj-Napoca, Victor Melenti Publishing house, 2001.
[44] Ţălu, Ştefan and Mihai Ţălu. "The influence of corrosion and pressure variation on the minimum safety factor of a 3D Hexagonal toroid with regular hexagonal cross-section used in manufacturing of LPG storage tanks." *Magazine of Hydraulics, Pneumatics, Tribology, Ecology, Sensorics, Mechatronics (HIDRAULICA)*, no. 3 (September 2018): 39-45.
[45] Ţălu, Mihai. "Determination of a set of admissible parameters in designing of LPG storage tanks considering a required safety factor." *Magazine of Hydraulics, Pneumatics, Tribology, Ecology, Sensorics, Mechatronics (HIDRAULICA)*, no. 3 (September 2018): 56-61.

Studying Transients in Water Supply Systems

Zoltán CSONGRÁDI[1]**,** Assistant professor PhD Student **Nikolett FECSER**[2]**,**
Bálint LAJTAI[3]

[1]PANNON-VÍZ Zrt., Országút u., Győr, H-9025 4., e-mail: muszakiig@pannon-viz.hu

[2] Széchenyi István University, 1 Egyetem tér, Győr, H-9026, e-mail: fecser.nikolett@sze.hu

[3] VAG Armaturen Hungary, Madarász Viktor str., Budapest, H-1138 47-49., e-mail: b.lajtai@vag-group.com

Abstract: *Transient operating states occur in water supply systems under pressure. Transient operating states place such extreme loads on the pipes that they might cause burst water pipes, so to be able to avoid damages and operation failures due to burst pipes they are needed to be studied and modelled. To highlight the importance of transient phenomena, we present the measurements carried out at Pannon-Víz Zrt (the local Hungarian Water Utility Service) and their results in our study.*

Keywords*: Transient, burst water pipe, pump, transient operating state*

1. Introduction

If the valve openings and closings, pump start/stopping are not carried out slowly enough in the systems of large water pipes at pumping stations, they might generate quick changes in pressure. In extreme situations, transient phenomena can endanger the soundness of the pipe itself. At a pump station a pump shutdown caused by a power failure can have so severe consequences that even pipe burst might occur if the automatic or controlled closing valves are designed or operated poorly.

2. The phenomenon of transiency

A transient operating state is a kind of flow in time and space which is initiated by the impacts of some occurrence started from a steady (stationary) state and lasts until the development of another steady state [1].
The main reasons of the occurrences of transient phenomena are:

- power failures at pump stations leading to stops and the changes of flow velocity during pump startups,
- a sudden change in flow at filling or emptying pipelines,
- isolating pipeline sections, operating valves too quickly leading to big flowrate changes,
- rinsings and the changes in flow rate occurring at the opening / closure the drains during water inspection [2].

Due to the reasons mentioned above it is necessary to analyze the transient states developing in the system.

If the quantity of the water in the pipe alters, the movement of the water in the pipe is not permanent. After closings and openings, the pressure in the pipe oscillates in the surroundings of the hydrostatic pressure with a gradually decreasing intensity. After a quick closing a positive, meanwhile after a quick opening a negative pressure surge or wave develops. [3]. These types of oscillations can be calculated and modelled. Its basic idea was worked out by Lorenzo Allievi, an Italian scientist, in 1904 [4].

3. The venue of the measuring process

Pannon-Víz ZRt, the largest water and sewage service in Győr-Moson-Sopron county, operates several regional drinking water supply systems. Our measuring instruments were installed at the booster station in Pápai út, Győr, and the reservoir in Hegyalja út. We applied 2 pieces of TRAREC® measuring instruments to monitor the transient state in the pipeline system. Model number LL1-12078 got installed in Pápai út and LL1-12078 in Hegyalja út. Figure 1 shows the distance between the two measuring instruments.

Fig. 1. Measurement venues (Pápai út-Hegyalja út)

The distance between the two measuring devices is 4700 meter. The pipes are NA600 asbestos-cement pipes. 3 pumps - a NP150/400 and two DAN250 type pumps - can be found in the booster station in Pápai út. Fig. 2 shows the position of the two measuring instruments.

Fig. 2. Measurement venues (Pápai út-Hegyalja út)

4. Describing the measuring instrument

The applied measuring instrument - in fig. 3 - was developed and patented by Budapest Waterworks.
TRAREC® comes from the shorter version of TRANSIENT RECORDER.

Main characteristics of the measuring instrument:

- patented measurement and evaluation system
- normal or high-frequency measuring method
- selective data storage for long measurements
- variable parameters for different applications [5]

Fig. 3. TRAREC® measuring instrument

Table 1 shows the parameters of the measuring instrument.

Table 1: TRAREC® the parameters of the measuring instrument

Pressure sensor	0 -15 bar; (maximum 40 bar)
Accuracy	0.1%
Measurement frequency	50-1000 measurements / sec
Data storage frequency	1 - 60 s
Data segmentation	20 bit
Duration of measurement	1-2 weeks
Data communication and charging	USB 2

Table 2 shows the calibration data of the measuring instrument and summarizes some measured values.

Table 2: TRAREC® calibration data of the measuring instrument

Parameters of the measuring instrument		
Name	LL1-12078	LL1-12079
Sequence number	12078	12079
Version	1.0	1.0
Serial number	12078	12079
Pressure range (mwc)	211.00 mwc	211.00 mwc
Calibration	0.86111	0.86466
Pressure shifting	-9.58 mwc	-10.20 mwc
Measurement		
Starting date	07.02.2018	07.02.2018
Sea level (m)	0.00 m	0.00 m
Frequency of measurements	256 Hz	256 Hz
Frequency of data collection (sec)	1 sec	1 sec
Transient		
Starting date	07.02.2018	07.02.2018
Length of time	12 days 00:00:00	12 days 00:00:00
Storage time (sec)	10 sec	10 sec
Pre-storage time (sec)	2 sec	2 sec
Monitoring the deviation	Yes	Yes
Maximum number of transients	1000 pcs	1000 pcs
Results		
Starting date	05:00 am 07.02.2018	07.02.2018
Finishing date	04:59 am 19.02.2018	19.02.2018
Number of stored transients	233 pcs (2472 sec)	578 pcs (7402 sec)
Number of detected transients	249 pcs	767 pcs

5. Presenting measurement results

We used the PressEval software for evaluating the results of the measurement. Measuring instrument LL1-12078 sensed 233 transients, while LL1-12079 perceived 578 transients. Analyzing transients I applied a 1- hour method, namely the number of occurrences of transients during an hour was evaluated.

Fig. 4 shows the measurements made by the two measuring instruments.

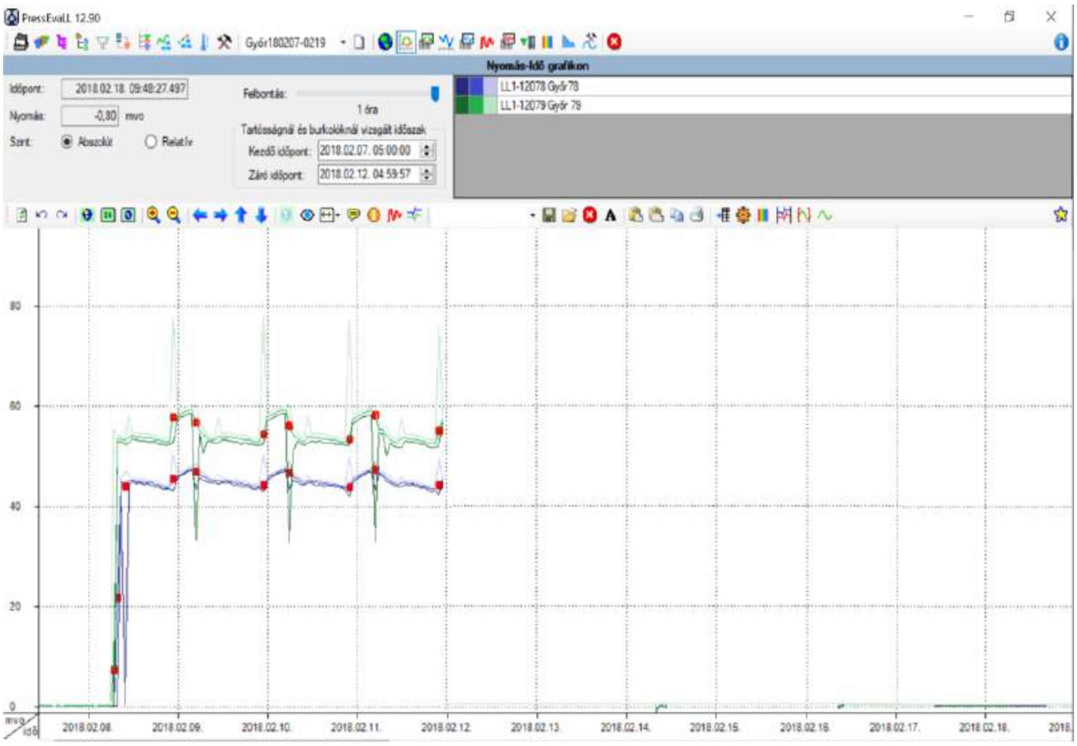

Fig. 4. Program PressEvaLL

Fig. 5 illustrates the measurements of LL1-12078 measuring instrument.

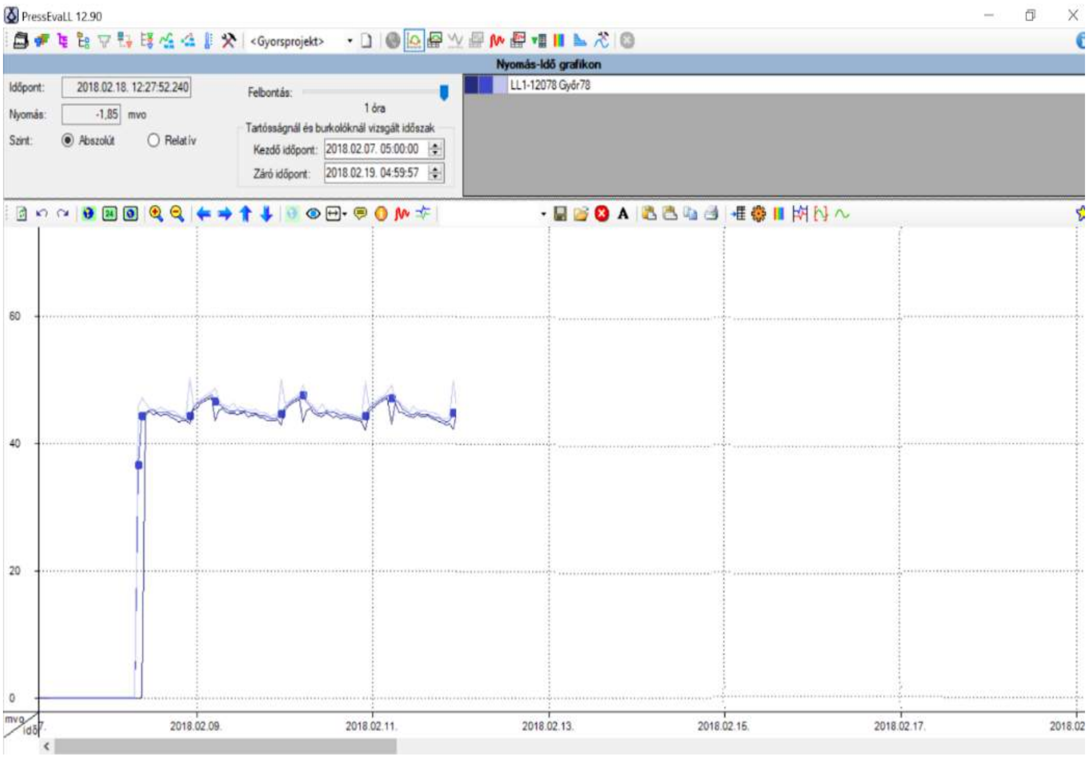

Fig. 5. Program PressEvaLL LL1-12078

Fig. 6 illustrates the measurements of LL1-12079 measuring instrument.

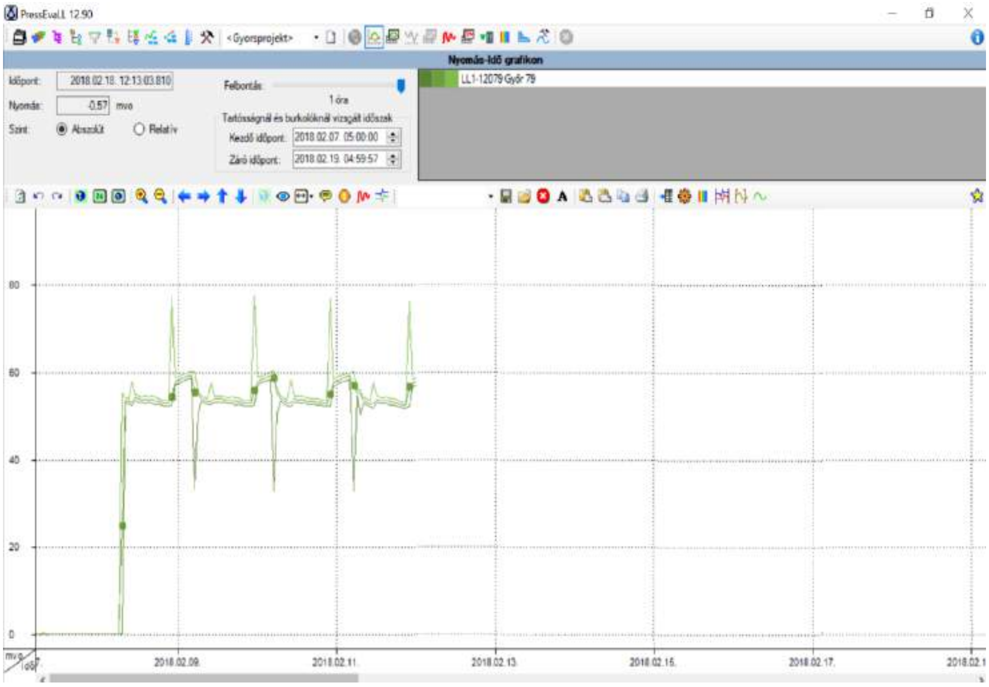

Fig. 6. Program PressEvaLL LL1-12079

In Table 3 I collected the absolute, minimum and maximum values of pressure changes.

Table 3: Pressure changes

Date [h:m:s]			Absolute change [bar]		Minimum change [bar]		Maximum change [bar]	
	Measurement instrument 79	Measurement instrument 78	Measurement instrument 79	Measurement instrument 78	Measurement instrument 79	Measurement instrument 78	Measurement instrument 79	Measurement instrument 78
08.02.	07:31:52		5.475		-5.488		93.833	
		08:11:14		4.499		-0.185		5.962
08.02.		09:41:01		4.299		-9.142		5.252
08.02.	22.41:47	22:41:51	2.462	0.708	-16.035	-4.452	15.822	1.9729
08.02.	05:04:10	05:04:33	2.326	0.471	-1.924	-1.079	1.639	1.661
09.02.	23:21:25	23:21:30	2.485	0.719	-15.537	-4.315	16.349	6.501
10.02	05:53:14	05:53:36	2.335	0.515	-2.195	-1.178	1.069	1.888
10.02	22:31:54	22:31:58	2.454	0.774	-15.978	-6.8	16.178	9.582
11.02	05:25:30	05:25:52	2.349	0.605	-1.696	-3.336	1.881	3.748
11.02	22:06:48	22:06:52	2.403	0.74	-15.864	-4.031	16.648	5.877
12.02	05:21:46	05:22:09	2.323	0.564	-2.366	-3.648	1.881	3.819
12.02	07:38:03		7.651		-46.995		7.412	
		07:54:46		4.641		-12.393		2.214

The process of the transient can be seen clearly from the table. E.g.: the transient starts its travelling at 22:41:47 and reaches the next measuring instrument at 22:41:51. The table demonstrates that the phenomenon of transiency is detectable in the system. The next task is to observe what causes the phenomenon of transiency.

6. Conclusion

In our study we intended to draw attention onto the existence of the phenomenon of pressure transiency and its importance. Our goal is to reveal what might cause the appearance of transient in the system. Later we are going to make a geometric and mathematical model.

References

[1] Pandula, Zoltán. *Csappantyú tranziens áramlásbeli viselkedését leíró modell / Model describing transient flow behavior of a damper.* Budapest, Hungary, 2003.
[2] Ludányi, László, Árpád Nagy, Péter Zimmer. *A Trarec tranziens nyomásmérő műszer és a PressEval Adatkezelő és feldolgozó szoftver*. Budapest, Hungary, 2004. http://www.tova-partner.hu/letoltesek/trarec.pdf
[3] György, István. *Vízügyi létesítmények kézikönyve. Szivattyúüzemi kézikönyv / Handbook of water facilities. Pump Manual*. Technical Publishing House, Budapest, Hungary, 1974, pp. 11-45.
[4] Szlivka, Ferenc. *Csővezetékekben fellépú tranzoens jelenségek / Transient phenomena in pipelines.* Budapest, Hungary, 2012. http://www.ontozesmuzeum.hu/download/7ViZGAZDHirtelenzaras.pdf
[5] Zimmer, Péter. *A tranziens mérés sikeres alkalmazása a vízveszteség-feltárás területén. Vízmű Panoráma.* Budapest, Hungary, 2007.

Studying the Influence of River Works on River Flow Regime with 1-D Hydraulic Modelling

As.Prof. PhD. Eng. **Marie-Alice GHIȚESCU[1],** Lect. PhD. Eng. **Albert Titus CONSTATIN[1]**

[1] Politehnica University Timisoara, alice.ghitescu@upt.ro, albert.constantin@upt.ro

Abstract: *The one-dimensional (1-D) hydraulic models are the most adequate for river modelling flow. This case study involves the rehabilitation of the CFR bridge, km 38 + 389, line 116 DII Simeria - Petrosani at Ruşor town, Hunedoara county. Therefore, the Ruşor River is being thought through, with a series of complex river works of the river bed and channel, in order to regulate the flows near CFR Bridge. To prevent future possible damages, a 1D hydrodynamic model of the Ruşor river sector was developed, highlighting the effect of the river regularization works. The hydraulic model was built with HEC-RAS 4.0 software, for two flow simulation scenarios: natural river flow and regulated river flow. Following the simulation of the hydrodynamic modelling, a significant reduction in the flow rates within the calculation reach was observed.*

Keywords: *1-D hydraulic modelling, river works, HEC-RAS.*

1. Introduction

In science, by modelling it understood the simplified reproduction of a real system that preserves the important characteristics and processes that take place in it.
Physical and mathematical models are suitable for research for a wide range of boundary conditions and the development of general design rules. Verification of final results requires field investigations and measurements as well as assessment of experiments and tests. [3]
In river modelling, the most common hydraulic models are the one-dimensional models (1D). Hydraulic computational models are constructed on the basis of conservation laws (mass preservation, energy conservation, moment conservation).
For the description of surface water flow in 1D system, the uniform flow equations and those of uniformly gradual flow are used. The following equations are used for uniform flow:

$$\frac{d_h}{d_x} = \frac{S_0 \cdot S_f}{1 \cdot F_r^2} \tag{1}$$

$$Q = \frac{1}{n} \cdot R^{\frac{1}{6}} \cdot \sqrt{R \cdot S_o} \cdot A \tag{2}$$

$$K = \frac{1}{n} AR^{\frac{2}{3}} \tag{3}$$

Where: -h is water depth (m);
- x is the measured distance along the river channel (m);
- S_o is the river bed slope;
- S_f is the friction slope;
- Q is river flow (m^3/s);
- K is river conveyance (m^3/s);
- A is wet surface (m^2);
- R is hydraulic radius (m);
- n is Manning's roughness coefficient ($s/m^{1/3}$);
- g is gravity acceleration (m/s^2).

2. Case Study

The purpose of the present paper is to show the influence of the proposed complex works on the river flow regime, in comparison with the natural (initial) river flow regime. This is made through hydraulic modelling of both scenarios for the 1 in 100 year return period flood event. The hydraulic modelling tool used for this is HEC-RAS software, for a one-dimensional hydrodynamic river channel model.

2.1 Hec-RAS modelling tool

The HEC-RAS software was developed at the Hydrologic Engineering Center (HEC), which is a division of the Institute for Water Resources (IWR), U.S. Army Corps of Engineers. HEC-RAS is a software that allows to perform one-dimensional steady flow hydraulics, one and two- dimensional unsteady flow river hydraulics computations; quasi unsteady and full unsteady flow sediment transport- mobile bed modelling; water temperature analysis and generalized water quality modelling (nutrient fate and transport). The HEC - RAS program is designed to perform one-dimensional and two-dimensional hydraulic computations for a full network of natural and artificial channels, overbank or floodplain areas, levee or embanked protected areas. And it can model the surface water profile in subcritical, supercritical or mixed flow [3], [4]. Depending on the flow regime (subcritical, supercritical, or mixed), the boundary conditions should be selected for different flow conditions, but also to determine which of these edge conditions can be used upstream or downstream or both.

2.2 Background description

The case study area is in Ruşor town, Hunedoara County, on the railway line CF 116 DII Simeria Petroşani at 38+989km, at the railway metal bridge. At km 38 + 989 there are two independent parallel bridges, each for one CF 116 Simeria-Petrosani line (see Figure 1) [1].

Fig. 1. Case study area of interest, Rusor River

In the bridge area at km 38 + 989, the banks of the Ruşor River bed have suffered due to floods, significant degradations that may endanger the proper behavior of foundations of existing bridges in the area. The current state of the river bed and railway infrastructure motivated the necessity to perform some complex works of regulation of the Ruşor River bed in the area of the railway bridge located on the railway line CF 116 Simeria-Petroşani between Băieşti - Pui stations, in Ruşor locality at km 38 989. The railway bridge has an opening of L = 19.0 m. In Figure 2 is illustrated an overview of the case study railway bridge.

Fig. 2. Bridge overview, Rusor River

2.3 Hydrodynamic modelling and numerical simulation

To assess the transit situation of flows with different probabilities of occurring on the watercourse along the bridge, it was necessary to build two numerical models, in two different flow regime scenarios. A numerical model represents the initial situation, the natural river flow regime, and the second numerical model represents the situation with the proposed works (supporting walls, bottom weir and stabilization river bed works), post-scheme model (regulated river flow regime). For the hydraulic modelling the total river reach length was 164m, with 21 cross sections considered, obtained from topographical survey. The railway bridge is located between cross sections ST13 to ST17. It was appreciated that cross section ST13 is the upstream bridge section, and ST17 is the downstream bridge cross section.
The roughness coefficients adopted for this study range between n=0.02-0.025 for the river bed, and between n=0.03-0.035 for the floodplains.
As modelling boundary condition upstream, a flow hydrograph was used, for the peak flow flood event 1 in 100 year return period $Q_{1\%}=105m^3/s$. The time length of the resulted flood flow hydrograph was 4 to 5hours, with recorded data every 2 minutes. For the downstream boundary condition, the normal depth was used.
In Fig. 3 are presented the river reach plan view for both scenarios: natural flow regime and regulated river flow regime.

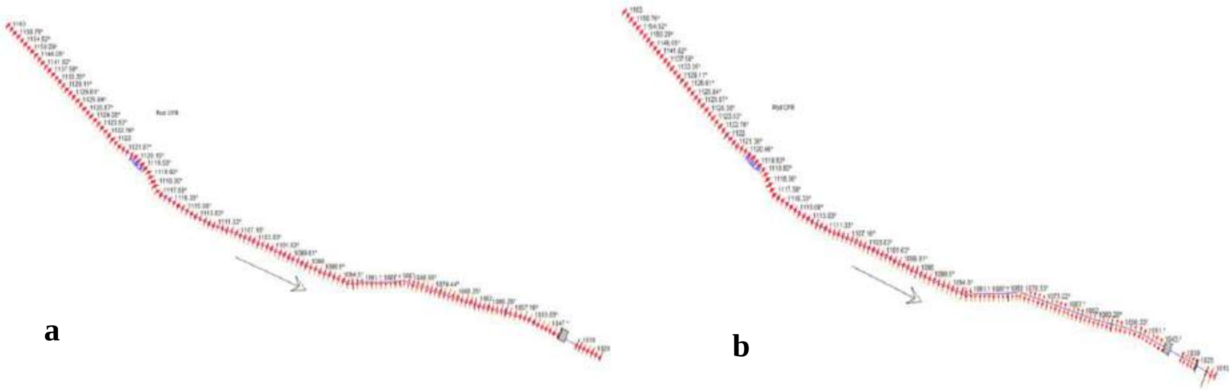

Fig. 3. River reach plan view **a.** Natural river flow regime, **b.** Regularized river flow regime, Rusor River

The ST13 cross section was considered to be the railway bridge cross section, and built accordingly, take into account the survey data and roughness coefficient (see Fig. 4).

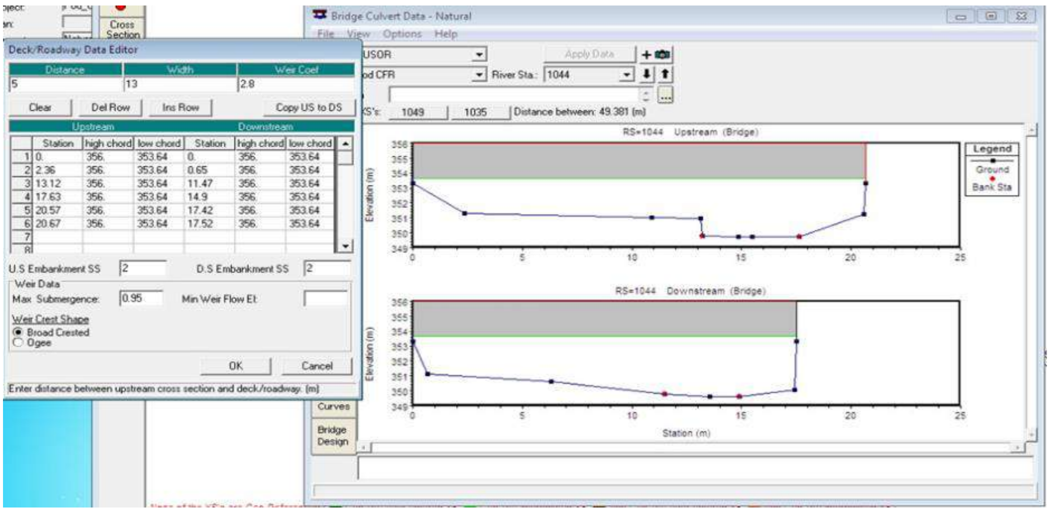

Fig. 4. River cross section at railway bridge, upstream and downstream view, Rusor River

As a change between the two flow regimes, in the regularised scenario, cascade bottom weirs were considered in the correspondingly cross sections (see Fig.5).

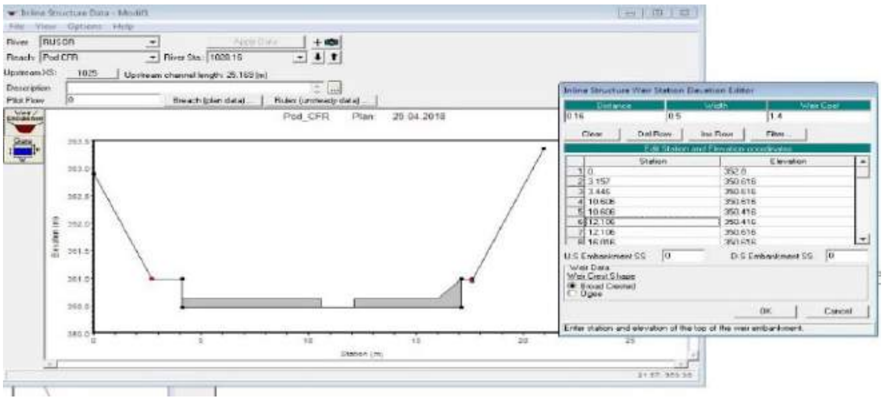

Fig. 5. River cross section at bottom weir, Rusor River

The river bed works were represented in the regularised flow scenario by the change in the roughness coefficient values and cross sections geometry (see Fig.6).

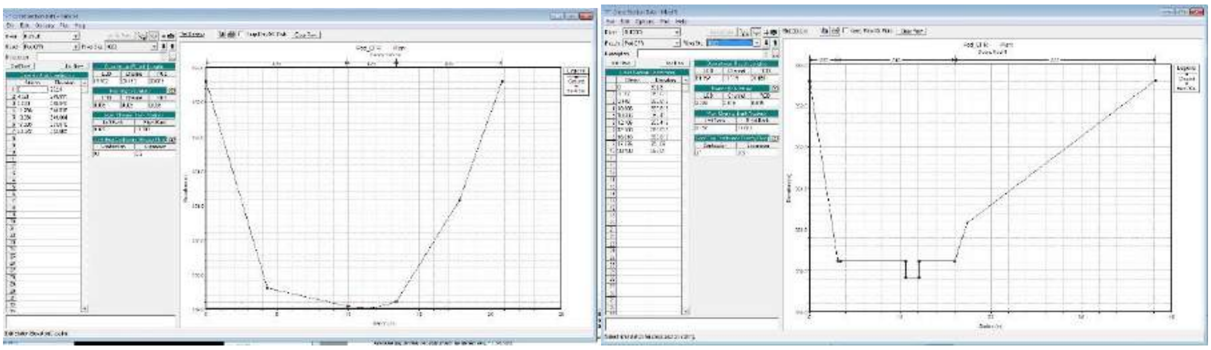

Fig. 6. Cross Section ST20 view **a.** Natural river flow regime, **b.** Regularized river flow regime, Rusor River

3. Results and Discussions

The modelling simulations of both flow regime scenarios outputs are illustrated as water levels in the following figures, Fig.7 to Fig. 12. The roughness coefficient Manning's n proved to be a significant sensitivity parameter. One of the majors constrains for the obtained results was the railway bridge soffit level, at 353.64maBSL. The water levels resulted over the hydraulic simulation in the bridge cross section had to be below the railway bridge by 1.0m, in order to prove the efficiency of the considered river works.

Fig. 7. Long profile view of Rusor River reach, natural river flow regime scenario

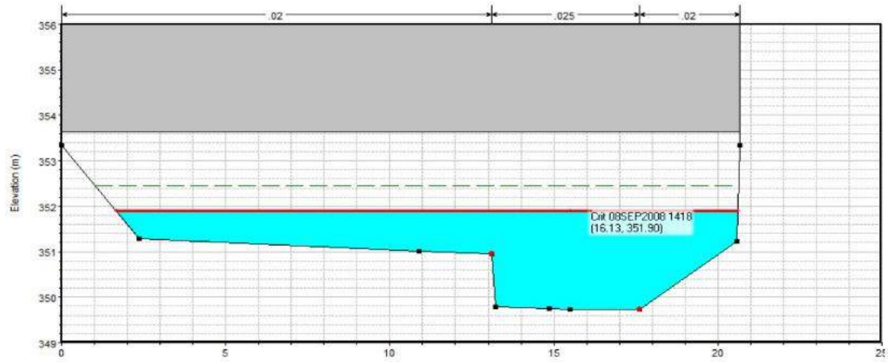

Fig. 8. Upstream Rusor River cross section at railway bridge, natural river flow regime scenario

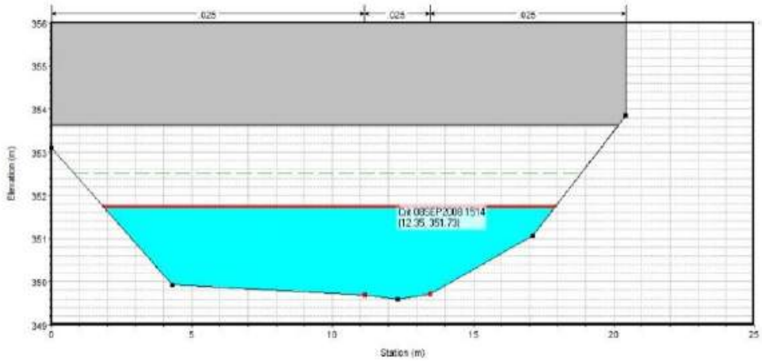

Fig. 9. Downstream Rusor River cross section at railway bridge, natural river flow regime scenario

In the following figures are illustrated the represented results obtained in the regularized river flow regime scenario.

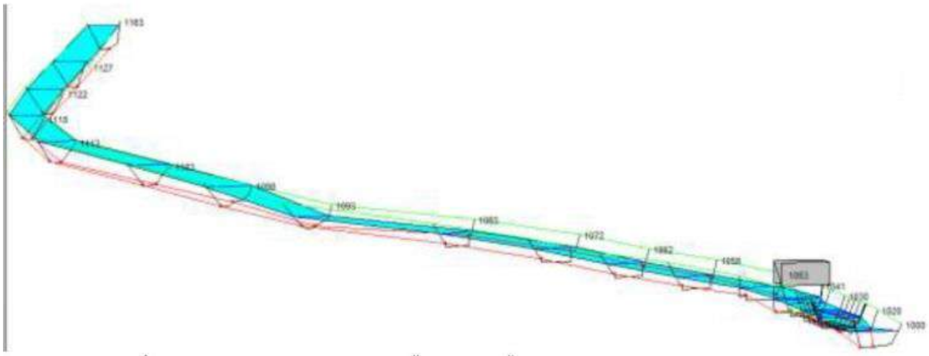

Fig. 10. Long profile view of Rusor River reach, regularised river flow regime scenario

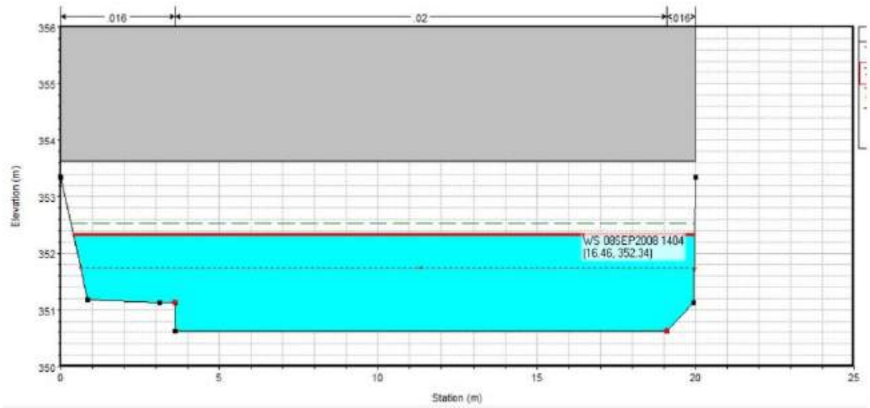

Fig. 11. Upstream Rusor River cross section at railway bridge, regularised river flow regime scenario

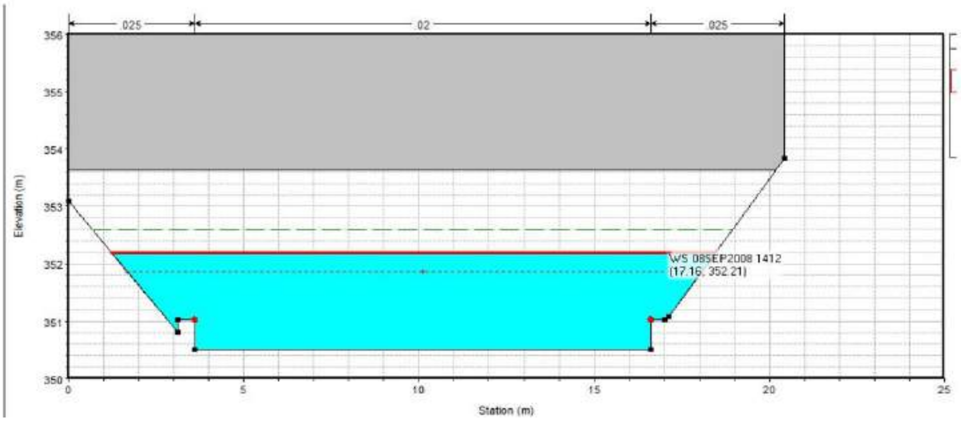

Fig. 12. Downstream Rusor River cross section at railway bridge, natural river flow regime scenario

From the modelling simulation, the results showed that in the natural flow regime scenario, the obtained velocities had range values between v_m = 3.5 - 6.8 m/s, where in the regularised flow regime the velocities vales obtained were in the range of v_m = 1.5 – 4.5 m/s.
Although, the water levels may show a small increase, the velocities which are an important factor in the railway bridge infrastructure stability, showed an overall decrease.

4. Conclusions

This case study presented in this paper illustrated the influence of river works on the natural river flow regime. A one-dimensional hydraulic model was built for this purpose, for two flow regime scenarios: natural flow regime and regulated river flow regime.
In the natural flow regime scenario, the obtained velocities had range values between v_m = 3.5 - 6.8 m/s, where in the regularised flow regime the velocities vales obtained were in the range of v_m = 1.5 – 4.5 m/s.
As a result of the model simulations, the outputs of the two flow regimes scenarios, showed a significant decrease of the flow rates in the computation sections of the regularised flow regime scenario, in comparison with the natural flow regime scenario.
Therefore, the proposed river works proved the expected impact on the river flow regimes, by decreasing the water levels and velocities in the railway bridge vicinity.

Acknowledgments

Acknowledgments to Administrația Bazinală de Apă Mureș for river flow recorded data.

References

[1] S.C. LONGHERSIN SRL Timisoara and Universitatea Politehnica Timișoara, Facultatea de Construcții, Departamentul de Hidrotehnică. *Proiect nr.: BC 104 / 15.11.2017 Reparație radier şi infrastructură albie râu Rușor în zona podului de la km 38+989, Linia 116 D II Simeria – Petroşani*.
[2] Popa, Radu. *Elemente de hidrodinamică a râurilor.* București, Editura Didactică și pedagogică, 1995.
[3] Ghitescu, Marie-Alice. *Analiza posibilităților și limitelor conceptelor de modelare a curgerilor în sistem 1D, 2D și 3D*. Timisoara, Editura Politehnica, 2010.
[4] Brunner, G.W.. HEC–RAS 4.1, *River Analysis System, Hydraulic Reference Manual*. USACE, November 2002.

ISSN 1453 – 7303 **"HIDRAULICA" (No. 3/2018)**
Magazine *of Hydraulics, Pneumatics, Tribology, Ecology, Sensorics, Mechatronics*

The Influence of Corrosion and Pressure Variation on the Minimum Safety Factor of a 3D Hexagonal Toroid with Regular Hexagonal Cross-Section Used in Manufacturing of LPG Storage Tanks

Assoc. Prof. PhD. Eng. **Ștefan ŢĂLU**[1,*], Assoc. Prof. PhD. Eng. **Mihai ŢĂLU**[2]

[1] Technical University of Cluj-Napoca, The Directorate of Research, Development and Innovation Management (DMCDI), Constantin Daicoviciu Street, no. 15, Cluj-Napoca, 400020, Cluj county, Romania. Corresponding author* e-mail: stefan_ta@yahoo.com

[2] University of Craiova, Faculty of Mechanics, Department of Applied Mechanics and Civil Engineering, Calea București Street, no. 107, 200512 Craiova, Dolj county, Romania. E-mail: mihai_talu@yahoo.com

Abstract: *This research was aimed to explore the minimum safety factor (SF) values of a three-dimensional (3D) hexagonal toroid with regular hexagonal cross-section used in manufacturing of LPG storage tanks from the automotive industry. Numerical simulations had been carried out to assess the influence of the corrosion and pressure variation on the minimum safety factor values. A polynomial interpolation was applied to provide a comparison between the surfaces or curves for which the SF has the minimum values. The development of the parametric 3D model (done in the AutoCAD Autodesk 2017 software, which was imported for analysis to SolidWorks 2017 software) on the actual conditions of the structure provides the decision-maker with the information necessary for making high-consequence decisions. The results of this study offer a fundamental understanding of the corrosion behavior of LPG storage tanks in exploitation environments.*

Keywords: *3D hexagonal toroidal LPG fuel tank, automotive industry, industrial engineering design, optimization methods, safety factor*

1. Introduction

Corrosion is a natural process defined as gradual degradation of metal caused by a chemical or electrochemical reaction with its environment. Many structural alloys corrode merely from exposure to moisture in air, but the process can be strongly affected by exposure to certain substances. Corrosion-related damage is accelerated by factors including the storage fuel tank's interaction with interconnected components and corrosive environmental conditions [1].
Corrosion protection of fuel storage tanks is a very important task which combines modern corrosion control methods with state-of-the-art technology to prevent storage fuel tanks from deteriorating. Common corrosion protection strategies include corrosion-resistant materials, application of coatings and/or linings as a barrier to the environment, and use of inhibiting chemicals in stored substances to control corrosion of the fuel storage tank interior.
Many researches have focused on technologies and innovation design strategies to create new models for the competitive market of fuel storage tanks [2-7].
Fuel storage tanks have complex shapes, mechanical and chemical resistance, range in size and complexity achieved through the combination of great design and manufacturing flexibility [8-15].
The modern engineering design of storage fuel tanks offers the perfect balance between safety, weight and cost to satisfy the demands of the competitive automotive market [16-19]. In order to meet these challenges, modern computer aided engineering (CAE) methods must be consistently applied throughout the manufacturing process.
3D CAD modelling of prototypes of storage fuel tanks used in automotive industry in an early phase of the design process with modern simulation tools is an indispensable requirement, as the design and optimization of subsystems is possible only within the complete product system [20-32]. In addition, to avoid expensive tests working with advanced materials and technology, various softwares with virtual computer aided engineering tools are challenged to quickly validate new models (In a hierarchical approach, the system, subsystems, components) while managing costs and protecting valuable test articles, which performs calculations in accordance with accepted national or international standards [33-41].

Factor of Safety (FoS), also known as Safety Factor (SF), in the technical literature can be computed using simplified approaches or more sophisticated methods with advanced numerical procedures. The factor of safety is often specified in a design code or standard [42-44].
In this research, starting from the aforementioned insights, a theoretical study was launched with the objective of researching the influence of the corrosion and pressure variation on the minimum safety factor values of a three-dimensional (3D) hexagonal toroid with regular hexagonal cross-section used in manufacturing of LPG storage tanks.
The performance analyses of investigated cases have a more dominant role in the understanding of the corrosion behavior of LPG storage tanks in exploitation environments.

2. Design methodology

In this research, it is used a 3D hexagonal toroid with regular hexagonal cross-section analyzed in our previous studies [14, 43].

2.1 Basic geometry of the parametric 3D model

The representative parametric 3D model generated by revolving of a closed generating curve C_G (a hexagon with rounded corners) along a closed guiding curve C_D (a hexagon with rounded corners) was used in this study, as shown in figure 1 [14].

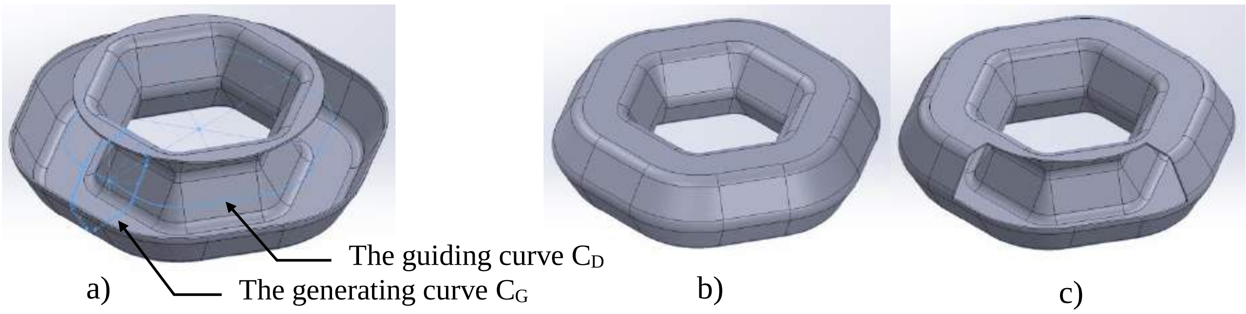

Fig. 1. The axonometric representation of the representative parametric 3D solid model

The following parameters were applied as input parameters to the 3D parametric model (figure 1): a) a closed generating curve C_G (a hexagon with a side value L = 175 mm, with rounded corners, radius R = 50 mm), and b) the guiding curve C_D (a hexagon with a side value L = 430 mm, with rounded corners, radius R = 180 mm).

2.2 Numerical analysis of the parametric 3D model

Based on the physical model, the modeling was done in the AutoCAD Autodesk 2017 software [39] and the numerical analysis was performed with SolidWorks 2017 software [40] with the Static, Thermal and Design Study modules. The design data used were:

- the tank material is AISI 4340 steel;
- the maximum hydraulic test pressure: p_{max} = 30 bar;
- the working temperature between the limits: T = -30 ^{0}C up to T = 60 ^{0}C;
- supporting surfaces located on the inferior side;
- the duration of the tank exploitation: n_a = 16 years;
- the corrosion rate of the material: v_c = 0.07 mm/years.

The safety factor (SF) of the parametric 3D model was computed as a result of the pressure variation within the permissible design limits (p_{max} = 0 up to 30 bar) and the maximum corrosion.
Numerical calculations were performed for: mesh standard type, solid mesh with quality high, automatic transition, Jacobian in 16 points, element size 10 mm, tolerance 1 mm, number of nodes 130215, number of elements 68415, maximum aspect ratio 26.30, number of degrees freedom 346152.
It can be seen that due to the geometry of the cover material, the boundary conditions, or the intensity of application or distribution of different loads occurring during exploitation, the safety factor has different values on the surface of the envelope, with values ranging from 1.399 to 14.974.

Table 1: The minimum safety factor

SF_{min} [-]	T = -30 ºC	T = -15 ºC	T = 0 ºC	T = 15 ºC	T = 30 ºC	T = 45 ºC	T = 60 ºC
p [bar]	-30	-15	0	15	30	45	60
2.5	4.769	6.360	8.807	13.625	14.26	14.974	9.264
5.0	4.15	4.986	6.233	8.268	12.05	10.053	8.281
7.5	3.477	4.04	4.813	5.928	7.646	7.400	6.404
10.0	2.989	3.393	3.917	4.619	5.598	5.853	5.216
12.5	2.619	2.922	3.301	3.784	4.416	4.839	4.398
15.0	2.330	2.566	2.852	3.204	3.645	4.125	3.801
17.5	2.098	2.287	2.510	2.778	3.104	3.505	3.346
20.0	1.908	2.062	2.241	2.452	2.702	3.003	2.988
22.5	1.749	1.877	2.024	2.195	2.393	2.626	2.700
25.0	1.615	1.723	1.846	1.986	2.147	2.333	2.462
27.5	1.499	1.592	1.696	1.814	1.947	2.099	2.262
30.0	1.399	1.480	1.569	1.669	1.781	1.908	2.051

The graphs of 3D surfaces (by type surf and fire) corresponding to the variation of minimum SF for SF_{min} (n_a = ct, p, T) taking into account the results from Table 1, are graphically shown in fig. 2.

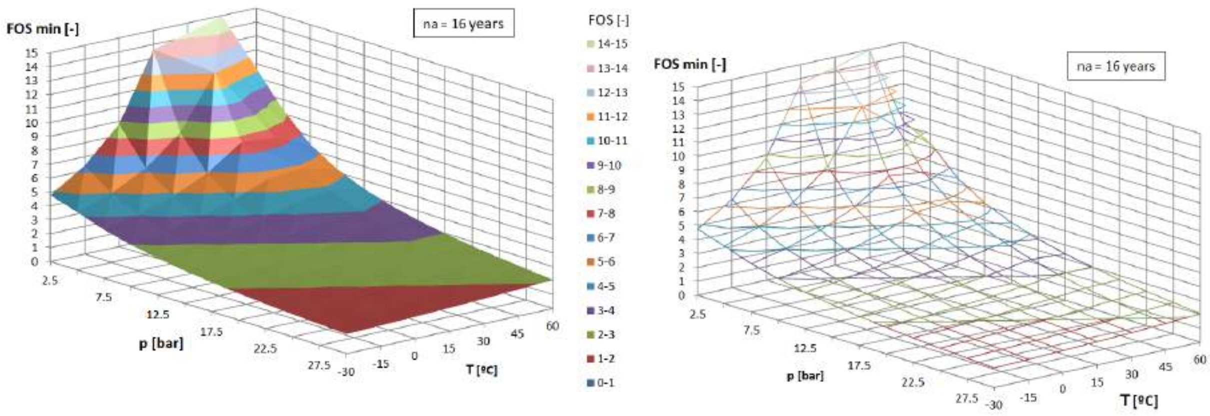

a) b)

Fig. 2. The 3D graphs SF_{min} (n_a = ct, p, T): a) surf type; b) fire type

The graphs of the isothermal coefficient variation curves, SF_{min} (n_a= ct, p, T = ct), are graphically shown in fig. 3.

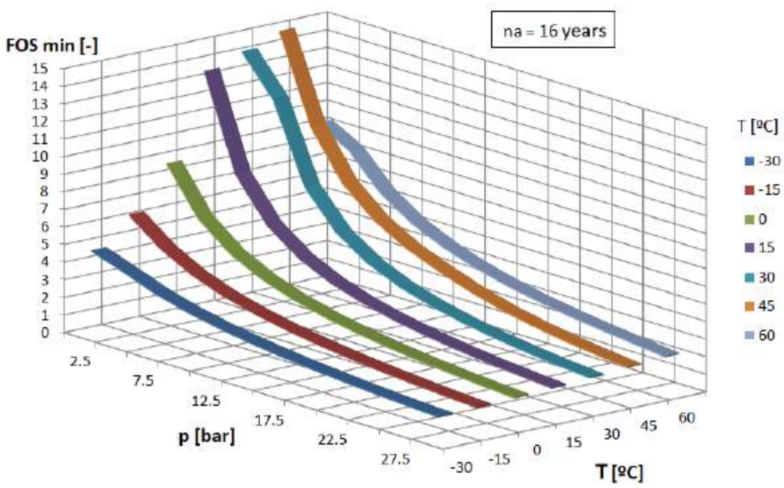

Fig. 3. The 3D graphs of the isothermal coefficient variation curves, SF_{min} (n_a= ct, p, T = ct)

The graphs and laws of the variance of resulting SF_{min} (n_a = ct, p, T), calculated through a polynomial interpolation using Microsoft Excel 2017 are shown in figs. 4 and 5.

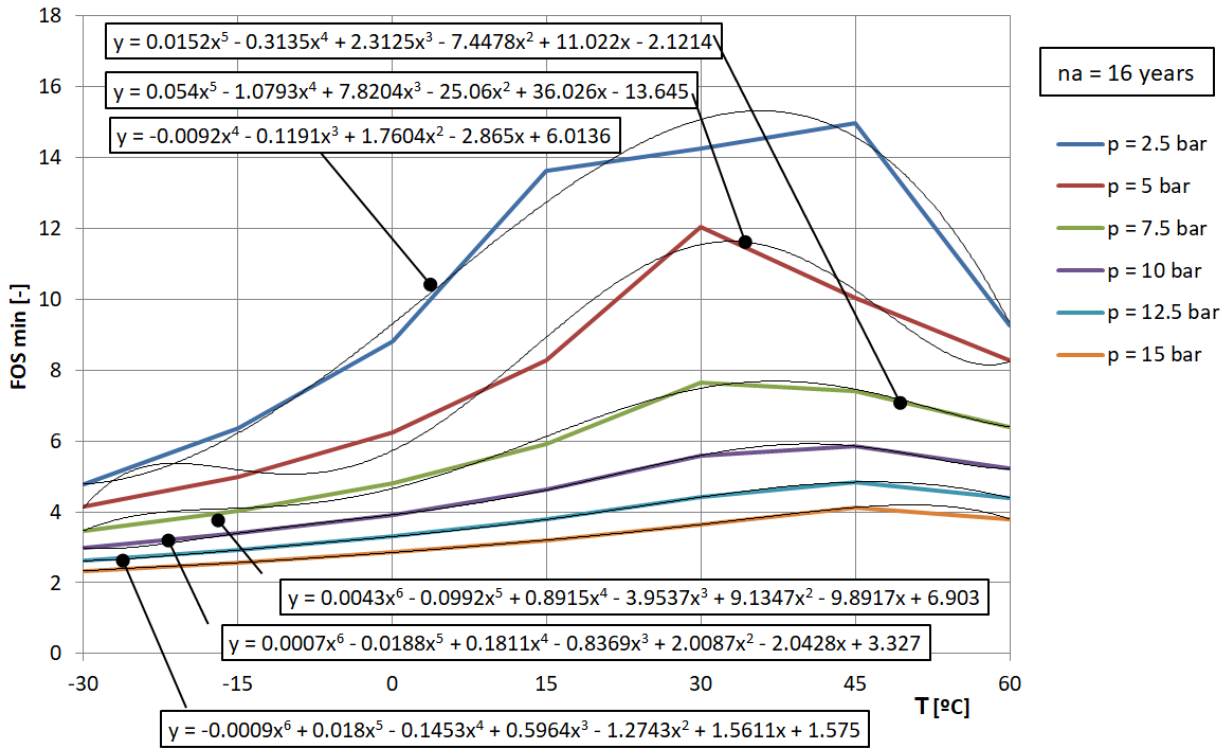

a)

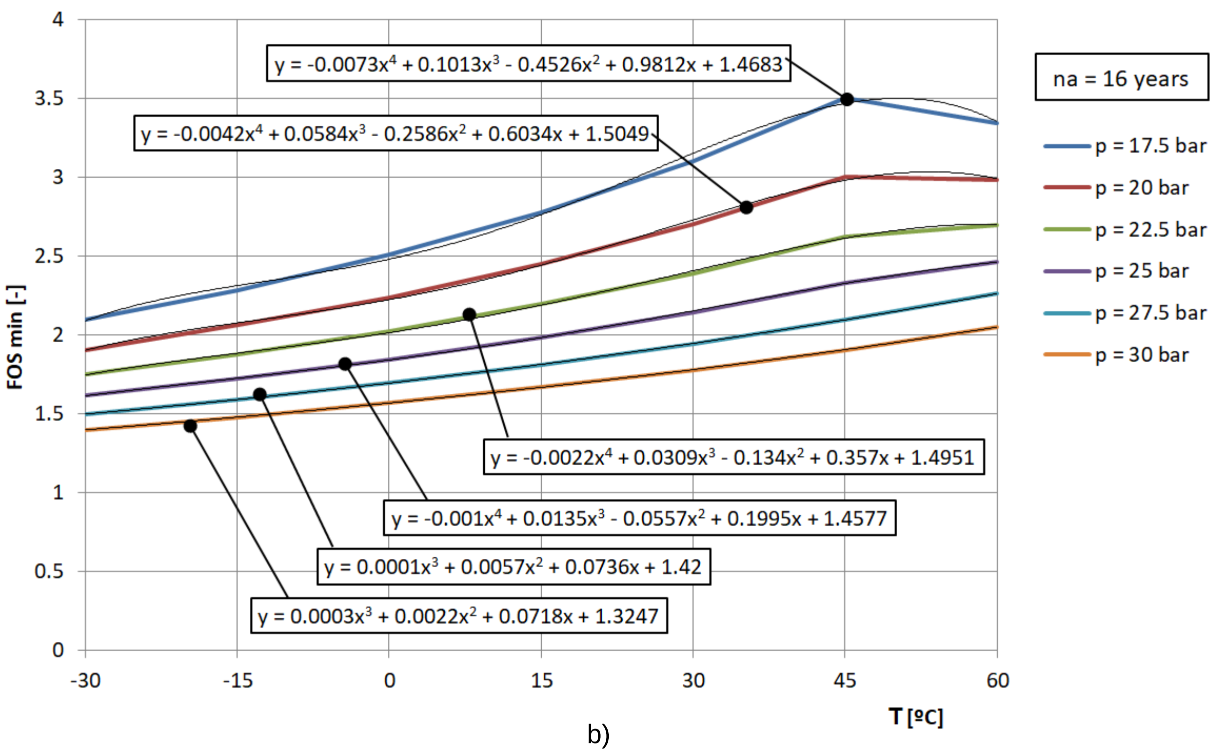

b)

Fig. 4. The 2D graphs and laws of the variance of resulting SF_{min} (n_a, p = ct, T)

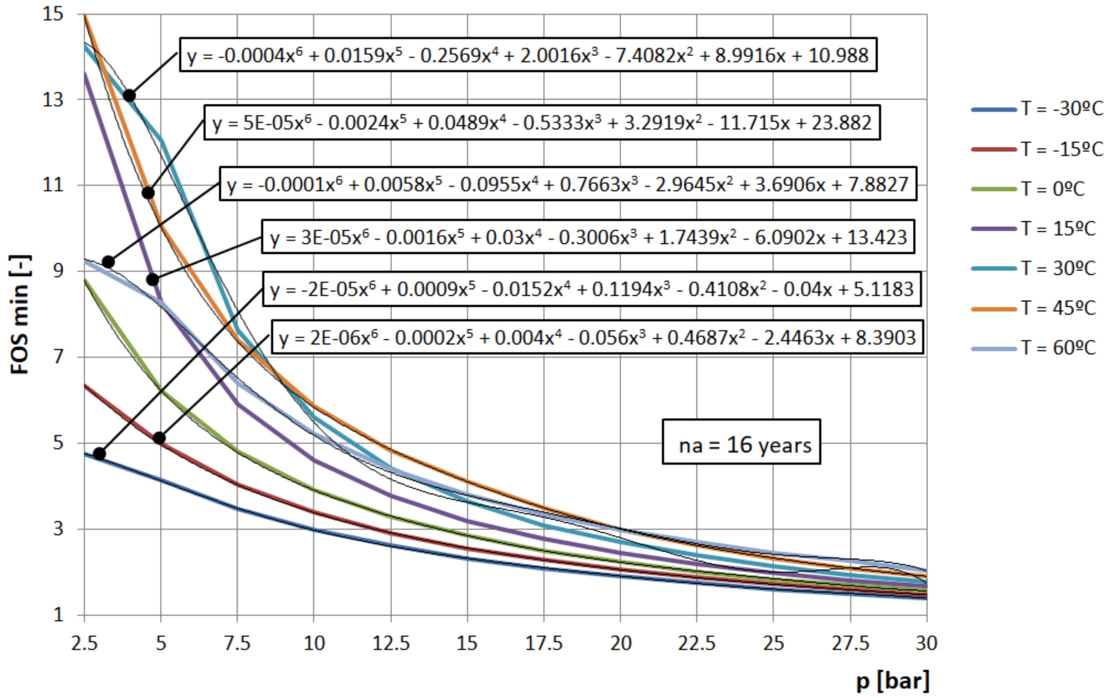

Fig. 5. The 2D graphs and laws of the variance of resulting SF_{min} (n_a, p, T = ct)

A direct determination of SF_{min} (n_a = ct, p, T) is shown in fig. 6.

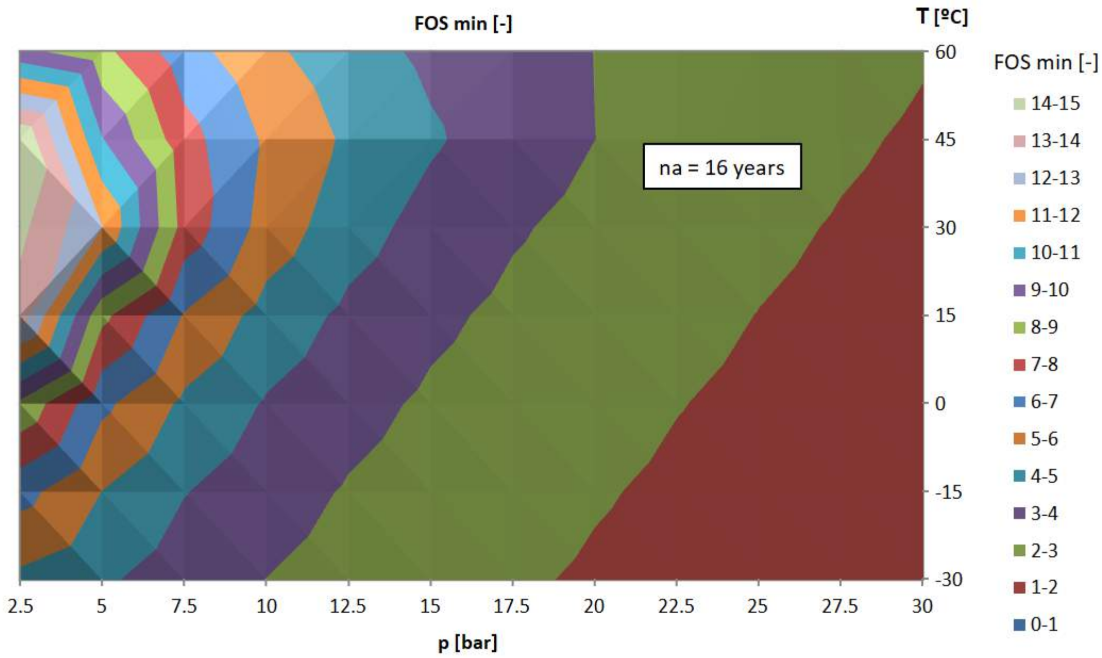

Fig. 6. The 2D graph of SF_{min} (n_a= ct, p, T)

3. Discussion

Following the SF analysis and the resulting graphs it has been found that:
- the graphical and analytical results of the mathematical dependencies determined by the laws of variation, allow for the determination of minimum SF considering the simultaneous influence of the corrosion and pressure;
- the obtained laws of variation highlight a major influence of pressure and temperature on the minimum SF. On the other hand, the minimum SF values decrease at lower temperatures (fig. 4) and increase at lower pressures (fig. 5).

4. Conclusions

Simulation results show that proposed method offer a major advantage and can lead to better applicability in the computational effort design of a 3D hexagonal toroid with regular hexagonal cross-section used in manufacturing of LPG storage tanks from the automotive industry.

Conflict of Interest: The authors declare that they have no conflict of interest.

References

[1] Mirza, Muhammad Mumtaz, Elansezhian Rasu, and Anjali Desilva. “Influence of Nano Additives on Protective Coatings for Oil Pipe Lines of Oman.” *International Journal of Chemical Engineering and Applications*, vol. 7, no. 4 (2016): 221-225.
[2] Ghiţă, C. Mirela, Anton C. Micu, Mihai Ţălu and Ştefan Ţălu. “Shape optimization of a thoroidal methane gas tank for automotive industry.” *Annals of Faculty of Engineering Hunedoara - International Journal of Engineering, Hunedoara, Romania*, Tome X, Fascicule 3 (2012): 295-297.
[3] Ghiţă, C. Mirela, Anton C. Micu, Mihai Ţălu and Ştefan Ţălu. “3D modelling of a gas tank with reversed end up covers for automotive industry.“, *Annals of Faculty of Engineering Hunedoara - International Journal of Engineering, Hunedoara*, *Romania*, Tome XI, Fascicule 3 (2013): 195-200.
[4] Ghiţă, C. Mirela, Anton C. Micu, Mihai Ţălu and Ştefan Ţălu. “Shape optimization of vehicle's methane gas tank.“ *Annals of Faculty of Engineering Hunedoara - International Journal of Engineering, Hunedoara, Romania*, Tome X, Fascicule 3 (2012): 259-266.
[5] Ghiţă, C. Mirela, Anton C. Micu, Mihai Ţălu and Ştefan Ţălu. “3D modelling of a shrink fitted concave ended cylindrical tank for automotive industry.“ *Acta Technica Corviniensis – Bulletin of Engineering, Hunedoara, Romania*, Tome VI, Fascicule 4 (2013): 87-92.
[6] Ghiţă, C. Mirela, Anton C. Micu, Mihai Ţălu, Ştefan Ţălu and Ema I. Adam. “Computer-Aided Design of a classical cylinder gas tank for the automotive industry.“ *Annals of Faculty of Engineering Hunedoara - International Journal of Engineering, Hunedoara*, *Romania*, Tome XI, Fascicule 4 (2013): 59-64.
[7] Ghiţă, C. Mirela, Ştefan C. Ghiță, Ştefan Ţălu and Simona Rotaru, “Optimal design of cylindrical rings used for the shrinkage of vehicle tanks for compressed natural gas.“ *Annals of Faculty of Engineering Hunedoara - International Journal of Engineering, Hunedoara*, Tome XII, Fascicule 3 (2014): 243-250.
[8] Ţălu, Ştefan and Mihai Ţălu. "The influence of deviation from circularity on the stress of a pressurized fuel cylindrical tank." *Magazine of Hydraulics, Pneumatics, Tribology, Ecology, Sensorics, Mechatronics (HIDRAULICA)*, no. 4 (December 2017): 34-45.
[9] Bică, Marin, Mihai Ţălu and Ştefan Ţălu. “Optimal shapes of the cylindrical pressurized fuel tanks.” *Magazine of Hydraulics, Pneumatics, Tribology, Ecology, Sensorics, Mechatronics (HIDRAULICA)*, no. 4 (December 2017): 6-17.
[10] Vintilă, Daniela, Mihai Ţălu and Ştefan Ţălu. “The CAD analyses of a torospheric head cover of a pressurized cylindrical fuel tank after the crash test.” *Magazine of Hydraulics, Pneumatics, Tribology, Ecology, Sensorics, Mechatronics (HIDRAULICA)*, no. 4 (December 2017): 57-66.
[11] Ţălu, Mihai and Ştefan Ţălu. "Analysis of temperature resistance of pressurized cylindrical fuel tanks." *Magazine of Hydraulics, Pneumatics, Tribology, Ecology, Sensorics, Mechatronics (HIDRAULICA)*, no. 1 (March 2018): 6-15.
[12] Ţălu, Mihai. "The influence of the corrosion and temperature on the Von Mises stress in the lateral cover of a pressurized fuel tank." *Magazine of Hydraulics, Pneumatics, Tribology, Ecology, Sensorics, Mechatronics (HIDRAULICA)*, no. 4 (December 2017): 89-97.
[13] Ţălu, Mihai and Ştefan Ţălu. "Design and optimization of pressurized toroidal LPG fuel tanks with variable section." *Magazine of Hydraulics, Pneumatics, Tribology, Ecology, Sensorics, Mechatronics (HIDRAULICA)*, no. 1 (March 2018): 32-41.
[14] Ţălu, Mihai and Ştefan Ţălu. "The optimal CAD design of a 3D hexagonal toroid with regular hexagonal cross-section used in manufacturing of LPG storage tanks." *Magazine of Hydraulics, Pneumatics, Tribology, Ecology, Sensorics, Mechatronics (HIDRAULICA)*, no. 2 (June 2018): 49-56.
[15] Ţălu, Ştefan and Mihai Ţălu. "Algorithm for optimal design of pressurized toroidal LPG fuel tanks with constant section described by imposed algebraic plane curves." *Magazine of Hydraulics, Pneumatics, Tribology, Ecology, Sensorics, Mechatronics (HIDRAULICA)*, no. 2 (June 2018): 14-21.
[16] Ţălu, Mihai and Ştefan Ţălu. “3D geometrical solutions for toroidal LPG fuel tanks used in automotive industry.“ *Advances in Intelligent Systems Research,* vol. 151 (2018): 189-193. DOI: 10.2991/cmsa-18.2018.44.
[17] Ţălu, Ştefan and Mihai Ţălu. “The Influence of corrosion on the vibration modes of a pressurized fuel tank used in automotive industry.“ *DEStech Transactions on Materials Science and Engineering,* (2018): 1-6. DOI: 10.12783/dtmse/icmsa2018/20560.

[18] Ţălu, Ştefan and Mihai Ţălu. “Constructive CAD variants of toroidal LPG fuel tanks used in automotive Industry.“ *Advances in Intelligent Systems Research,* vol. 159 (2018): 27-30. DOI: 10.2991/mmsa-18.2018.7.

[19] Ţălu, Mihai and Ştefan Ţălu. “Optimal engineering design of a pressurized paralepipedic fuel tank.“ *Annals of Faculty of Engineering Hunedoara - International Journal of Engineering, Hunedoara, Romania*, Tome XVI, Fascicule 2 (2018): 193-200.

[20] Ţălu, Ştefan. *Limbajul de programare AutoLISP. Teorie şi aplicaţii. (AutoLISP programming language. Theory and applications)*. Cluj-Napoca, Risoprint Publishing house, 2001.

[21] Țălu, Mihai. *Calculul pierderilor de presiune distribuite în conducte hidraulice. (Calculation of distributed pressure loss in hydraulic pipelines).* Craiova, Universitaria Publishing house, 2016.

[22] Ţălu, Mihai. *Mecanica fluidelor. Curgeri laminare monodimensionale. (Fluid mechanics. The monodimensional laminar flow).* Craiova, Universitaria Publishing house, 2016.

[23] Țălu, Mihai. *Pierderi de presiune hidraulică în conducte tehnice cu secțiune inelară. Calcul numeric și analiză C.F.D. (Hydraulic pressure loss in technical piping with annular section. Numerical calculation and C.F.D.)*, Craiova, Universitaria Publishing house, 2016.

[24] Ţălu, Ştefan. *Geometrie descriptivă. (Descriptive geometry)*, Cluj-Napoca, Risoprint Publishing house, 2010.

[25] Valencia, Garcia. *Geometría descriptiva, paso a paso*. Primera edición, Bogotá, Colombia, D.C, editorial Ecoe Ediciones, 2009.

[26] Florescu-Gligore, Adrian, Magdalena Orban and Ştefan Ţălu. *Cotarea în proiectarea constructivă şi tehnologică. (Dimensioning in technological and constructive engineering graphics).* Cluj-Napoca, Lithography of The Technical University of Cluj-Napoca, 1998.

[27] Florescu-Gligore, Adrian, Ştefan Ţălu and Dan Noveanu. *Reprezentarea şi vizualizarea formelor geometrice în desenul industrial. (Representation and visualization of geometric shapes in industrial drawing).* Cluj-Napoca, U. T. Pres Publishing house, 2006.

[28] Racocea, Cristina and Ştefan Ţălu. *Reprezentarea formelor geometrice tehnice în axonometrie. (The axonometric representation of technical geometric shapes).* Cluj-Napoca, Napoca Star Publishing house, 2011.

[29] Ţălu, Ştefan and Cristina Racocea. *Reprezentări axonometrice cu aplicaţii în tehnică. (Axonometric representations with applications in technique).* Cluj-Napoca, MEGA Publishing house, 2007.

[30] Ţălu, Ştefan and Mihai Ţălu. “CAD generating of 3D supershapes in different coordinate systems.“ *Annals of Faculty of Engineering Hunedoara - International Journal of Engineering, Hunedoara, Romania*, Tome VIII, Fascicule 3 (2010): 215-219.

[31] Ţălu, Ştefan and Mihai Ţălu. “A CAD study on generating of 2D supershapes in different coordinate systems.“ *Annals of Faculty of Engineering Hunedoara - International Journal of Engineering, Hunedoara, Romania*, Tome VIII, Fascicule 3 (2010): 201-203.

[32] Niţulescu, Theodor and Ştefan Ţălu. *Aplicaţii ale geometriei descriptive şi graficii asistate de calculator în desenul industrial. (Applications of descriptive geometry and computer aided design in engineering graphics).* Cluj-Napoca, Risoprint Publishing house, 2001.

[33] Ţălu, Ştefan. *Reprezentări grafice asistate de calculator. (Computer assisted graphical representations).* Cluj-Napoca, Osama Publishing house, 2001.

[34] Ţălu, Ştefan. *Grafică tehnică asistată de calculator. (Computer assisted technical graphics)*. Cluj-Napoca, Victor Melenti Publishing house, 2001.

[35] Ţălu, Ştefan. *AutoCAD 2005*. Cluj-Napoca, Risoprint Publishing house, 2005.

[36] Ţălu, Ştefan and Mihai Ţălu. *AutoCAD 2006. Proiectare tridimensională. (AutoCAD 2006. Three-dimensional designing)*. Cluj-Napoca, MEGA Publishing house, 2007.

[37] Ţălu, Ştefan. *AutoCAD 2017*. Cluj-Napoca, Napoca Star Publishing house, 2017.

[38] Nedelcu, Dorian. *Proiectare și simulare numerică cu SolidWorks*. *(Digital Prototyping and Numerical Simulation with SolidWorks)*. Timişoara, Eurostampa Publishing house, 2011.

[39] *** Autodesk AutoCAD 2017 software.

[40] *** SolidWorks 2017 software.

[41] Ţălu, Ştefan. *Micro and nanoscale characterization of three dimensional surfaces. Basics and applications*. Napoca Star Publishing House, Cluj-Napoca, Romania, 2015.

[42] Bîrleanu, Corina and Ştefan Ţălu. *Organe de maşini. Proiectare şi reprezentare grafică asistată de calculator. (Machine elements. Designing and computer assisted graphical representations).* Cluj-Napoca, Victor Melenti Publishing house, 2001.

[43] Ţălu, Mihai and Ştefan Ţălu. "The influence of corrosion and temperature variation on the minimum safety factor of a 3D Hexagonal toroid with regular hexagonal cross-section used in manufacturing of LPG storage tanks." *Magazine of Hydraulics, Pneumatics, Tribology, Ecology, Sensorics, Mechatronics (HIDRAULICA)*, no. 3 (September 2018): 16-25.

[44] Ţălu, Mihai. "Determination of a set of admissible parameters in designing of LPG storage tanks considering a required safety factor." *Magazine of Hydraulics, Pneumatics, Tribology, Ecology, Sensorics, Mechatronics (HIDRAULICA)*, no. 3 (September 2018): 56-61.

Water Flow Transition on a Hydropower Virtually Developed Sector of Bârzava River in the Town of Reșița

Assist.prof.PhD.Eng. **Alina-Ioana POPESCU-BUŞAN [1],** Assoc.prof.PhD.Eng. **Gheorghe LAZĂR[2],** Lect. PhD.Eng. **Albert Titus CONSTANTIN[3],** Lect. PhD.Eng. **Şerban-Vlad NICOARĂ[4]**

[1] POLITEHNICA University Timişoara, alina.popescu-busan@upt.ro

[2,3,4] POLITEHNICA University Timişoara

Abstract: *A water flow numerical modelling is developed on the paper for a given sector on Bârzava River where a hydropower associated deviation is assumed, in case of accidental high waters in the Town of Reșița. The model includes two gate-controlled overflowing steps, two water catchments, a headrace pipe of 3052 m in length and 1.10 m in diameter, two energy dissipaters and one micro-hydropower station endowed with two hydroelectric turbines. The flow simulation by the designed numerical model looks to establish the special water levels along the covered sector on the river course and to discuss with respect to the gross head and installed power at an afforded micro-hydropower arrangement. Two specific running situations were assumed, the common running status when the upstream entering section receives the medium multiannual flow and the accidental running status when the entering section is to receive a specified time related flow along the entire considered analysis period of 59 hours.*

Keywords: *River flow, micro-hydropower, numerical model.*

1. General considerations; specific topographical and hydrological data

Bârzava River originates in the Semenic Mountains, Caraș-Severin County, a formation in the Banat Mountains that belong with the Western Carpathians. The river has a receiving basin of 1190 km^2 and a length of 166 km, which from 127 km lay on Romanian territory. Arising in Caraș-Severin County, Bârzava crosses the south of Timiș County and the Province of Vojvodina in The Republic of Serbia where finally reaches the Danube-Tisa Channel. For a length of 3.8 km the river establishes the Romanian-Serbian border. Țerova Rivulet is a right-side tributary of Bârzava River with the joining point in Reșița Town.
The river modelled sector and the hydropower deviation lays on the administrative territory of Reșița Municipality [1], the site being bordered at south (upstream) by the Railway Iron Bridge and at north by the road bridge on Calea Timișoarei Boulevard. Thus, the considered sector spreads over a length of about 6040 m (figure 1).

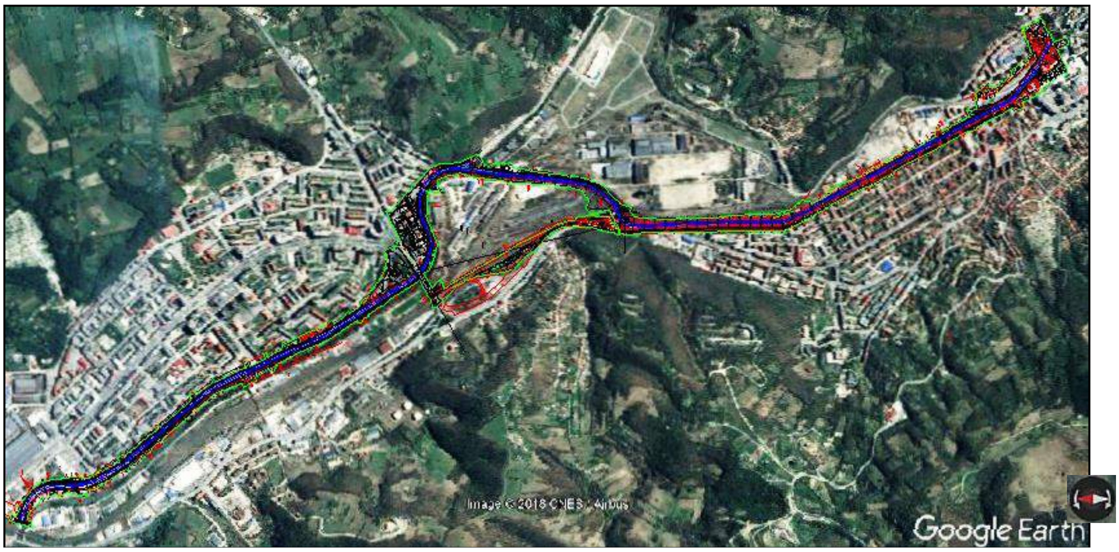

Fig. 1. Aerial view of the modelled sector on Bârzava River in the Town of Reșița with the overlaid topographic measurements plan

Based on the supplied topographical specialized information (Stereo 70 measurements) a specific geometry database (of 6394 distinct geographic coordinates points) was created for the considered river sector, representing the terrain plan view and 121 watercourse cross sections that properly points out the minor and major streambed.
In order to estimate a specific flow transition – water levels and velocity developments in time for any cross section – along the sector related to Reșița Town, the following data had to be obtained: maximum flow values of the particular occurrence probabilities 5% and 1% (according to national regulations with respect to the water arrangement importance and location); high-waters phenomenon development (hydrographer); terrain roughness coefficients for the streambed; flow hydro-energy gradient or flow-level curve corresponding to the downstream ending cross section. The water flow values for different occurrence probabilities together with the high-water development curves possible to happen on the modelled sector were supplied by the "Romanian Waters" National Administration, Banat Water Basin Administration, as presented in table 1. As about the high-waters hydrographer that is to be considered in Reșița, its development and maximum value (corresponding to the 1% probability of occurrence, 142 m^3/s) can be observed in figure 2, given by curve d. The water flow value of 20 m^3/s is to be added as the contribution of Țerova Rivulet, assuming the possible overlapping of its particular hydrographer.

Table 1: Hydrological data

River		Bârzava
Referring point		Traian Vuia Square in Reșița Town
Receiving basin (km^2)		218
Controlled flow	1 %	142
	5 %	78

The main foreseen hydraulic structures related to the model – two gate-controlled overflowing steps, two water catchments, a headrace pipe of 3052 m in length and 1.10 m in diameter, two energy dissipaters and one micro-hydropower station endowed with two hydroelectric turbines [1] – are considered of the IVth importance class (constructions of low importance) as stipulated by the national regulations given their dimensions and capacity.
Consequently, the dimensioning and verification water flow occurring probabilities are to be considered of 5% and 1%.

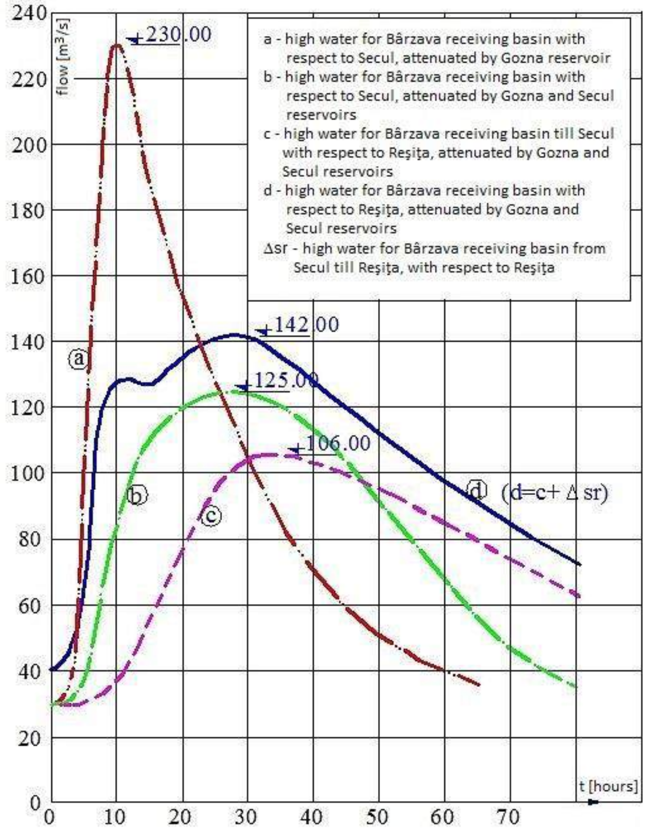

Fig. 2. High-waters hydrographers developments on the modelled river sector in the Town of Reșița, as determined under the conditions of existing upstream water arrangements

The geometrical development d supplied by figure 2 was assigned as transiting the entering upstream section of Bârzava River studied sector, while the additional flow brought by Țerova Rivulet was assigned on the route to the joining section.
The numerical model developed by the help of the performant software package HEC-RAS v.5.03 [2, …, 5] considers thus a possible transiting high-waters wave that eventually reaches the maximum flow value of 162 m^3/s on the downstream section at the road bridge on Calea Timișoarei Boulevard.

2. Numerical modelling, revealed results

The Bârzava River streambed geometry in the Town of Reșița was modelled for a sector length of 6042 m, considering a succession of 155 straight segments delimitated by 156 cross section (121 of which as according to the actual topographic measurements, while the rest of 35 being considered by linear interpolation). The entire path of the numerical model was organized in 5 sectors marked as one can find in the general scheme on bottom part of figure 3.

Fig. 3. General plan scheme (bottom) with marked cross sections (as developed by HEC-RASv.5.03) from the upstream entering position "6042.80*" to the outgoing one "0.00"; the detailed positions PT106 (upper left, "57.43") and PT44 (upper right, "3842.40") of the main hydraulic structures

The cross sections cut up to the major streambed, both sides of the river, their geometry being referred to a start point on the outside edge of the left bank top. The profiles location (identification) is performed by the help of a metric counter (a real number) with respect to the downstream end of the modelled river sector [2, 3].
The discretized path involves 11 bridges and foot-bridges, 2 overflowing steps (with the positions PT44 and PT106) with their accompanying constructions (water catchments and energy dissipaters), a headrace side pipe (with its entering section near the PT44 position) and a micro-hydropower station (MHC-3 in the vicinity of position PT106). This last structure is furnished with two hydro-electric outfits of Axial/Propeller type (bulb turbine, figure 4) of the following designed parameters: group1 (as fuelled by the 3052 m length headrace pipe) – $H_{gross-31}$ = 14.39 m, $Q_{inst-31}$ = 2 m^3/s, $P_{gross-31}$ = 282.33 KW and group2 – $H_{gross-31}$ = 1.76 m, $Q_{inst-31}$ = 2m^3/s, $P_{gross-31}$ = 34.53 KW.
There are also considered a couple of virtual structures, a side type structure at position PT44 (metric location "3842.40" and furthermore associated to the entrance in the headrace pipe on "3052.03") to control and monitor the running regimes and transit flow, and an overflowing retaining (barrage) structure type in the vicinity of position PT106 (metric location "57.43") to model some local and longitudinal head losses.
A transitory hydraulic regime correlated to the required high-waters development phenomenon (hydrographer d in figure 2) was engaged by the designed model and the followed analysis results

reflect two specific running situations: the common running status when the upstream entering section PT0 (metric location "6042,80*") receives the medium multiannual flow Q_m = 3.63 m^3/s and the Țerova tributary brings the adding flow $Q_{mȚ}$ = 0.30 m^3/s (infused along the particular time interval between 00:00 and 02:50 of the day "23OCT2017"), and respectively the accidental running status when the entering section is to receive the specified time related flow along the entire considered analysis period of 59 hours (from 00:00 on 23OCT2017 to 11:00 on 25OCT2017).

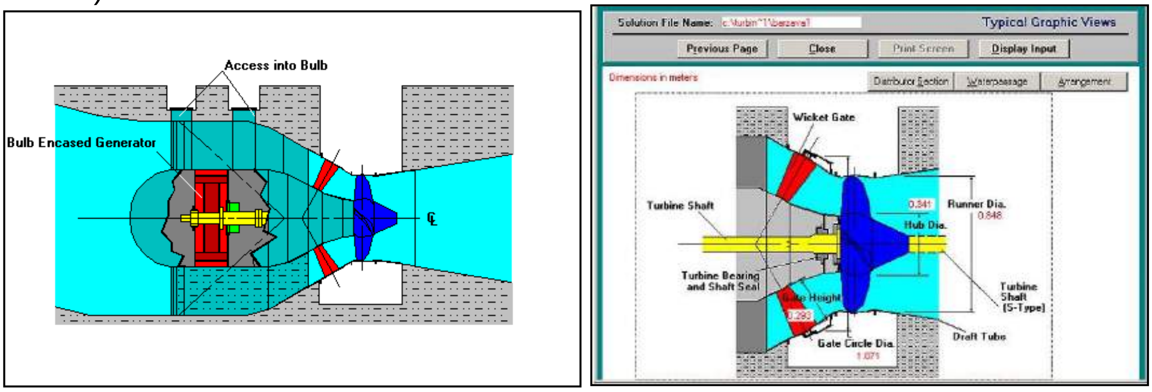

Fig. 4. Characteristic elements a the considered Axial/Propeller hydroelectric turbine

A flap gate covering a rectangular gap of 19.48m width and 2.00m height is modelled on the ridge of each overflowing step, by the help of which the water retention height can be controlled (during a common running status) or that can be completely opened to allow the accidental nigh-waters passing away (during the accidental running status). The alluvia settled in time upstream of the steps/catchments (positions PT44 and PT106) is to be washed by the help of uprising flat gates of 0.80m width and 1.00m height each.

Figure 5 presents the cross sections corresponding upstream and downstream the overflowing step at the position PT44 during the common running status, showing the obtained water level (metric location "3846.03" for upstream and respectively "3831.74*", "3824.60*" and "3796.02" for downstream). The cross sections associated to the structures at position PT106 – overflow step, water catchment and micro-hydropower station – for the common running status are presented by figure 6 (metric locations "760.66*" and "754.43" for upstream and "740.73*" for downstream).

As regarding the accidental running status, conventional results corresponding to the cross sections associated to the structures at position PT44 are presented by figure 7 for the specific time moments 00:10, 04:50 and 06:00 on 23OCT2017 and 11:00 on 25OCT2017 (the end of the given time period). Similarly, figure 8 present the results on cross sections associated to the structures at PT106 for the time moments 00:10, 04:40 and 06:00 on 23OCT2017 and 11:10 on 25OCT2017.

The longitudinal profiles along the 5 analysed sectors of the numerical model, showing the water level development, are presented by figure 9 – common running status at 00:10 on 23OCT2017 and figure 10 – accidental running status at 04:40 and 06:00 on 23OCT2017 and 11:00 on 25OCT2017.

3. Conclusions

Looking to analyse the water levels development under required conditions with respect to the flow transition and a virtual accomplishment of a micro-hydropower arrangement on a particular sector of Bârzava River in the Town of Reșița a thorough numerical model was developed by the help of HEC-RAS v.5.03 dedicated software. Based on this result two aspects regarding this specific arrangement can be judged, meaning the basic parameters and running procedure for the foreseen hydropower development and the transit capacity of the virtual endowed streambed under accidental flow. Therefore, two fundamental running situations were considered for the studied refurbished river sector, one reflecting the common running status of transiting the medium multiannual flow and the other one that covers an accidental running status of transiting the 1% apparition probability high-waters flow wave.

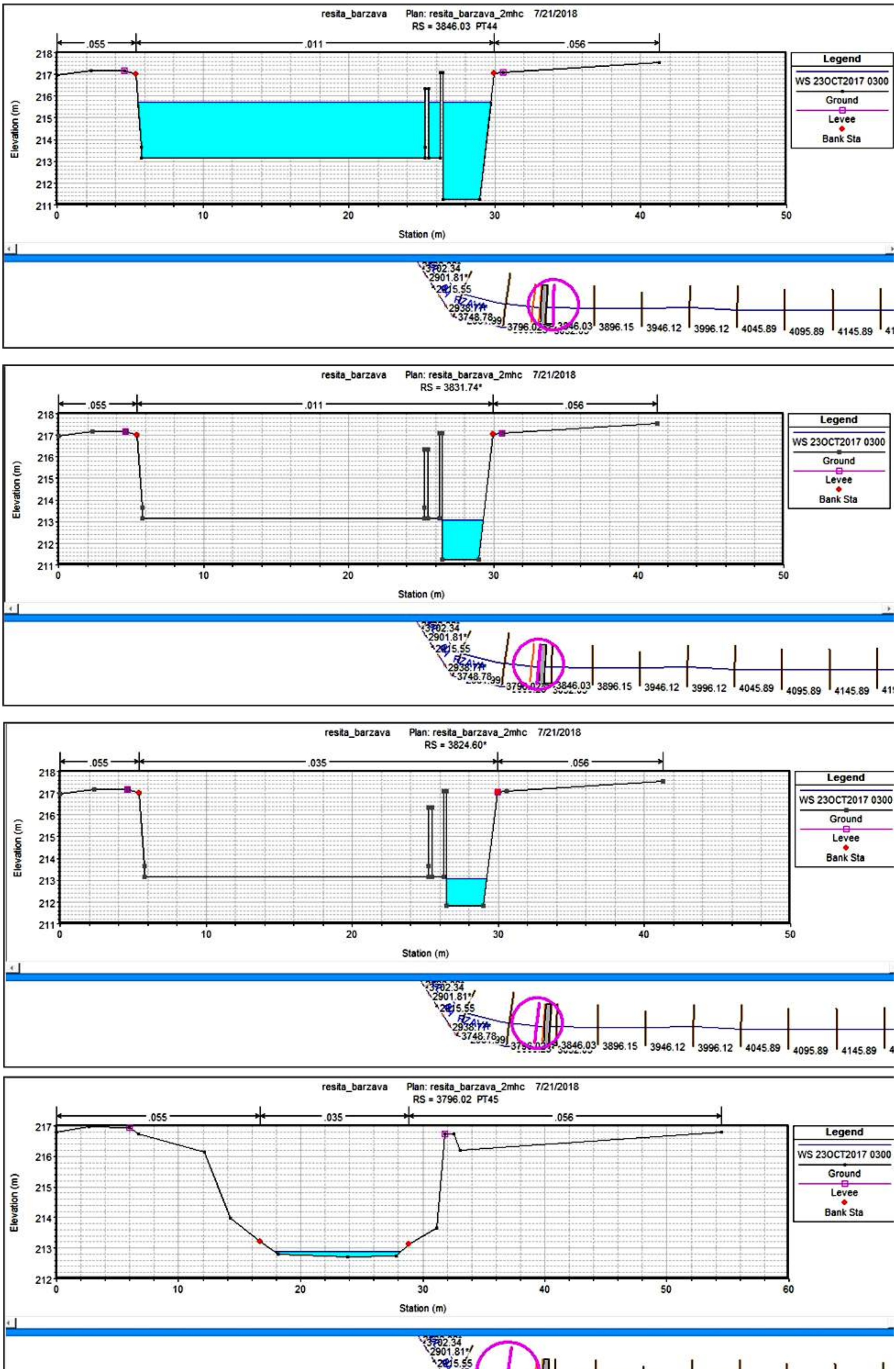

Fig. 5. Cross sections associated upstream (upper) and downstream to structures at PT44 showing the water level produced by the common running status

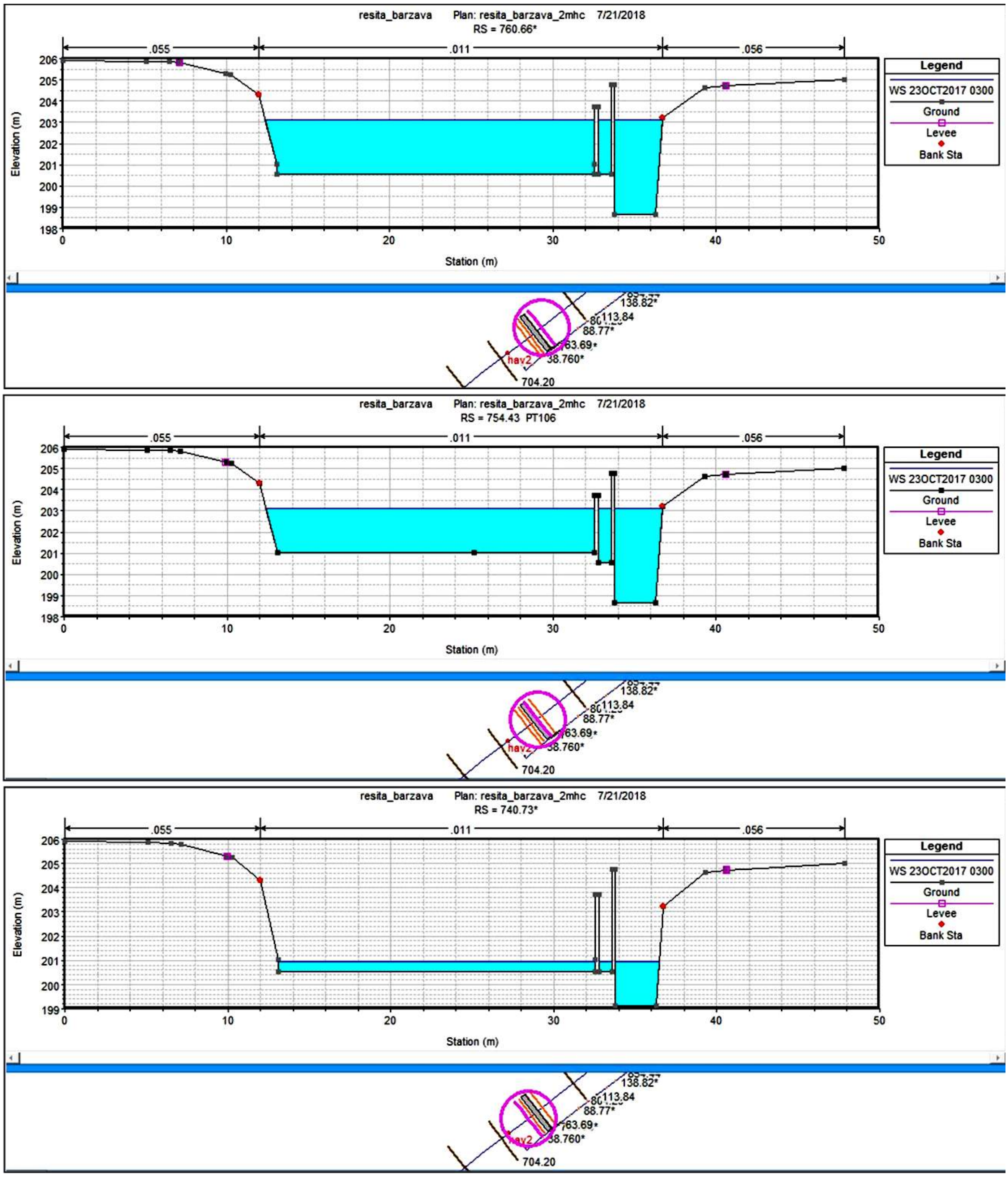

Fig. 6. Cross sections associated upstream and downstream (lower) to structures at PT106 (overflow step, catchment and micro-hydropower station) showing the water level produced by the common running status

Going through the reached results (see the moment 00:10 on 23OCT2017) one can engage the numerical values that define the running parameters for the usual running status of the two power groups designed for the MHC-3 micro-hydropower station:

- the gross head of the first group, as fuelled with the installed discharge $Q_{inst-31}$ = 2 m^3/s by a 3052 m long headrace pipe, results as the level difference $H_{gross-31}$ = 215.73 – 201.34 = 14.39 m, which leads to the gross installed power $P_{gross-31} = 9.81 \times Q_{inst-31} \times H_{gross-31} = 9.81 \times 2 \times 14.39 = 282.33$ kW;
- the gross head for the second group, designed as at an on-step power station supplied with an installed discharge $Q_{inst-32}$ = 2 m^3/s, results as $H_{gross-32}$ = 203.10 – 201.34 = 1.76 m, which may allow a gross installed power $P_{gross-32} = 9.81 \times Q_{inst-32} \times H_{gross-32} = 9.81 \times 2 \times 1.76 = 34.53$ kW.

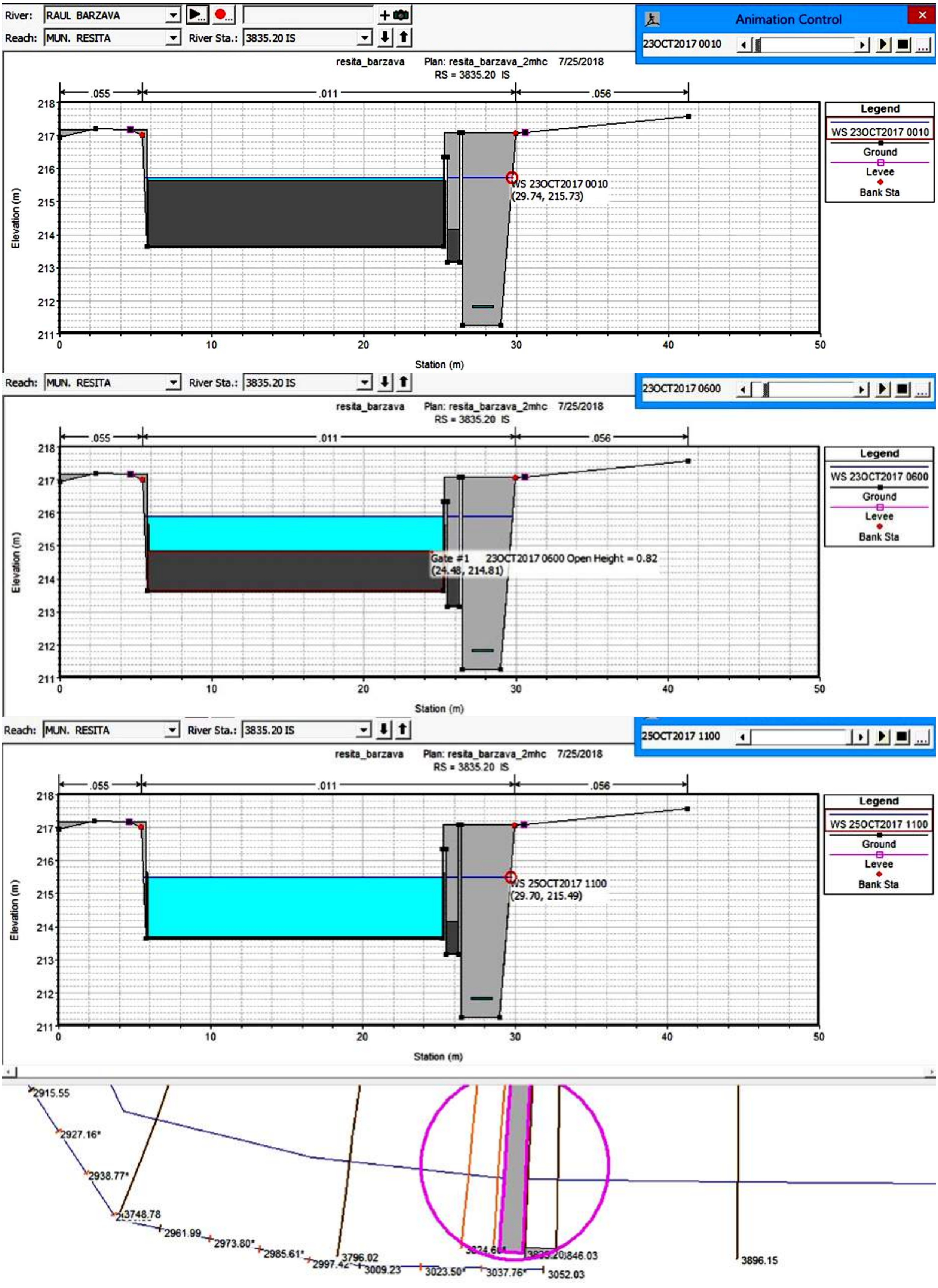

Fig. 7. Cross section associated to structures at PT44 showing the water level produced by the accidental running status for some specific operation conditions and moment of time: flap gate in closed position at 00:10 on 23OCT2017 (upper), flap gate in partially opened position (0.82m) at 06:00 on 23OCT2017 and flap gate in completely opened position at 11:00 on 25OCT2017 (lower)

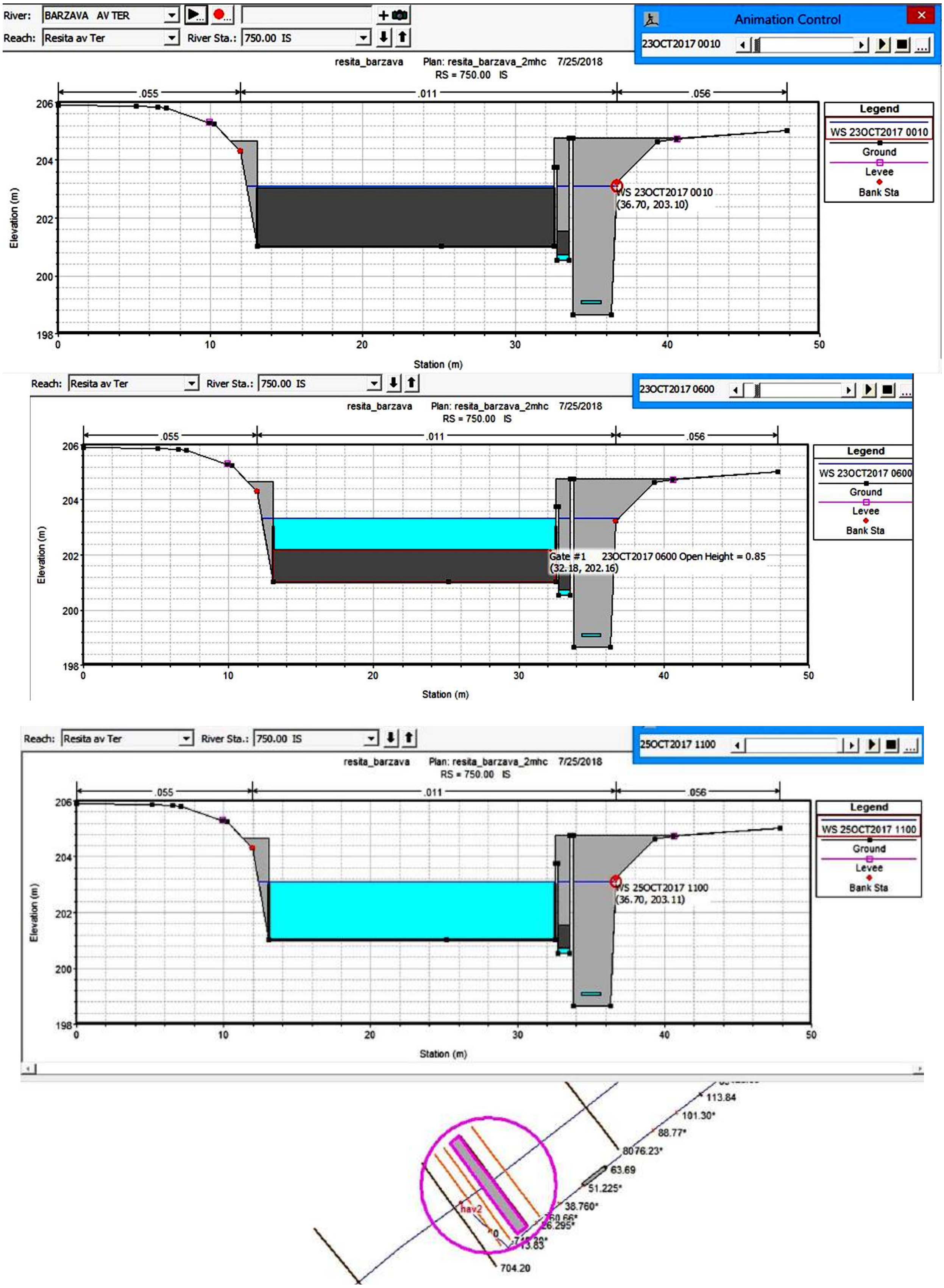

Fig. 8. Cross section associated to structures at PT106 showing the water level produced by the accidental running status for some specific operation conditions and moment of time: flap gate in closed position at 00:10 on 23OCT2017 (upper), flap gate in partially opened position (0.85m) at 06:00 on 23OCT2017 (middle) and flap gate in completely opened position at 11:00 on 25OCT2017 (lower)

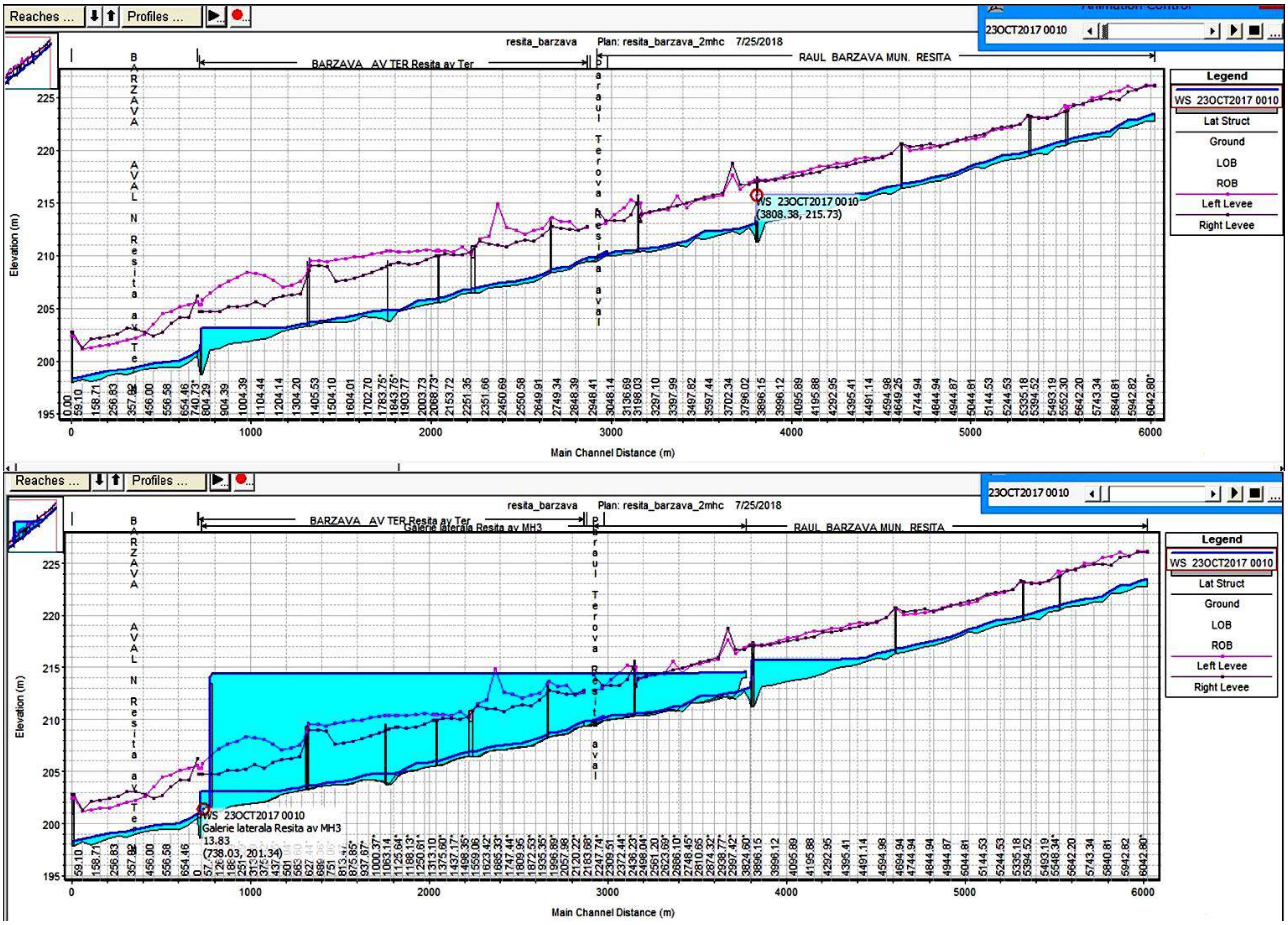

Fig. 9. Longitudinal profiles showing the water level development along the studied sector on Bârzava River in the Town of Reșița, corresponding to the common running status of transiting the multiannual flow $Q_m = 3.63 m^3/s$ (moment of time 00:10 on 23OCT2017), displaying only the river-course hydraulic profile (upper) and displaying the overlaid hydraulic profile of the side headrace pipe (lower)

It can be so estimated that the total gross installed power for the presented micro-hydropower development would reach about 316.86 kW under usual running regime given by the mean multiannual flow.

As about the situation produced by the accidental high-waters wave, there can be noticed from the longitudinal water levels time development with respect to the side framing bank levels that the already regulated river valley cross section would still be able to discharge the required maximum flow of 1% apparition probability, obviously under the circumstances of manoeuvring the flap gates on the overflowing steps down to the complete opening of the flow section. There can be concluded that the stipulated high-waters flow can transit the furbished river sector along the populated area under mandatory safety conditions.

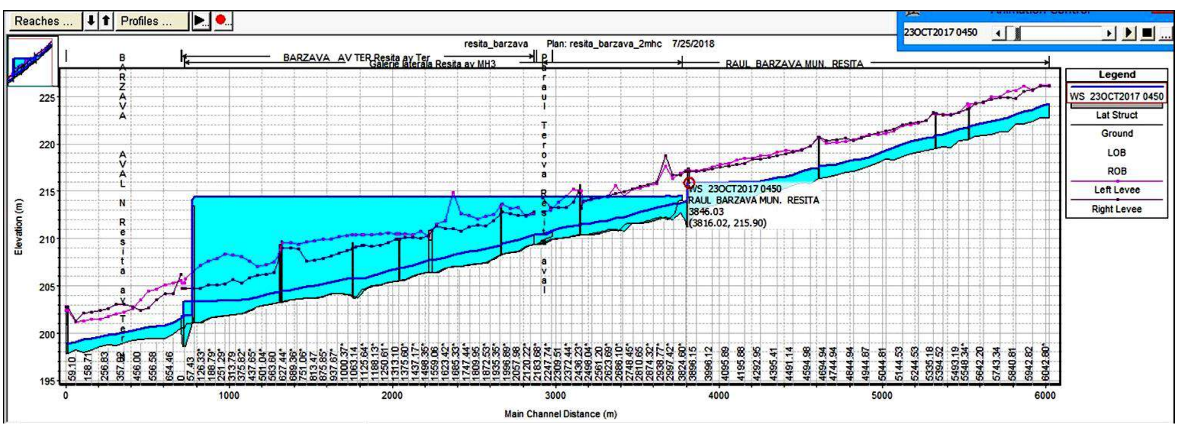

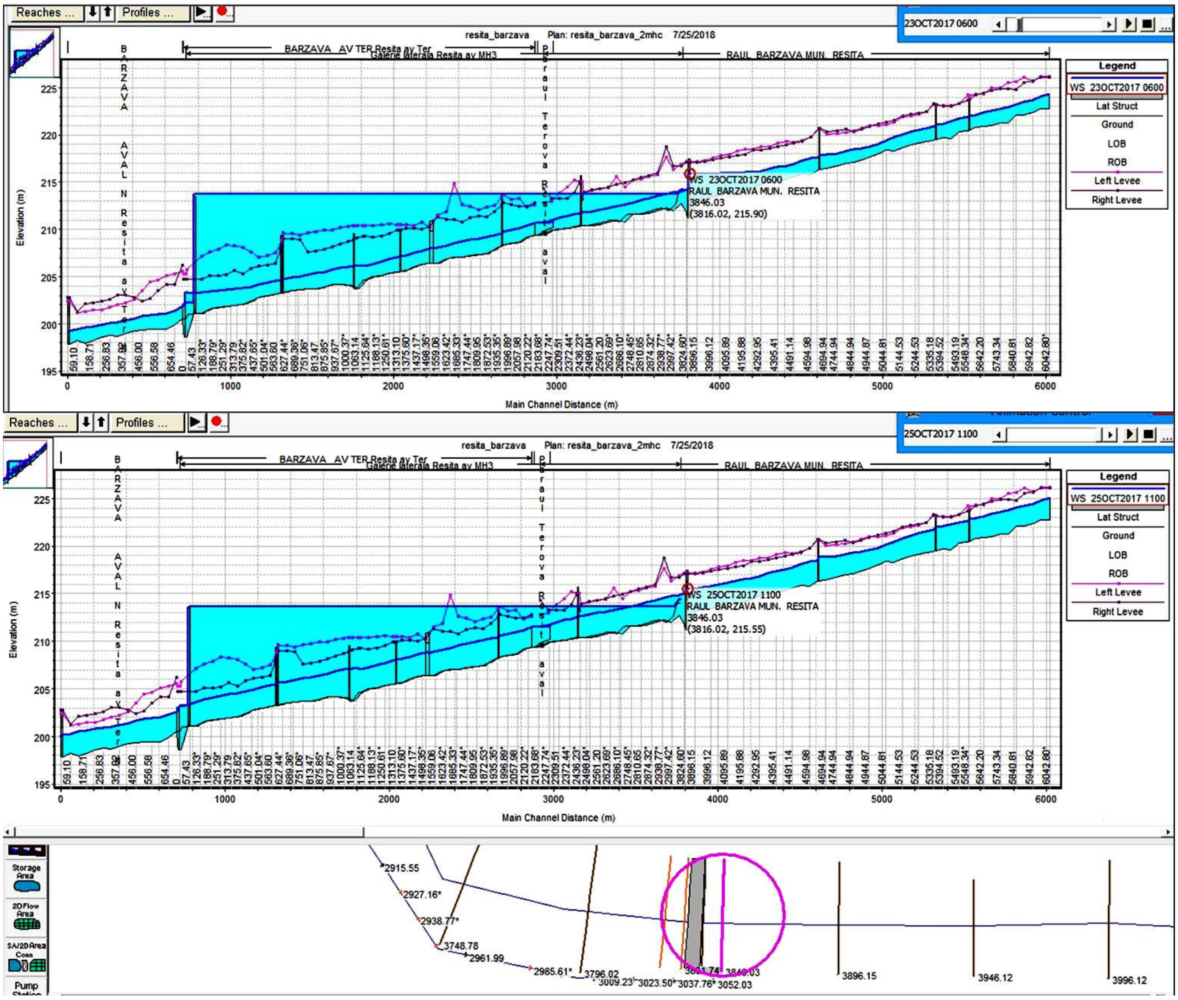

Fig. 10. Longitudinal profiles showing the water level development along the studied sector on Bârzava River in the Town of Reșița (overlaying the hydraulic profile of the side headrace pipe), corresponding to the accidental running status of high-waters flow $Q_{1\%}$ at some given moments of time: 04:50 (previous page) and 06:00 (middle) on 23OCT2017 and 11:00 on 25OCT2017 (lower)

References

[1] ***, *Technical Contract no.15/01.03.2018 - Elaborarea studiului de fezabilitate pentru microhidrocentrale pe Râul Bârzava ca soluție adaptată local pentru investiții în infrastructura de energie regenerabilă și utilități publice, Reșița, România / Feasibility study for small hydro power plants on Bârzava River as locally adapted solution for investments in renewable energy and public utilities infrastructure, Reșița, Romania*. POLITEHNICA University Timişoara, Faculty of Civil Engineering, Department of Hydrotechnical Engineering, Timişoara, March 2018.

[2] Brunner, G.W.. *HEC-RAS – River Analysis System, Hydraulic Reference Manual – version 4.1*. US Army Corps of Engineers, January 2010.

[3] Brunner, G.W.. *HEC-RAS 4.1 – River Analysis System, User's Manual – version 4.1*. US Army Corps of Engineers, January 2010.

[4] Brunner, G.W., S.S. Piper, M.R. Jensen, B. Chacon."Combined 1D and 2D Modelling with HEC–RAS." Paper presented at the World Environmental and Water Resources Congress, Austin, Texas, May 17-21, 2015.

[5] Brunner, G.W.. *HEC-RAS 4.1 – River Analysis System, Application Guide – version 4.1*. US Army Corps of Engineers, January 2010.

Determination of a Set of Admissible Parameters in Designing of LPG Storage Tanks Considering a Required Safety Factor

Assoc. Prof. PhD. Eng. **Mihai ŢĂLU**

University of Craiova, Faculty of Mechanics, Department of Applied Mechanics and Civil Engineering, Calea București Street, no. 107, 200512 Craiova, Dolj county, Romania. E-mail: mihai_talu@yahoo.com

Abstract: *In this study a method to determine a set of admissible parameters in designing of a three-dimensional (3D) hexagonal toroid with regular hexagonal cross-section used in manufacturing of LPG storage tanks from the automotive industry was proposed. A design methodology was applied to determine the safety factor (SF) values according to manufacturing objectives. The numerical simulations of a 3D model with parametric features (created in AutoCAD Autodesk 2017 software, and then analyzed with SolidWorks 2017 software) was applied in correlation with computation of confidence intervals of the safety factor. The proposed flexible numerical simulation framework offer an efficient workflows for integration of data and software packages for coupled process simulations to demonstrate its capabilities. Numerical results were stored in structured data formats to allow for an integrated 3D visualization and result interpretation. Results have shown that the proposed method is useful in CAD design of LPG storage tanks from the automotive industry.*

Keywords: *3D hexagonal toroidal LPG fuel tank, automotive industry, industrial engineering design, optimization methods, safety factor*

1. Introduction

The automobile market in the world of 2018 offers more buying options than in previous years, meaning different styles, sizes, quality and luxury levels or performance. Automotive market is set to grow due to expansion of vehicle production, changing lifestyle, increases in living standard, rising disposable income, rapid urbanization, and favorable government initiatives.

Automotive fuel tanks are used in passenger cars, light commercial vehicles and heavy commercial vehicles. Continuous investments in fuel tank market for the development of efficient, cost effective, with a high shelf life product by various manufacturers are expected to create immense market potential over the upcoming years. In addition, increasing sale of electric vehicles along with rising investments in hybrid vehicles is expected to open new growth avenues.

The current automotive fuel tank market is segmented, based on the capacity of fuel tank, into less than 45 L, 45 L – 75 L, and greater than 75 L. In addition, there is a high demand for automotive fuel tank of 45 L – 75 L due to rise in demand for multi-utility vehicles and sports-utility vehicles. On the other hand, the passenger car segment is expected to dominate the market as compared to the commercial vehicle.

The fuel tanks have complex shapes [1-6], high mechanical and chemical resistance [7-11], in various models manufactured from materials (such as plastic, steel, and aluminum materials) [12-16], with different prices and advanced safety features [17-25]. Due to lightweight capability, aluminum is the most widely used and reduces the overall weight of the vehicle.

A variety of design recommendations are used in the structural design of a storage fuel tank [26-34] according to its intended use, size, structure type, materials, service life, in order to assure life safety and to maintain its essential functions [35-37].

There are various Computer-Aided Engineering softwares for specialized design of storage fuel tanks, which performs calculations in accordance with national and international standards [38-47].

In the technical literature, Factor of Safety (FoS), also known as Safety Factor (SF), can be computed based on different methodologies with advanced numerical procedures, according the national and international standards. In addition, confidence intervals of the SF in calculated due to uncertainty and exploitation conditions, data errors, and model structural inadequacies [48].

Our research aims to determine a set of admissible parameters in designing of a 3D hexagonal toroid with regular hexagonal cross-section used in manufacturing of LPG storage tanks from the automotive industry. The obtained results can be applied at the design or control stage of the LPG storage tank.

2. Design methodology

In our previous studies [14-16], an optimal design of a 3D hexagonal toroid with regular hexagonal cross-section was performed.

2.1 Basic geometry of the parametric 3D model

Let's consider the parametric 3D model generated by revolving of a closed generating curve C_G (a hexagon with rounded corners) along a closed guiding curve C_D (a hexagon with rounded corners) as shown in figure 1 [14].

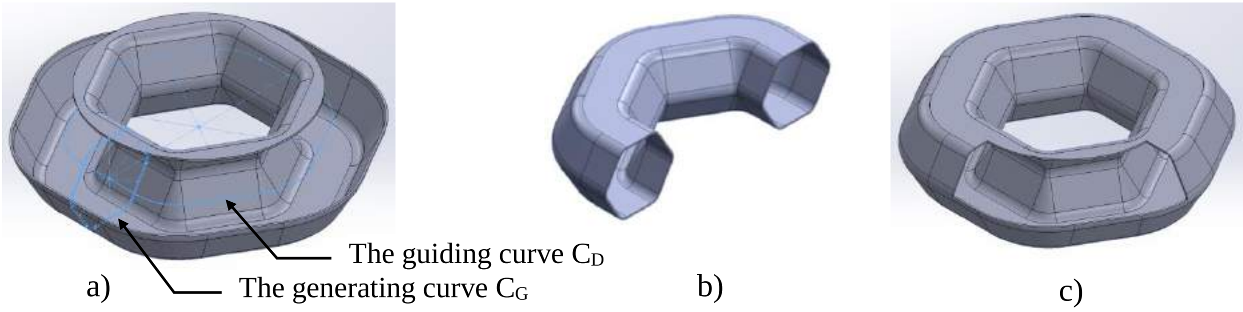

Fig. 1. The axonometric representation of the parametric 3D solid model

The following parameters were applied as input parameters to the 3D parametric model (figure 1): a) a closed generating curve C_G (a hexagon with a side value L = 175 mm, with rounded corners, radius R = 50 mm), and b) the guiding curve C_D (a hexagon with a side value L = 430 mm, with rounded corners, radius R = 180 mm).

2.2 Computational model

Based on the physical model, the parametric model was created in AutoCAD Autodesk 2017 software [45] and numerical analysis was performed with SolidWorks 2017 software [46] with the Static, Thermal and Design Study modules. The design data used were:

- the tank material is AISI 4340 steel;
- the maximum hydraulic test pressure: p_{max} = 30 bar;
- the working temperature between the limits: T = -30 ^{0}C up to T = 60 ^{0}C;
- supporting surfaces located on the inferior side;
- the duration of the tank exploitation: n_a = 16 years;
- the corrosion rate of the material: v_c = 0.07 mm/years.

In our previous study [15], the graph of 3D surfaces (by type surf) corresponding to the variation of minimum SF for SF_{min} (n_a, T), are graphically shown in fig. 2 [15].

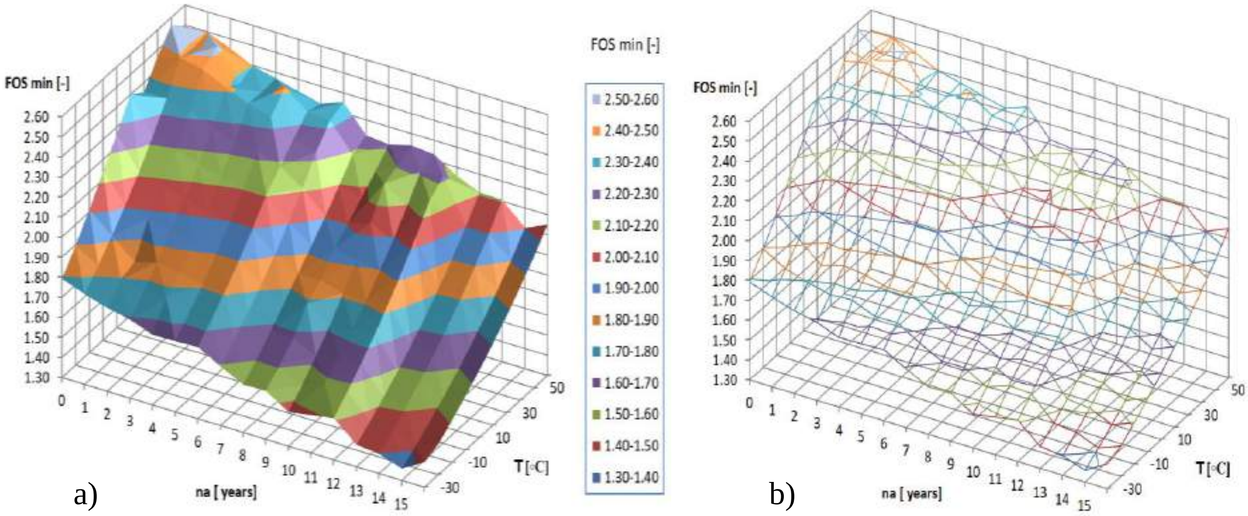

Fig. 2. The 3D graphs SF_{min} (n_a, T): a) surf type; b) fire type

Let's consider that the required safety factor is: $SF_{imp} = 1.6$
If the 3D surface of SF_{min} (n_a, T) (from fig. 2, shown as surf type) is intersected by a horizontal plane (with a height of SF_{imp}), it is obtained a 3D graph with $SF > SF_{imp}$, as shown in fig. 3.

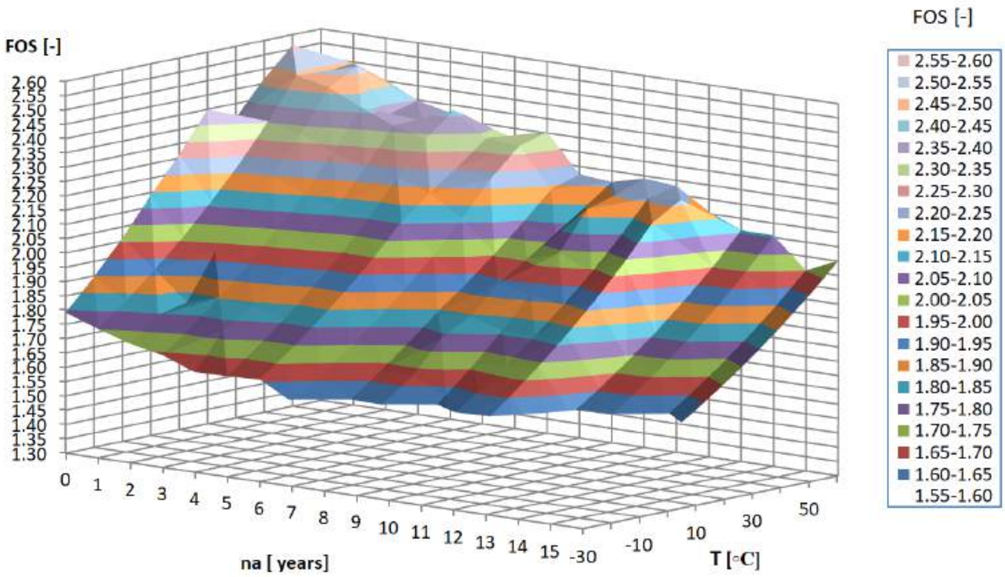

Fig. 3. The 3D graph SF_{min} (n_a, T) shown as surf type, for $SF > SF_{imp}$

A direct determination of 2D graph of SF_{min} (n_a, T), for $SF \geq SF_{imp}$ and $SF < SF_{imp}$ is shown in fig. 4.

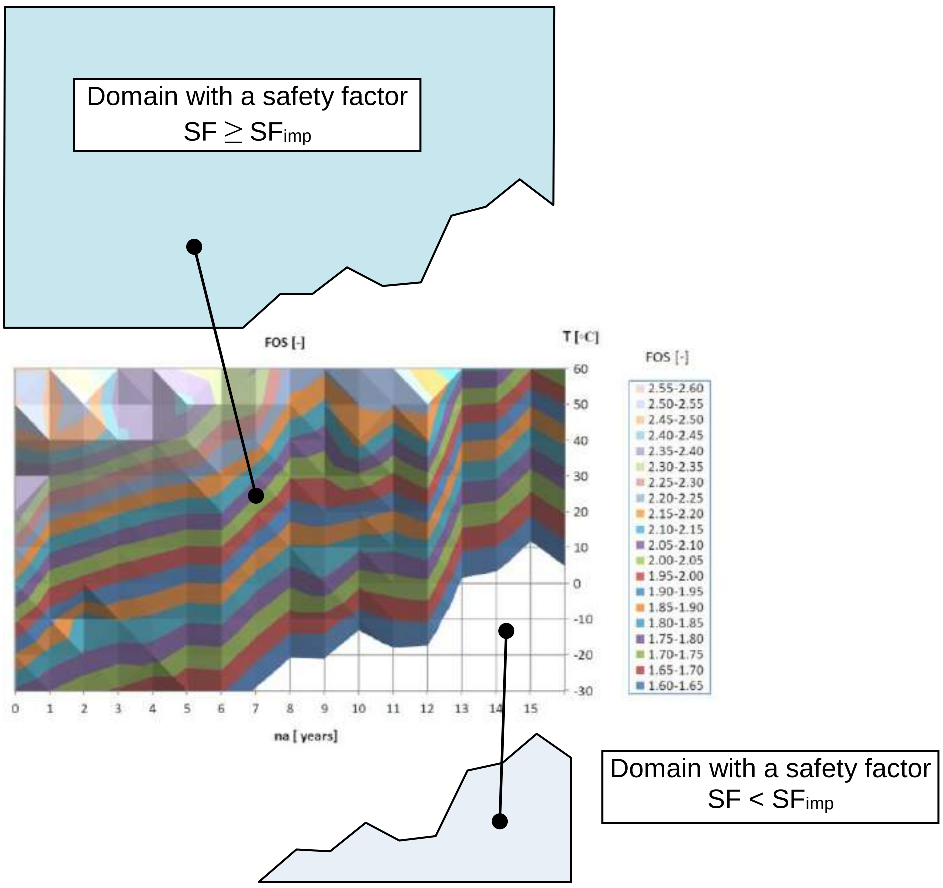

Fig. 4. The 2D graph of SF_{min} (n_a, T), for $SF > SF_{imp}$ and $SF < SF_{imp}$

The corresponding 2D graphs of the isothermal coefficient variation curves, SF_{min} (n_{ao}, T_o) with improper work parameters domain, are graphically shown in fig. 5.

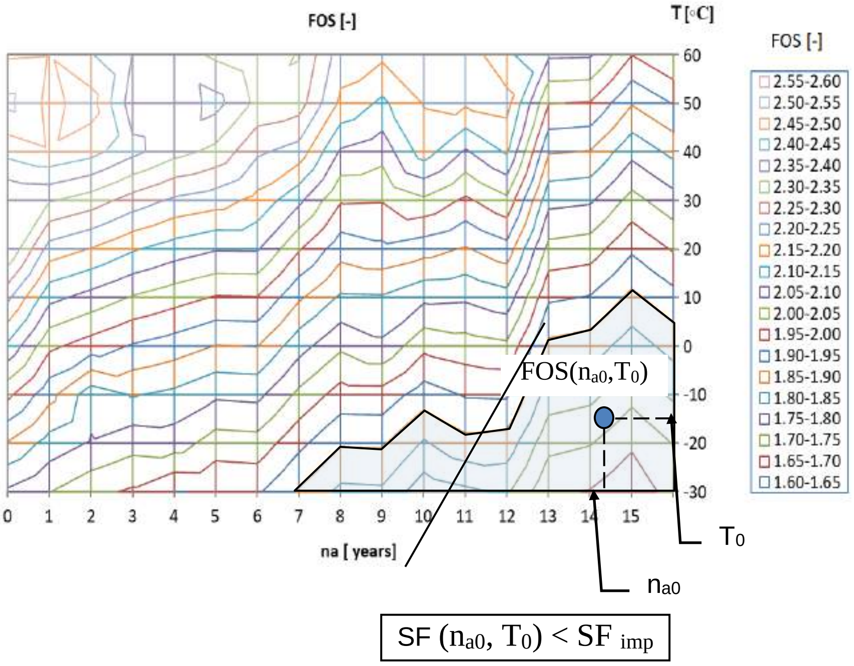

Fig. 5. The 2D graphs of the isothermal coefficient variation curves, SF_{min} (n_a, T), with domain SF (n_{a0}, T_0) < SF $_{imp}$

Finally, the contour of the planar domain can be described by curves obtained by polynomial interpolation, corresponding to each contour, which allow the analytical calculation relations of the domain, which lead to the rapid determination if a function point characterized by working parameters n_{a0} and T_0, belongs to proper working domain.

3. Discussion

Following the SF analysis and the resulting graphs for the parametric 3D model structure through the method of finite elements it has been found that:
- this method uses specialized computing software based on Finite element methods (FEM);
- this method can be applied at the design stage or during the control stage;
- graphical representations (in 2D or 3D), associated with the analytical curves determined by polynomial interpolation, delimitates the validity domain for which SF $\geq$ SF_{imp}.

4. Conclusions

The proposed method identifies a set of admissible work parameters for which SF $\geq$ SF_{imp}, structured, on algorithmic details of how to efficiently implement it, and on pre- and postprocessing steps.

Conflict of Interest: The authors declare that they have no conflict of interest.

References

[1] Ghiţă, C. Mirela, Anton C. Micu, Mihai Ţălu and Ştefan Ţălu. "Shape optimization of a thoroidal methane gas tank for automotive industry." *Annals of Faculty of Engineering Hunedoara - International Journal of Engineering, Hunedoara, Romania*, Tome X, Fascicule 3 (2012): 295-297.
[2] Ghiţă, C. Mirela, Anton C. Micu, Mihai Ţălu and Ştefan Ţălu. "Shape optimization of vehicle's methane gas tank." *Annals of Faculty of Engineering Hunedoara - International Journal of Engineering, Hunedoara, Romania*, Tome X, Fascicule 3 (2012): 259-266.

[3] Ghiţă, C. Mirela, Anton C. Micu, Mihai Ţălu and Ştefan Ţălu. "3D modelling of a gas tank with reversed end up covers for automotive industry.", *Annals of Faculty of Engineering Hunedoara - International Journal of Engineering, Hunedoara*, *Romania*, Tome XI, Fascicule 3 (2013): 195-200.
[4] Ghiţă, C. Mirela, Anton C. Micu, Mihai Ţălu, Ştefan Ţălu and Ema I. Adam. "Computer-Aided Design of a classical cylinder gas tank for the automotive industry." *Annals of Faculty of Engineering Hunedoara - International Journal of Engineering, Hunedoara*, *Romania*, Tome XI, Fascicule 4 (2013): 59-64.
[5] Ghiţă, C. Mirela, Anton C. Micu, Mihai Ţălu and Ştefan Ţălu. "3D modelling of a shrink fitted concave ended cylindrical tank for automotive industry." *Acta Technica Corviniensis – Bulletin of Engineering, Hunedoara, Romania*, Tome VI, Fascicule 4 (2013): 87-92.
[6] Ghiţă, C. Mirela, Ştefan C. Ghiță, Ştefan Ţălu and Simona Rotaru, "Optimal design of cylindrical rings used for the shrinkage of vehicle tanks for compressed natural gas." *Annals of Faculty of Engineering Hunedoara - International Journal of Engineering, Hunedoara*, Tome XII, Fascicule 3 (2014): 243-250.
[7] Bică, Marin, Mihai Ţălu and Ştefan Ţălu. "Optimal shapes of the cylindrical pressurized fuel tanks." *Magazine of Hydraulics, Pneumatics, Tribology, Ecology, Sensorics, Mechatronics (HIDRAULICA)*, no. 4 (December 2017): 6-17.
[8] Ţălu, Ştefan and Mihai Ţălu. "The influence of deviation from circularity on the stress of a pressurized fuel cylindrical tank." *Magazine of Hydraulics, Pneumatics, Tribology, Ecology, Sensorics, Mechatronics (HIDRAULICA)*, no. 4 (December 2017): 34-45.
[9] Vintilă, Daniela, Mihai Ţălu and Ştefan Ţălu. "The CAD analyses of a torospheric head cover of a pressurized cylindrical fuel tank after the crash test." *Magazine of Hydraulics, Pneumatics, Tribology, Ecology, Sensorics, Mechatronics (HIDRAULICA)*, no. 4 (December 2017): 57-66.
[10] Ţălu, Mihai. "The influence of the corrosion and temperature on the Von Mises stress in the lateral cover of a pressurized fuel tank." *Magazine of Hydraulics, Pneumatics, Tribology, Ecology, Sensorics, Mechatronics (HIDRAULICA)*, no. 4 (December 2017): 89-97.
[11] Ţălu, Mihai and Ştefan Ţălu. "Analysis of temperature resistance of pressurized cylindrical fuel tanks." *Magazine of Hydraulics, Pneumatics, Tribology, Ecology, Sensorics, Mechatronics (HIDRAULICA)*, no. 1 (March 2018): 6-15.
[12] Ţălu, Mihai and Ştefan Ţălu. "Design and optimization of pressurized toroidal LPG fuel tanks with variable section." *Magazine of Hydraulics, Pneumatics, Tribology, Ecology, Sensorics, Mechatronics (HIDRAULICA)*, no. 1 (March 2018): 32-41.
[13] Ţălu, Ştefan and Mihai Ţălu. "Algorithm for optimal design of pressurized toroidal LPG fuel tanks with constant section described by imposed algebraic plane curves." *Magazine of Hydraulics, Pneumatics, Tribology, Ecology, Sensorics, Mechatronics (HIDRAULICA)*, no. 2 (June 2018): 14-21.
[14] Ţălu, Mihai and Ştefan Ţălu. "The optimal CAD design of a 3D hexagonal toroid with regular hexagonal cross-section used in manufacturing of LPG storage tanks." *Magazine of Hydraulics, Pneumatics, Tribology, Ecology, Sensorics, Mechatronics (HIDRAULICA)*, no. 2 (June 2018): 49-56.
[15] Ţălu, Mihai and Ştefan Ţălu. "The influence of corrosion and temperature variation on the minimum safety factor of a 3D Hexagonal toroid with regular hexagonal cross-section used in manufacturing of LPG storage tanks." *Magazine of Hydraulics, Pneumatics, Tribology, Ecology, Sensorics, Mechatronics (HIDRAULICA)*, no. 3 (September 2018): 16-25.
[16] Ţălu, Ştefan and Mihai Ţălu. "The influence of corrosion and pressure variation on the minimum safety factor of a 3D Hexagonal toroid with regular hexagonal cross-section used in manufacturing of LPG storage tanks." *Magazine of Hydraulics, Pneumatics, Tribology, Ecology, Sensorics, Mechatronics (HIDRAULICA)*, no. 3 (September 2018): 39-45.
[17] Ţălu, Mihai and Ştefan Ţălu. "3D geometrical solutions for toroidal LPG fuel tanks used in automotive industry." *Advances in Intelligent Systems Research,* vol. 151 (2018): 189-193. DOI: 10.2991/cmsa-18.2018.44.
[18] Ţălu, Ştefan and Mihai Ţălu. "Constructive CAD variants of toroidal LPG fuel tanks used in automotive Industry." *Advances in Intelligent Systems Research,* vol. 159 (2018): 27-30. DOI: 10.2991/mmsa-18.2018.7.
[19] Ţălu, Ştefan and Mihai Ţălu. "The Influence of corrosion on the vibration modes of a pressurized fuel tank used in automotive industry." *DEStech Transactions on Materials Science and Engineering,* (2018): 1-6. DOI: 10.12783/dtmse/icmsa2018/20560.
[20] Ţălu, Mihai and Ştefan Ţălu. "Optimal engineering design of a pressurized paralepipedic fuel tank." *Annals of Faculty of Engineering Hunedoara - International Journal of Engineering, Hunedoara, Romania*, Tome XVI, Fascicule 2 (2018): 193-200.
[21] Ţălu, Mihai, Ştefan Ţălu, Germán Valencia García and Imre Kiss, "The CAD parametric modeling of particular shapes of fuel storage tanks." *Annals of Faculty of Engineering Hunedoara - International Journal of Engineering, Hunedoara, Romania*, Tome XVI, Fascicule 3 (2018): 107-111.

[22] Ţălu, Mihai and Ştefan Ţălu. "Numerical analysis of cylindrical fuel tanks thermal behaviour." *Annals of Faculty of Engineering Hunedoara - International Journal of Engineering, Hunedoara, Romania*, Tome XVI, Fascicule 3 (2018): 153-160.

[23] Domanski, Jerzy and Grzegorz Zywica, "Optimization of the construction of a pressure tank using CAD/CAE systems." *Technical Sciences*, no. 10 (2007): 41-59. DOI: 10.2478/v10022-007-0006-4.

[24] Düren, Tina, Lev Sarkisov, Omar M. Yaghi and Randall Q. Snurr, "Design of new materials for methane storage." *Langmuir*, vol. 20, no. 7 (2004): 2683–2689. DOI: 10.1021/la0355500.

[25] Jörg B. Multhoff. "Integrated Structural Analysis of Composite Pressure Vessels: A Design Tool." ASME 2016 Pressure Vessels and Piping Conference, vol. 6A: Materials and Fabrication, Vancouver, British Columbia, Canada, July 17–21, 2016. Paper no. PVP2016-63603, pp. V06AT06A045; 10 pages. DOI:10.1115/PVP2016-63603.

[26] Ţălu, Ştefan. *Geometrie descriptivă. (Descriptive geometry)*, Cluj-Napoca, Risoprint Publishing house, 2010.

[27] Valencia, Garcia. *Geometría descriptiva, paso a paso*. Primera edición, Bogotá, Colombia, D.C, editorial Ecoe Ediciones, 2009.

[28] Florescu-Gligore, Adrian, Magdalena Orban and Ştefan Ţălu. *Cotarea în proiectarea constructivă şi tehnologică. (Dimensioning in technological and constructive engineering graphics).* Cluj-Napoca, Lithography of The Technical University of Cluj-Napoca, 1998.

[29] Florescu-Gligore, Adrian, Ştefan Ţălu and Dan Noveanu. *Reprezentarea şi vizualizarea formelor geometrice în desenul industrial. (Representation and visualization of geometric shapes in industrial drawing).* Cluj-Napoca, U. T. Pres Publishing house, 2006.

[30] Racocea, Cristina and Ştefan Ţălu. *Reprezentarea formelor geometrice tehnice în axonometrie. (The axonometric representation of technical geometric shapes).* Cluj-Napoca, Napoca Star Publishing house, 2011.

[31] Ţălu, Ştefan and Cristina Racocea. *Reprezentări axonometrice cu aplicaţii în tehnică. (Axonometric representations with applications in technique).* Cluj-Napoca, MEGA Publishing house, 2007.

[32] Ţălu, Ştefan and Mihai Ţălu. "CAD generating of 3D supershapes in different coordinate systems." *Annals of Faculty of Engineering Hunedoara - International Journal of Engineering, Hunedoara, Romania*, Tome VIII, Fascicule 3 (2010): 215-219.

[33] Ţălu, Ştefan and Mihai Ţălu. "A CAD study on generating of 2D supershapes in different coordinate systems." *Annals of Faculty of Engineering Hunedoara - International Journal of Engineering, Hunedoara, Romania*, Tome VIII, Fascicule 3 (2010): 201-203.

[34] Niţulescu, Theodor and Ştefan Ţălu. *Aplicaţii ale geometriei descriptive şi graficii asistate de calculator în desenul industrial. (Applications of descriptive geometry and computer aided design in engineering graphics).* Cluj-Napoca, Risoprint Publishing house, 2001.

[35] Țălu, Mihai. *Calculul pierderilor de presiune distribuite în conducte hidraulice. (Calculation of distributed pressure loss in hydraulic pipelines).* Craiova, Universitaria Publishing house, 2016.

[36] Ţălu, Mihai. *Mecanica fluidelor. Curgeri laminare monodimensionale. (Fluid mechanics. The monodimensional laminar flow).* Craiova, Universitaria Publishing house, 2016.

[37] Țălu, Mihai. *Pierderi de presiune hidraulică în conducte tehnice cu secțiune inelară. Calcul numeric și analiză C.F.D. (Hydraulic pressure loss in technical piping with annular section. Numerical calculation and C.F.D.)*, Craiova, Universitaria Publishing house, 2016.

[38] Ţălu, Ştefan. *Limbajul de programare AutoLISP. Teorie şi aplicaţii. (AutoLISP programming language. Theory and applications)*. Cluj-Napoca, Risoprint Publishing house, 2001.

[39] Ţălu, Ştefan. *Grafică tehnică asistată de calculator. (Computer assisted technical graphics)*. Cluj-Napoca, Victor Melenti Publishing house, 2001.

[40] Ţălu, Ştefan. *Reprezentări grafice asistate de calculator. (Computer assisted graphical representations).* Cluj-Napoca, Osama Publishing house, 2001.

[41] Ţălu, Ştefan. *AutoCAD 2005*. Cluj-Napoca, Risoprint Publishing house, 2005.

[42] Ţălu, Ştefan and Mihai Ţălu. *AutoCAD 2006. Proiectare tridimensională. (AutoCAD 2006. Three-dimensional designing)*. Cluj-Napoca, MEGA Publishing house, 2007.

[43] Ţălu, Ştefan. *AutoCAD 2017*. Cluj-Napoca, Napoca Star Publishing house, 2017.

[44] Nedelcu, Dorian. *Proiectare și simulare numerică cu SolidWorks*. *(Digital Prototyping and Numerical Simulation with SolidWorks)*. Timişoara, Eurostampa Publishing house, 2011.

[45] *** Autodesk AutoCAD 2017 software.

[46] *** SolidWorks 2017 software.

[47] Ţălu, Ştefan. *Micro and nanoscale characterization of three dimensional surfaces. Basics and applications*. Napoca Star Publishing House, Cluj-Napoca, Romania, 2015.

[48] Bîrleanu, Corina and Ştefan Ţălu. *Organe de maşini. Proiectare şi reprezentare grafică asistată de calculator. (Machine elements. Designing and computer assisted graphical representations).* Cluj-Napoca, Victor Melenti Publishing house, 2001.

Fluid Flow Particularities within Hydraulic Working Circuit

Assistant professor PhD Eng. **Fănel ȘCHEAUA**[1]

[1] Dunarea de Jos University of Galati, Domneasca Street 47, e-mail: fanel.scheaua@ugal.ro

Abstract: *As is known from the principles of fluid mechanics, the flow phenomenon of the working fluid within a hydraulic circuit is always accompanied by energy losses that are inevitably determined by the frictional forces with the pipe walls, the geometric shape of the pipeline used in the circuit but also the inner walls roughness of the circuit pipeline which interacts with the fluid. The fluid environment is used within the hydro-static systems in order to transmit the energy representing the support which, by simply circulating in the circuit to the execution organs, causes different device movements (rotation or translation) as a result of directly action. Forced flow of the working fluid inside the circuit is a complex phenomenon of continuous or non-permanent flow which involves the general laws and equations of the customized fluid mechanics for specific working situations of the hydro-static drive systems.*

Keywords: *Fluid, flow, laminar, turbulence, simulation, three-dimensional modelling*

1. Introduction

It is known that hydraulic and pneumatic drives have seen an unprecedented development in recent years due to increased use in the working systems of machines and equipment used in most industrial branches. At present time there is no industry branch that does not benefit from the supply of hydraulics and/or pneumatics in order to perform various tasks that simplify user activities.
Thus, industrial applications are known related to systems in stationary equipment involving fixed machines such as hydraulic presses, molding hammers, or various cutting equipment, as well as equipment present in mobile machinery represented by excavators, loaders, self-drilling, bulldozers and mowers.

2. Model of laminar flow for the working fluid

The hydro-static driving system is designed as a system that can operate permanently, the flow of the working fluid takes place within a working circuit that consists of active components (pump, motor) but also other components that allow the adjustment of the pressure values or flow rate in the circuit.
The flow pattern of the working fluid within the circuit pipelines can be considered laminar if the fluid viscosity is at a high level, the flow diameter is small relative to the duct length in which the flow occurs, or the fluid velocity is below the admissible limit value. Since mineral oil is mainly used in hydro-static drive circuits, the admissible flow velocity is up to 12 m/s. The usual circulating oil velocity values inside the driving circuit lines are in the range of 5-8 m/s.
Due to the adhesion forces occurring at the contact surface between the working fluid and the pipe walls, the change phenomenon of the circulation velocity values occurs as the fluid moves inside the pipe (Figure 1).

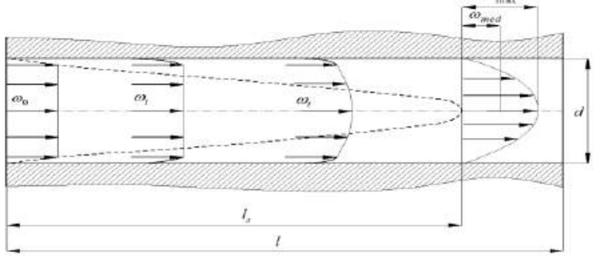

Fig. 1. Laminar flow model inside a circular pipeline

The continuous change in the flow velocity through the pipe is possible up to the pipeline axis when a parabolic distribution of flow velocity values is encountered (Hagen-Poiseuille) and the pipe length at which these velocity values changes occur is considered a stabilization length that can be calculated using the relationship: [1], [3]

$$l_S = 0.0575 \cdot d \cdot \mathrm{Re} \tag{1}$$

where d- pipe diameter;
Re – Reynolds number (adimensional);

$$\mathrm{Re} = \frac{\omega_{med} \cdot d}{\upsilon} \tag{2}$$

ω_{med} - average velocity value;
υ – fluid kinematic viscosity.
The average flow velocity of the working fluid within a hydro-static system can be assumed according the following relation:

$$\omega_{med} = \frac{Q_p}{A_n} \tag{3}$$

where:
Q_p – the pump volumetric flow rate;
A_n –cross-sectional area of the pipe.
Load losses during the flow of the working fluid through the hydrostatic actuator system pipeline are described as pressure drops generated by fluid inertia forces and viscosity forces. Darcy's relationship describes the pressure drop across a pipeline between two points: [1], [3]

$$\Delta_p = p_1 - p_2 = \lambda \cdot \frac{\rho}{2} \cdot \frac{l}{d} \cdot \omega_{med}^2 \tag{4}$$

Δ_p – the pressure drop on the pipe;
ρ - fluid density;
l,d – length and nominal pipe diameter;
ω_{med} – average flow velocity;
λ - linear loss coefficient.
During the operation of the hydrostatic system, the load losses (pressure drops) must be defeated by the actuator pump. The specific load loss linear coefficient parameter describes the losses magnitude in the isothermal or non-isothermal laminar flow regime specific to the hydrostatic drive circuit. The laminar flow regime for a fluid is evaluated by the Reynolds limit number having a value of Rel = 2320 value, and for mineral oils used predominantly Rel relays about 2000.

3. Turbulent flow pattern of the working fluid

For the turbulent flow model of the working fluid the laminar boundary layer at the pipe inlet becomes immediately turbulent increasing towards the pipe center of over a stabilizing length of about 25-40 pipe diameters. (Figure 2).

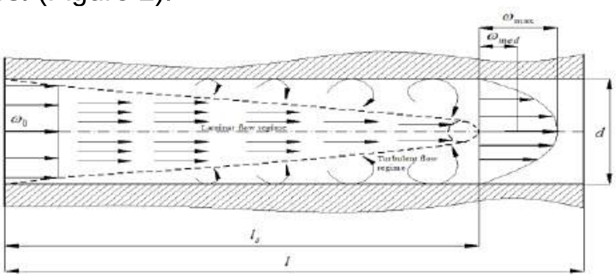

Fig. 2. Turbulent flow model inside a circular pipeline

For the turbulent flow model the Reynolds number is characterized by Re> 2320 or Re> 2000 for mineral oils. For the turbulent flow model, the load losses (pressure drops) on the grid are evaluated by the Darcy equivalent relationship, being heavily influenced by the roughness of the pipe walls, the working agent temperature and the hydraulic circuit path geometry.

The loss factor can be computed with Blasius, or Prandtl-Karman: [1], [2]

– Blasius for $4 \cdot 10^3 < \mathrm{Re} < 10^5$

$$\lambda = \frac{0.3164}{\sqrt[4]{\mathrm{Re}}} \tag{5}$$

– Prandtl-Karman for $3 \cdot 10^3 < \mathrm{Re} < 10^7$

$$\frac{1}{\lambda} = \frac{2}{\rho} \cdot \mathrm{Re} \cdot \sqrt{\lambda} - 0.8 \tag{6}$$

4. Fluid flow simulation on the virtual model

The fluid flow simulation on the circular pipeline model is accomplished on virtual three-dimensional model. The velocity circulation is declared in the range of 5 and 7 m/s corresponding to the specific velocity of the working fluid within a hydrostatic actuation system.

The reference pressure is 300 bar, the working fluid density is 900-905 kg/m3 (mineral oil), and the viscosity specific to mineral oils is in the range of 17-63 cSt, (table 1).

Table 1: Mineral oil properties

Mineral oil	H18A	H32A	H46A	H60A
Kinematic viscosity (cSt)	17-21	27-33	44-49	58-63
Density (g/cm3)	0.900	0.900	0.905	0.905

The pipeline diameter values are presented in table 2.

Table 2: Inner diameter values for pipeline

Duct inner diameter					
6.5	8	10	13	16	19

The pipeline virtual model analysis was designed to view the speed, pressure and flow pattern of the working fluid.

The model is a circular duct with two inlets and an outlet, the inside diameter is 19 mm and the total length is 300 mm, the working fluid is a mineral oil (H32A, H60A) having a density of 0.900 and 0.905 g/cm3, the kinematic viscosity of 33 and 63 cSt.

Four distinct cases were analysed in which specific rates of inlet velocity as well as kinematic viscosity values of the working fluid were reported (Table 3).

Table 3: Initial data for the four cases

Case number	**Fluid density (kg/m3)**	**Kinematic viscosity (cSt)**	**Inlet velocity 1 (m/s)**	**Inlet velocity 2 (m/s)**
1	900	33	3	5
2	900	33	5	7
3	905	63	3	5
4	905	63	5	7

The model used for the analysis is shown in Figure 3, along with the meshing network and solid and fluid domains in the model assembly.

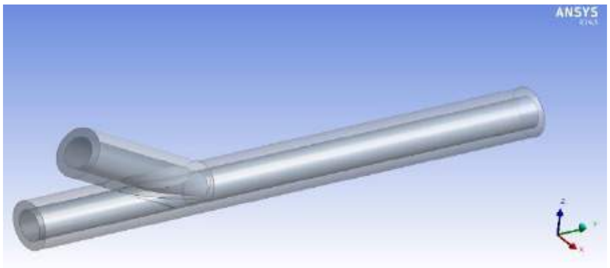

a) Pipe model

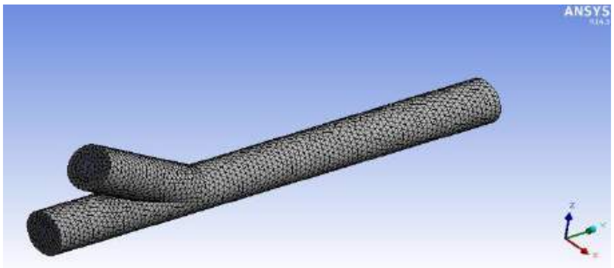

b) Mesh network

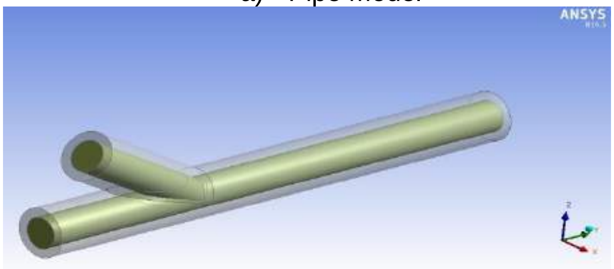

c) Fluid domain

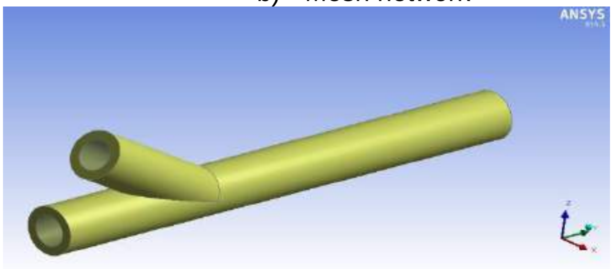

d) Solid domain

Fig. 3. Three-dimensional model for the pipeline

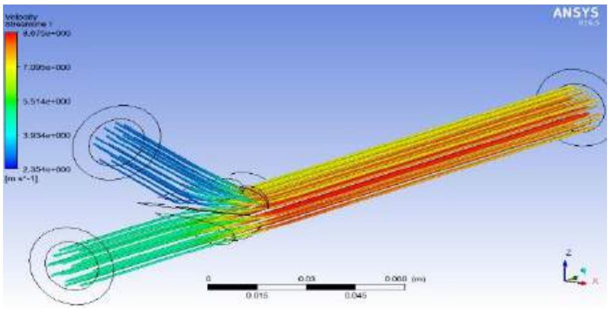

a) Fluid velocity

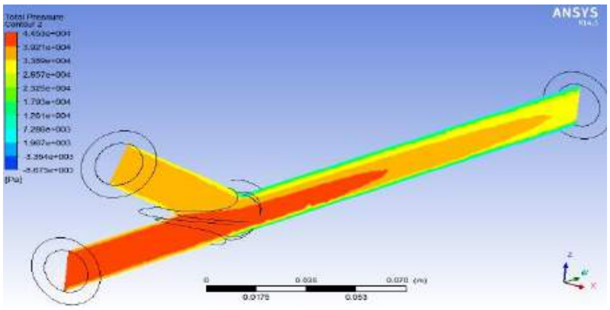

b) Total pressure

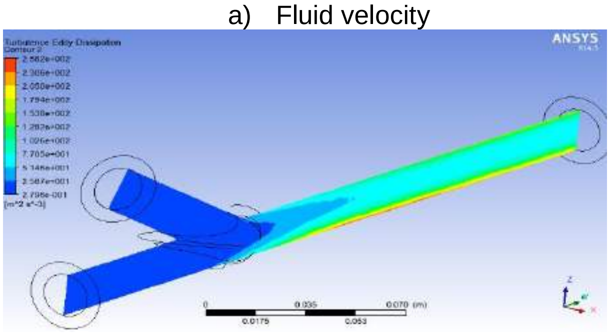

c) Turbulence eddy dissipation

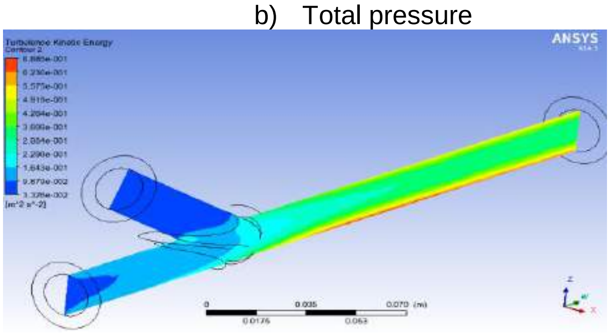

d) Turbulence kinetic energy

Fig. 4. The obtained results for case 1

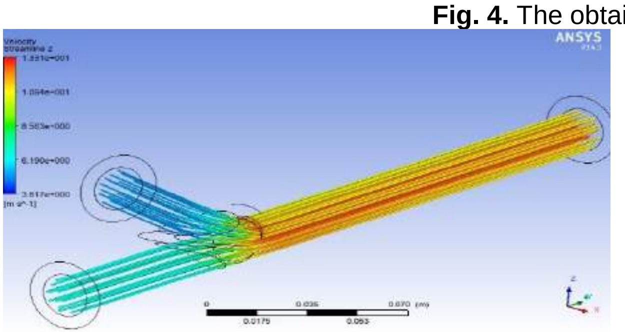

a) Fluid velocity

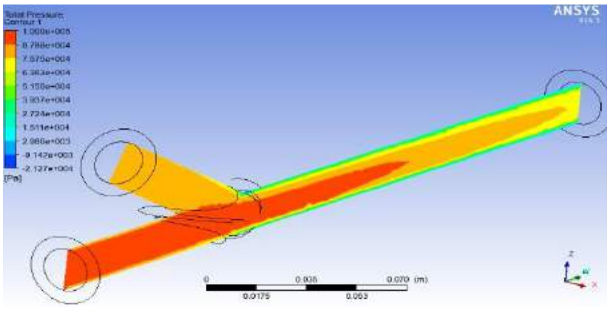

b) Total pressure

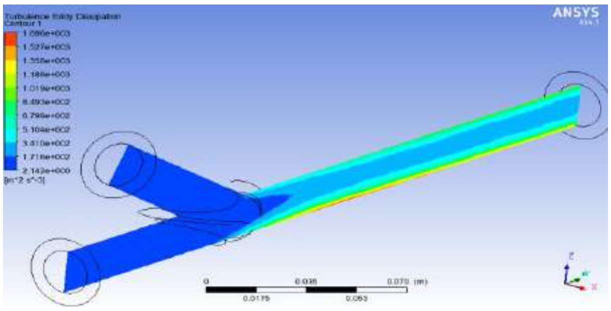

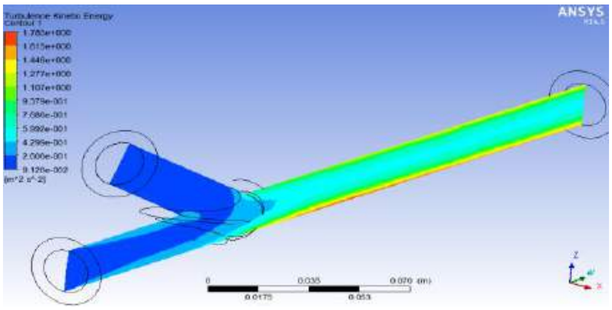

c) Turbulence eddy dissipation d) Turbulence kinetic energy

Fig. 5. The obtained results for case 2

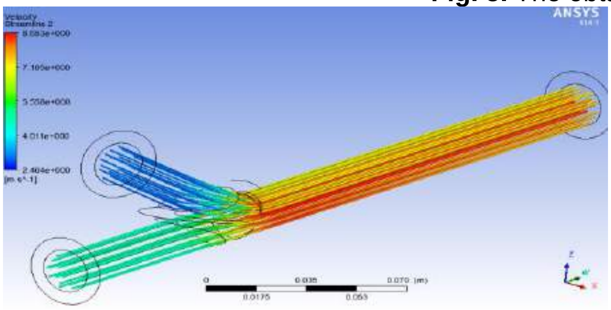

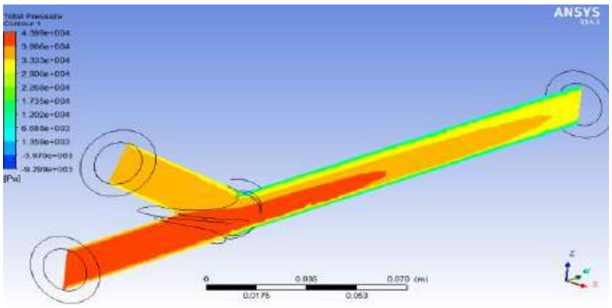

a) Fluid velocity b) Total pressure

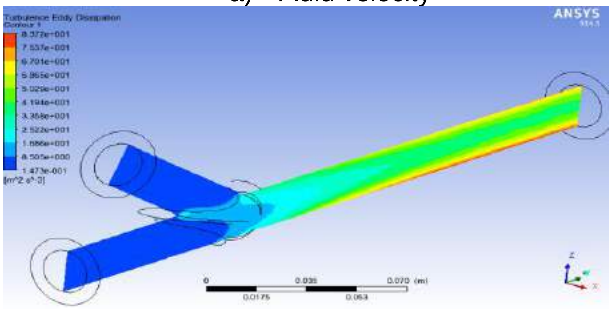

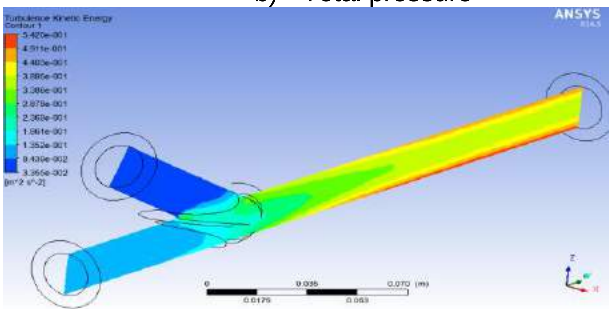

c) Turbulence eddy dissipation d) Turbulence kinetic energy

Fig. 6. The obtained results for case 3

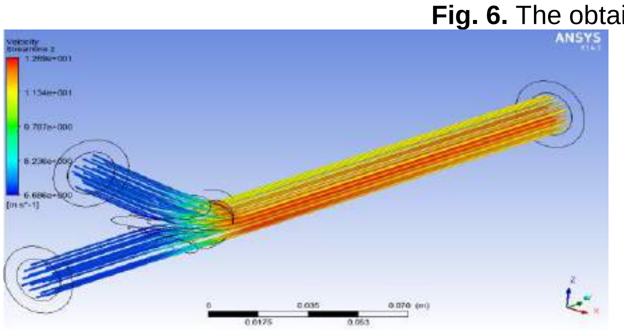

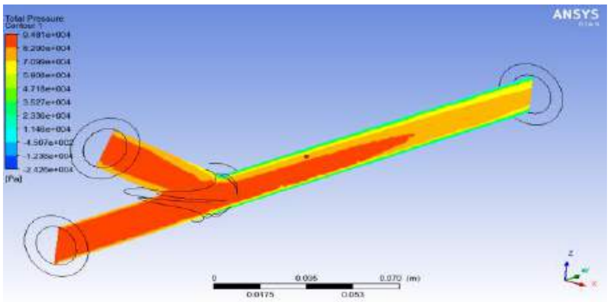

a) Fluid velocity b) Total pressure

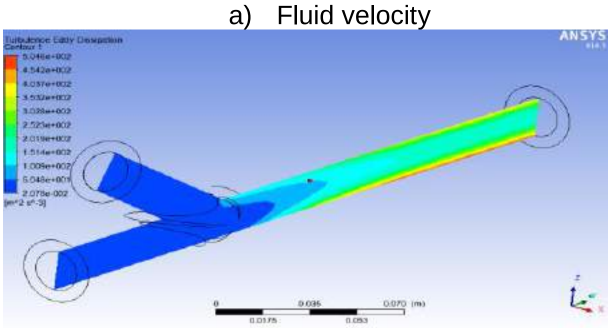

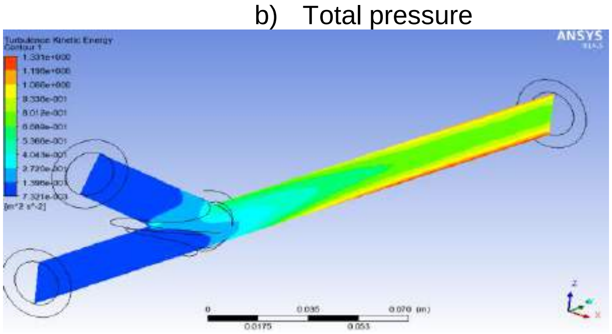

c) Turbulence eddy dissipation d) Turbulence kinetic energy

Fig. 7. The obtained results for case 4

Table 4: The obtained result values

	Case 1	Case 2	Case 3	Case 4
Fluid velocity (m/s)	8.67	13.31	8.65	12.89
Total pressure (Pa)	44530	100000	43990	94810
Turbulence eddy dissipation (m2/s3)	256.2	1696	83.72	504.6
Turbulence kinetic energy (m2/s2)	0.68	1.78	0.54	1.33

The obtained results show the flow pattern of the working fluid inside the pipe, according to the declared inlet values. A laminar flow model can be observed in the area of the two entrances but becomes turbulent after the fluid flowing from the two intakes makes the mixture.
The values obtained are specific to each case, depending on the declared initial calculation data.

5. Conclusions

Flow aspects of the working fluid through the circular pipes have been presented in this paper, highlighting the laminar and turbulent regime as well as the conditions in which they occur during the operation of a hydrostatic drive system.
For example, a numerical analysis was carried out on the virtual model of a pipeline that is crossed by a hydraulic fluid with the properties of a mineral oil.
The results show the values of flow velocity, total pressure and turbulence recorded at the analysed fluid region for each analysed case.

References

[1] Axinti, S., and F. D. Scheaua. *Introduction to industrial hydraulics/ Introducere în hidraulica industrială.* ISBN 978-606-696-032-8, Galati, Editura Galati University Press, 2015.
[2] Axinti, G., and A. S. Axinti. *Fluid Power Systems/ Acţionări hidraulice şi pneumatice.* Vol I-V. Chişinău, Editura Tehnica-Info, 2008-2012.
[3] Vasilescu, Al. A.. *Fluid Mechanics/ Mecanica fluidelor*. Ministerul Educaţiei şi Învăţământului, Universitatea din Galaţi, Galaţi, 1979.

ISSN 1453 – 7303 **"HIDRAULICA" (No. 3/2018)**
Magazine *of Hydraulics, Pneumatics, Tribology, Ecology, Sensorics, Mechatronics*

Automatic Electro-Hydraulic System for a P.E.T. Waste Baling Press

Lect.PhD.Eng. **Iulian-Claudiu DUȚU**[1], Prof.PhD.Eng. **Edmond MAICAN**[1],
Prof.PhD.Eng. **Sorin-Ștefan BIRIȘ**[1], Lect.PhD.Eng. **Mihaela-Florentina DUȚU**[1]

[1] University Politehnica of Bucharest, iulian_claudiu.dutu@upb.ro

Abstract: *Environmental protection is one of the leading factors when designing modern industrial machinery, their increased overall energy efficiency requiring the use of new industrial design concepts, smart driving circuits and digital concepts* [1]*. Classic industrial machinery is supposed to be changing in the next few years due to the development of INDUSTRY 4.0 concept for manufacturing technologies* [1]*. Improving energy efficiency, in most of the cases implies designing new driving schematics and their complexity seems to be significantly increasing. Rapid development of electronics technology and software industry supported the need for energy efficiency, but fluidic – hydraulic and pneumatic – installations are performing not so well on this field. There are known various constructive solutions for directional valves that traditional fluidic manufacturers promote, in order to improve overall energy efficiency* [2]*, but those solutions are centered on specific industrial application of group of applications. In a narrower case, a hydraulic P.E.T. waste baling press must be optimized taking into consideration productivity, ease-of-use, flexibility, energy efficiency and reduced maintenance costs* [3]*. Digital hydraulics might be a solution that can meet all the above criteria, but in the case of a small capacity P.E.T. waste press, retrofitting costs depreciation is poor. In this paper the authors propose a simple and energy efficient electro-hydraulic driving system for a small capacity P.E.T. waste baling press that was modeled using FluidSIM Hydraulic software environment.*

Keywords: *P.E.T. waste press, electro-hydraulic, FluidSIM*

1. Introduction

Modern industrial design must include modeling and simulation activities for engineering concepts or existing machines, using a *virtual tool* such as FluidSIM software environment. There are available on the market various modeling and simulation software environments, offering specialized packages of programs that are oriented on a single field of engineering (hydraulics, electrics, mechanics etc.) or on cross-field engineering (electro-hydraulics, mechatronics etc.). When modeling a physical object or a system, there must be taken into account, from the beginning, some hypothesis that induce, negligible or not, errors in the model itself. A simple physical object, in most cases, can be modeled similar to reality, but a much more complex object or a system – which comprises simple and/or complex objects – cannot be modeled having no discrepancies between reality and virtual environment. These discrepancies can lead to serious errors when simulating the model. Another aspect of modeling is not the object of modeling itself, but the model of the environment where the actions of the object are taking place. Here, also, a model of the reality having no errors is, yet, impossible to obtain. Errors in modeling can arise when trying to produce a mathematical model for the constraints between components of a system or between system's components and the working environment. Nowadays, powerful modeling and simulation tools can reduce "reality to virtual" errors, using component libraries that can be customized according to the real object or system's characteristics.
Hydraulic systems are used in numerous industrial fields, where main advantages of hydraulic drives cannot be overcome using other driving solutions (electric, pneumatic, mechanic, etc.) [4], [5,] [6], even though their reliability is considered to be medium and having relatively high energy losses. The authors propose in this paper new hydraulic and electric automation schematics for a small capacity P.E.T. waste baling press, modeling both the hydraulic and electrical parts using FluidSIM Hydraulics software environment.
The hydraulic and electrical schematics that the authors propose can be used on a P.E.T. waste baling press, having electro-hydraulic directional valves and a relay based electrical schematic.

2. Hydraulics system

Schematic of the hydraulic system that the authors propose is given in figure 1. As it is figured, the hydraulic schematic has a simple construction and can be used as a base for other engineering applications such as lifting systems or elevators.
The hydraulic system comprises a 7 liters hydraulic oil tank, which is used as primary source of fluid and return lines connection. Filter *F1* is mounted on the inlet port of a fixed-displacement hydraulic pump *P1* which is driven, through a flexible coupling, by a three-phase 1,5 kW asynchronous electric motor *ME*. The pump is used to convert the mechanical energy generated by the electrical motor into hydraulic energy, having a maximum flow of 4,9 l/min at n = 1450 rev/min. A pressure-relief valve *SP1* is used to limit the working pressure at 290 bar, being activated in case of an overload or the system has a fault that rises pressure to abnormal values.

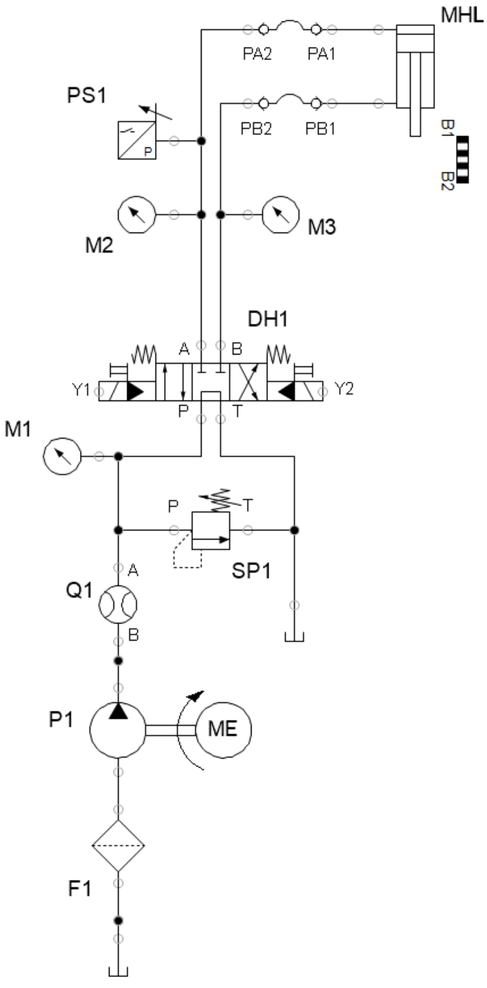

F1: hydraulic oil filter
P1: fixed-displacement pump
Q1: flowmeter
SP1: pressure-relief valve
M1 … M3: pressure gauges
DH1: electro-hydraulic directional valve
PS1: pressure switch
PA1/*PA2, PB1*/*PB2*: flexible pressure lines
MHL: double-acting hydraulic linear motor

Fig. 1. Hydraulics Schematic of the Driving System

Pressurized fluid flows through the *P1* to *DH1* hydraulic circuit and then returns into the hydraulic oil tank. *DH1* is a 4/3 bypass mid-position electro-hydraulic directional valve. This type of directional valve allows the hydraulic pump to be unloaded while the hydraulic linear motor *MHL* has the ports blocked. This implies that the motor is locked into its current position, as long as the directional valve is in central position. There must be taken into consideration that the directional valve has metal-to-metal fit spool and it cannot block totally the hydraulic oil flow, implying that when an outside force is exerted on *MHL*, its rod will move very little even though the 4/3 directional valve *DH1* is in center position. On *DH1*, *P* is the pressure in port, *T* is the tank out port, *A* and *B* are pressure in/out ports for the hydraulic linear motor.

DH1 directional valve has two springs for centering the spool in absence of any electrical or mechanical command. The spool can move under the action of manual or electrical commands, having two electromagnets *Y1* and *Y2*, one for *P-A*, *B-T*, connections and the other one for *P- B* and *A-T* connections (see figure 1).
MHL is a double acting unilateral rod hydraulic linear motor is connected to the directional valve using two flexible pressure lines (hoses) *PA1-PA2* and *PB1-PB2*. The motor is mounted in vertical position because of the physical configuration of the pressing chamber in the P.E.T. waste press (see figure 2).
In the hydraulic schematic, *M1*, *M2* and *M3* are pressure gauges used to monitor pressure values in the hydraulic circuits and *PS1* is a pressure activated switch used in the electrical automation schematic for stopping the pressing cycle and returning the press platter in its home position, unless other conditions are met for P.E.T. bale evacuation. *Q1* is a flow-meter.

Fig. 2. P.E.T. waste electro-hydraulic baling press

In figure 2 is shown a constructive type for a P.E.T. waste baling electro-hydraulic press available in *D009* laboratory of Faculty of Biotechnical Systems (U.P.B.).
The components in the hydraulic schematic are the following:

Table 1: Hydraulic equipment

Equipment type	Schematic symbol	General parameters
Hydraulic pump	*P1*	fixed-displacement, 4.9 l/min
Directional valve	*DH1*	4/3 bypass mid-position, electric control
Hydraulic motor	*MHL*	double acting, unilateral rod ϕ50xϕ40x620 mm
Pressure-relief valve	*SP1*	manual adjustment safety valve, 315 bar
Hydraulic oil filter	*F1*	ESA22
Hydraulic oil type	-	HLP22
Tank volume	-	7 liters

3. Electrical schematic

Schematic of the electrical system that the authors propose is given in figure 3. The authors have designed and modeled using *FluidSIM Hydraulics* a relay logic automation schematic in order to materialize operation phases of the P.E.T. waste press, as are described in table 2 (see below).

As one can see in figure 1, the directional valve *DH1* has two driving electromagnets, *Y1* and *Y2* that need to be controlled in operation phases of the pressing cycle. The electrical schematic is using a 24VDC power supply for both the driving (electromagnets) and relay-automation parts. In the schematic (see figure 3) it was not figured the power supply or the start circuit for the three-phase asynchronous electrical motor.

In figure 3, *S0* is a mushroom-type NC emergency STOP button having *H0* as optical indicator (lamp) for signaling that the P.E.T. waste press was switched ON and is currently in *stand-by* mode.

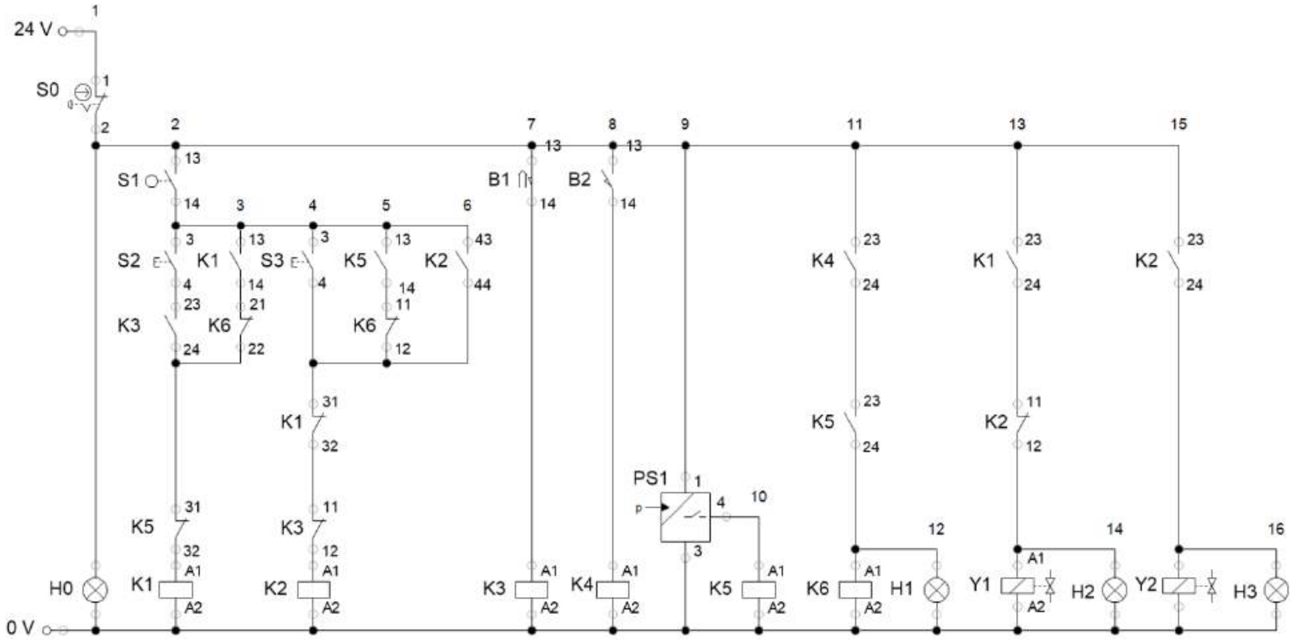

Fig. 3. Electrical schematic of the driving system

In the schematic above, figure 3, there are six electromagnetic control relays, *K1* … *K6*, that provide the operation logic. Pairs of relays' NO and NC contacts are connected in parallel or in series circuits in order to materialize operational phases given in table 2.

Fig. 4. Mounting detail of door switch (left) and *B2* limit switch (right)

One roller switch *S1* is used for disabling manual commands when the pressing chamber door is open, for human operator safety. The pressing plate is descending when *MHL* cylinder rod is extending and coil of *Y1* electromagnet of *DH1* is energized and it is ascending when cylinder rod is retracting and coil of *Y2* electromagnet is energized. There cannot be energized the coils of *Y1* and *Y2* electromagnets at the same time. The relay logic prevents this non-sense case to be encountered in normal operating cycle. If the pressing chamber door is accidentally or intentionally

opened, the current movement (extend/retract) will immediately stop, locking the pressing plate into its current position.
Button *S2* is used to start the automated pressing cycle after loading the P.E.T. waste into the pressing chamber and for safety reasons, the pressing will start only when the door is closed and the pressing plate is in home position (full retracted), travel limit switch *B1* through one NO contact of relay *K1* provides this second start condition. Self-latching of *START pressing* command is done by series circuit NO *K1* and NC *K6*. This command is inhibited when the door was opened while the pressing plate was in movement.
Button *S3* is a semi-automatic command for returning the pressing plate to its home position, *press plate retract*, being active only when:

- pressing chamber door was opened while the pressing plate was in movement (up/down) and it needs to be returned to home position, cylinder rod retracted;
- the P.E.T. waste press is in *bale out* mode, when travel limit switch *B2* and pressure switch *PS1* are both active at the same time.

This command is also self-latching through one NO contact of relay *K2*. Series circuit NO *K5* and NC *K6* is the automatic command for pressing plate retraction to home position after it was started with *S2*. When pressing the P.E.T. waste, the pressing force encounters two opposing forces, one given by the resistance to pressing of the P.E.T. mass and one given by the friction between the P.E.T. waste and the pressing chamber's lateral walls. In order to counterbalance these two forces, the hydraulic pressure in the active cylinder chamber increases to a maximum value determined by the degree of compaction of the P.E.T. bale. This is implying a pressure peak on the pressure switch line, activating its output and energizing *K5* relay's coil. While not in *bale out* mode, NC *K6* is closed and NO *K5* will be closed therefore the pressing plate will return automatically into its home position.
In table 2 is given the operation logic of the P.E.T. waste baling press, as the authors designed it, where *0* is *no operation/retract* (*MHL*), *1* is *operation/extension* (*MHL*), *X* is *state does not matter* and *LK* is *locked* into current position.

Table 2: Operation logic

Functional phase \ Schematic symbol	S0	S1	S2	S3	Y1	Y2	B1	B2	PS1	MHL
Emergency STOP (manual)	1	X	X	X	X	X	X	X	X	LK
Stand-by mode	0	0	0	0	0	0	1	0	0	0
START pressing (auto)	0	1	1	0	1	0	1	0	0	1
Press plate retract (auto)	0	1	0	0	0	1	0	X	1	0
Press plate retract (semi auto)	0	1	0	1	0	1	0	X	X	0
Bale out (auto-stop)	0	1	0	0	0	0	0	1	1	LK

Vertical position of *B2* travel limit switch is related to bale's height, while its length and width (usually for this type/size of press: L×w×h: 800×600×600mm, weight 70kg) are determined by the physical characteristics of the pressing chamber. Modifying *B2* vertical position will modify accordingly bale size and weight. The degree of compaction can be adjusted by modifying the setpoint value of pressure switch *PS1*, a lower value mean a lower compaction degree. A higher compaction degree of the bale can be obtained in the same mode, but it must be taken into consideration the maximum working pressure of the system, pressure-relief valve setpoint and safety regulations.
Pressing cycle is entering *bale out* mode when both *B2* and *PS1* are activated, optically signaled by lamp *H1*. The human operator can now safely open the pressing chamber door and bind the bale using metal wire or plastic ties, while the pressing plate is locked into last position (*Y1* and *Y2* not energized). After binding, the bale must be evacuated from the pressing chamber, but in the first place the pressing plate must be returned to home position by closing the door and pressing *S3*. The P.E.T. press enters into s*tand-by* mode and the door can now be opened to evacuate the

bale. A new pressing cycle can be started with *S2* after loading the pressing chamber and closing the door.

Table 3: Electric equipment

Equipment type	Schematic symbol	General parameters	Constructive model
Electrical motor (figure 1)	*ME*	1.5kW, 3 phase asynchronous motor	ASU 90L-4
Valve electromagnet	*Y1*, *Y2*	24 VDC, 1A,	HC-16, KVN193
Mushroom type STOP switch	*S0*	emergency STOP with housing, 1 NO, 1 NC,	MSG13400RD
Door switch	*S1*	proximity limit switch, 1 NO, 1 NC	ELOBAU 17127113
Manual NO switch	*S2, S3*	pushbutton with green indicator light	MST14100C
Relay	*K1 … K6*	miniature control relay, 24VDC, 4 CO contacts, 6A	PT 6A 4C 24VDC
Pressure switch	*PS1*	adjustable pressure switch, micro-switch commutation	F4YX3TG/150D/P2P1
Optical indicators	*H0 … H3*	indicator LED light 24V AC/DC	BZ501210-B (*H0*) BZ501213-B (*H1, H2*) BZ501211-B (*H3*)

4. Conclusions

Engineering field of electro-hydraulics has encountered a large development in the past years because of rapid technological advances, especially in electronics, IT and material's science. Modern P.E.T. waste presses use closed-loop analogic, digital or hybrid control, depending on its pressing capacity and functional requirements, most advanced constructive types use PLCs. The authors propose in this paper a simple and energy efficient electro-hydraulic automation schematic. Future work, the authors will try to obtain a simulation model for the solution presented in this paper and analyze its adequacy.

Acknowledgments

This work has been funded by University Politehnica of Bucharest, through the "Excellence Research Grants" Program, UPB – GEX 2017. Identifier: UPB- GEX2017, contract. No. 56/2017 (DIGIPRESS)".

References

[1] http://www.hydraulicspneumatics.com, Accessed September 3, 2018.
[2] Jelali, M., and A. Kroll. *Hydraulic servo-systems: modelling, identification and control*. Springer Science & Business Media, 2012.
[3] https://eu.hsm.eu, Accessed September 5, 2018.
[4] Dumitrescu, Liliana, Polifron – Alexandru Chiriță, Iulian Duțu, and Cristian Mărculescu. "Energy efficiency of multifunction vehicles in technological Speed drive." Paper presented at the 17th International Multidisciplinary Scientific GeoConference SGEM 2017, Albena, Bulgaria, June 27-July 6, 2017.
[5] Popescu, Teodor Costinel, Polifron-Alexandru Chirita, and Alina Iolanda Popescu. "Increasing energy efficiency and flow rate regularity in facilities, machinery and equipment provided with high operating pressure and low flow rate hydraulic systems." Paper presented at the 18th International Multidisciplinary Scientific GeoConference SGEM 2018, Albena, Bulgaria, June 30-July 9, 2018.
[6] Chirita, Polifron-Alexandru, Corneliu Cristescu, Liliana Dumitrescu, Alexandru-Daniel Marinescu, and Carmen-Anca Safta. "Improving the energy efficiency of multifunction motor vehicles by equipping them with hydrostatic pumps with load sensing." Paper presented at the 18th International Multidisciplinary Scientific GeoConference SGEM 2018, Albena, Bulgaria, June 30-July 9, 2018.

A Method to Address the Fixing of Sealing Deficiencies at the "Ostrovul Mic" Left Bank, "Râul Mare - Downstream" Water Development

Lect. PhD.Eng. **Albert Titus CONSTANTIN**[1], Assoc.Prof. PhD.Eng. **Gheorghe LAZĂR**[2], Assist.Prof. PhD.Eng. **Alina-Ioana POPESCU-BUŞAN**[3], Lect. PhD.Eng. **Şerban-Vlad NICOARĂ**[4]

[1] POLITEHNICA University Timişoara, albert.constantin@upt.ro

[2,3,4] POLITEHNICA University Timişoara

Abstract: *The present paper proposes a method for approaching the remediation of sealing deficiencies from the left bank of Ostrovul Mic water reservoir at km1+300 (Raul Mare – Downstream water development) by executing a drain at the bottom of the side embankment downstream face. The results of the remedy are highlighted by checking the flow both as a permanent regime and as transitional regime hypothesis on a 2D numerical model.*

Keywords: *Embankment, sealing, water infiltration, interception drain, 2D numerical modelling.*

1. General considerations

The hydro-power arrangement Ostrovul Mic (figure 1) is located at a distance of about 20 km from the Town of Haţeg, in the surrounding area of Ostrovul Mic village. The specific water development consists from a low retaining concrete dam, a hydro-power station and side enclosing embankments. The main uses of the arrangement are the electric power production, the water flow adjustment on river Râul Mare and the farm land irrigations. The concrete overflow dam accomplished towards the right bank is of "storied" type, with a tympan (H = 22,50 m), an over-spilling hood and a bottom discharger endowed with 4 tainter gates (4,00x4,00m^2) and 2 flap gates (10,00x2,50m^2). The usual water retention level is set at 465,00 mSL. The power station Ostrovul Mic is situated on the retention section towards the left side and is endowed with two Kaplan turbines. The installed flow of 90 m^3/s and its nominal head of 20 m leads to an installed power of 15.90 MW [1].

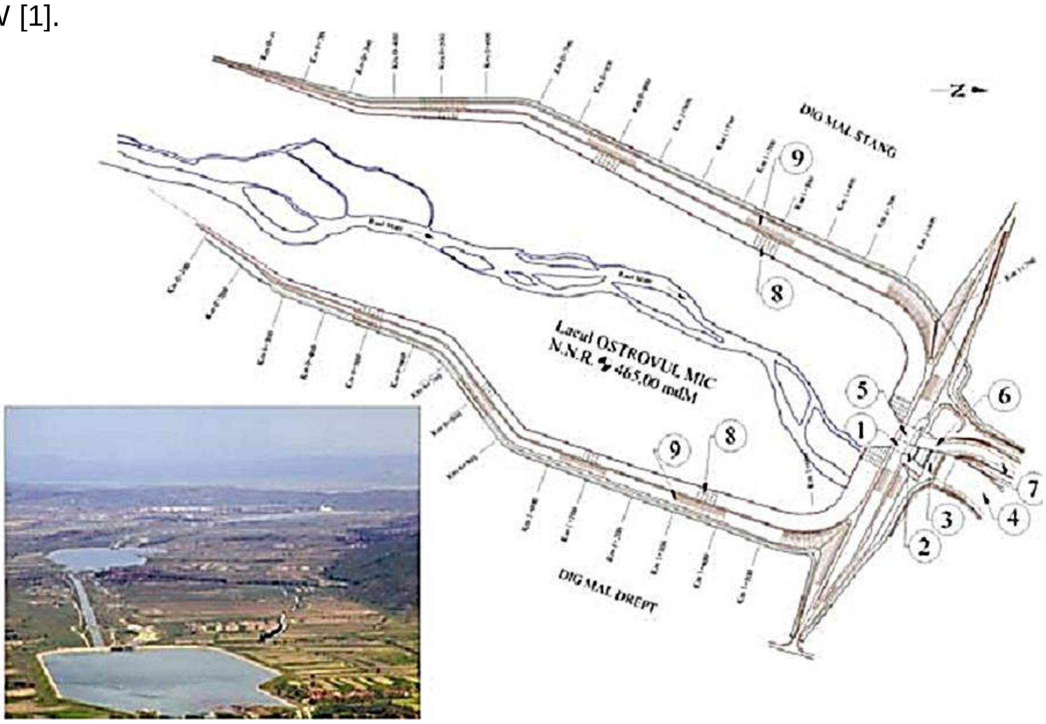

Fig. 1. Plan view and panoramic photo of the Ostrovul Mic water development. 1. overflow dam, 2-3. first and second steps of the energy dissipater, 4. high waters canal, 5. hydro-power station, 6. apron basin, 7. tale-race canal, 8. reinforced concrete face, 9. grassy downstream face.

Due to significant exfiltration accompanied by material entrainment from the enclosing embankments (especially at the left bank dike) the water development runs on level restrictions, meaning substantial energy and consequently financial losses. The enclosing ballast embankments of trapezoidal cross section have a 4.00m wide crest and faces slopes of 1:2.0 and 1:1.8 (upstream / downstream). The filling material – ballast – was obtained from the reservoir basin. The sealing is accomplished by an upstream reinforced concrete face (slabs 4.00x5.00m^2) of 0.15-0.20 m thickness and an underground slurry (bentonite) wall. The concrete face is upper ended by a water wave concrete turning parapet of 0.50 m height. The slabs joint gaps were sealed with bituminous mastic while the expansion joints are additionally sealed with glued straps.
The base ground layer – marl – is to be found at a depth of about 8…10 m from the natural ground level and therefore the underground sealing groin was difficult to be properly done by the following technological solution: the concrete face was to be deepened with about 4 m under the ground level, the remained depth was trench opened by excavation down to the base layer and filled with bentonite, a reinforced concrete supporting beam was accomplished on top of the slurry groin. Unfortunately, engaging this accomplishment procedure led to at least two types of inconveniences: there are zones where the trench excavation did not reach the marl layer, as it clearly proves to be the case on the left bank embankment at km1+276 where there is a bentonite uncovered gap of about 1…2m depth under the slurry groin (an exfiltration funnel developed here along the first 10 years of running the water arrangement, nourishing multiple springs on the downstream face and in the alongside safety counter duct); there are zones where it seems that the supporting beam does not properly vertically overlays with the slurry filled trench. It also needs to be mentioned the advantage offered by the embankment ballast fill granulometry which creates a solid skeleton hardly to be destabilised by exfiltration.
Along the 1996…1999 time period of running several exfiltration zones appeared and developed on the left side embankment downstream face (berm level) and its alongside duct, specifically at km0+790, km1+300 and km1+670, reaching an exfiltration discharge of 196 l/s. Geotechnical studies were then performed by digging three wells right down to the marl base layer (441,5 mSL) [2, 3]. Following the heavy rains of 12-14 July 1999, developing in torrents of extraordinary flow level, the water turbidity in the reservoirs maintained itself at very high values (as yellowish brownie viscous fluid) for about two months and it was noticed that the exfiltration at km1+300 seized for 8 days in order to reaper in the beginning at a half of its prior rate. The reservoir was emptied in October 2000, several operations being performed: longitudinal and transversal drainage of the berm, local repairing of the concrete face joints sealing and filling the exfiltration funnel at km1+276. As a result, the exfiltration at km0+790 and km1+670 were put out for good and the one at km1+300 seized to run on for a short period of time (80 days), reappearing with about 50% from its previous rate. The water level correlated exfiltration evolution, mentioning also two intervention moments (the natural generated one and the technological one), is presented by figure 2.

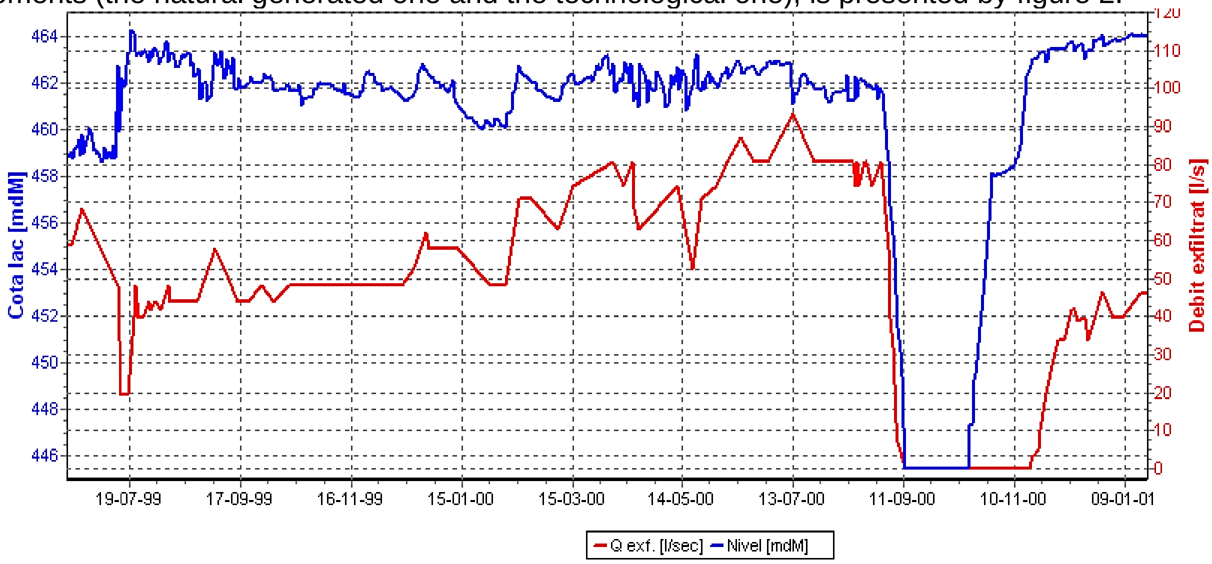

Fig. 2. Correlated exfiltration development on the left bank embankment of Ostrovul Mic reservoir

Given the importance of this also interesting subject, the present paper aims to bring on the light an approach method for sealing deficiency turnaround in the zone of km1+300 at the left side embankment of Ostrovul Mic water reservoir. An interception drain is suggested at the bottom level of the embankment downstream face while the infiltration discharge is then checked by a 2D numerical model on which several accompanying works are considered.

2. Wedging the numerical model under stationary and transitory regimes

The numerical model of the study case was built following the boundary conditions according to data appropriately supplied by the owner of Raul Mare – Downstream water arrangement [1]. These conditions include results obtained by measurements performed by infrared photography technics [2]. The outgoing levels of infiltration curve – from 456.00 to 457.20 mSL [4] – was established by analysing the thermal investigations results. Consequently, the numerical model was attuned with respect to the material permeability and anisotropy [5] based on this available data. This stage of the numerical study was performed both for the stationary and transitory regimes as presented here. The corresponding three established basic situations were as follows:

a. Stationary regime – developed for the fixed water level of 462.50 mSL in the Ostrovul Mic reservoir (figure 3)

b. Stationary regime – developed for the fixed water level of 465.00 mSL in the Ostrovul Mic reservoir (figure 4)

c. Transitory regime – developed for a maximum initially water level in the Ostrovul Mic reservoir imposed at 462.30 mSL (figure 5)

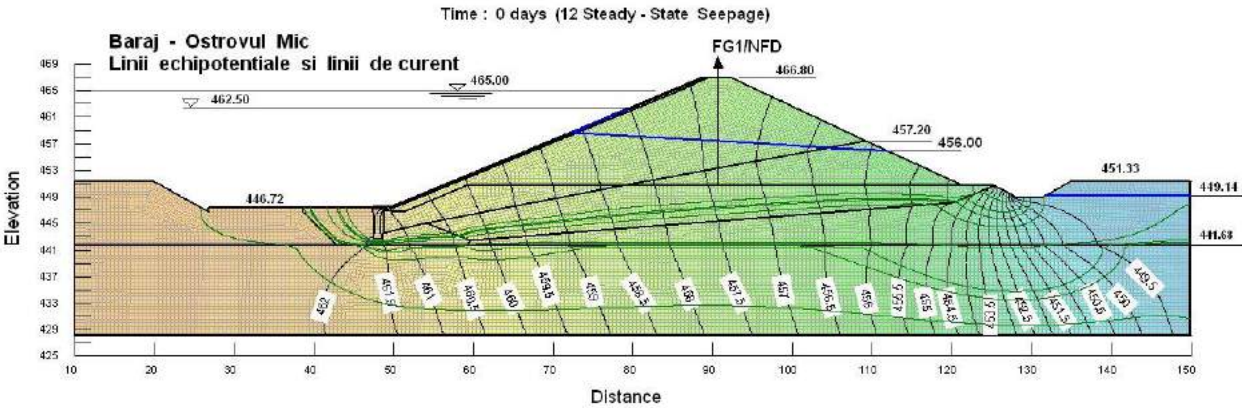

1		0 days						
2	Distance	Water Flux (m³/days)			Nivel in lac=		462.5	mdM
3	0	-696.212						
4	0.551981	-391.884			-300.304			
5	1.067746	-207.388			-154.542			
6	1.583511	-145.048			-90.8872			
7	2.099277	-113.617			-66.7052			
8	2.615042	-93.5043			-53.4129			
9	3.130807	-80.3007			-44.8213			
10	3.646572	-81.1091			-41.6248			
11	4.168245	-33.791			-29.9702			
12			Qtotal_exf_contracai		-782.27	mc/zi =	-9.054	l/s

Fig. 3. Equipotential and flow current lines corresponding to the upstream level of 462.50 mSL

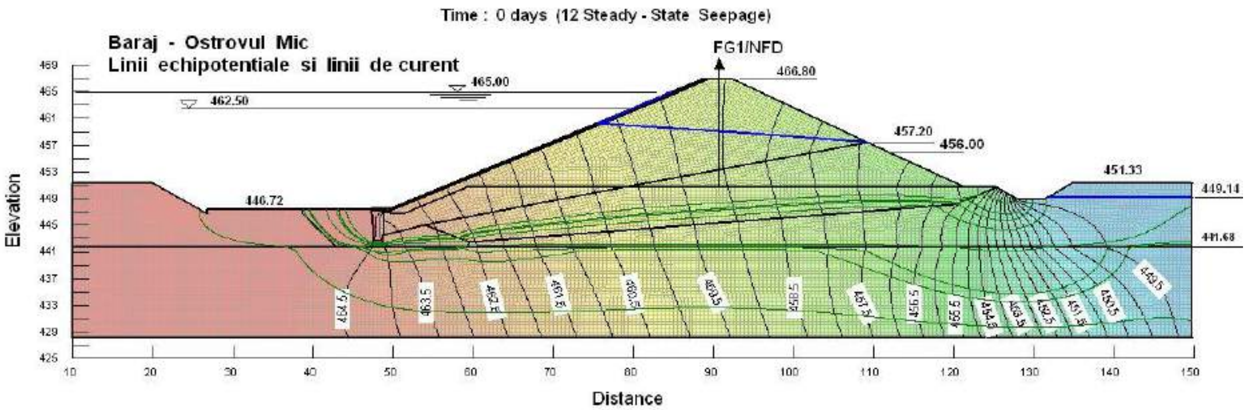

1		0 days						
2	Distance	Water Flux (m³/days)			Nivel in lac la =	465	mdM	
3	0	-824.109						
4	0.551981	-463.874			-355.471349			
5	1.067746	-245.486			-182.931594			
6	1.583511	-171.694			-107.5834858			
7	2.099277	-134.489			-78.95921155			
8	2.615042	-110.681			-63.22503963			
9	3.130807	-95.0522			-53.0551139			
10	3.646572	-96.0091			-49.27137345			
11	4.168245	-39.9986			-35.47578577			
12			Qtotal_exf_contracana		-925.9729532	mc/zi =	-10.717	l/s

Fig. 4. Equipotential and flow current lines corresponding to the upstream level of 465.00 mSL

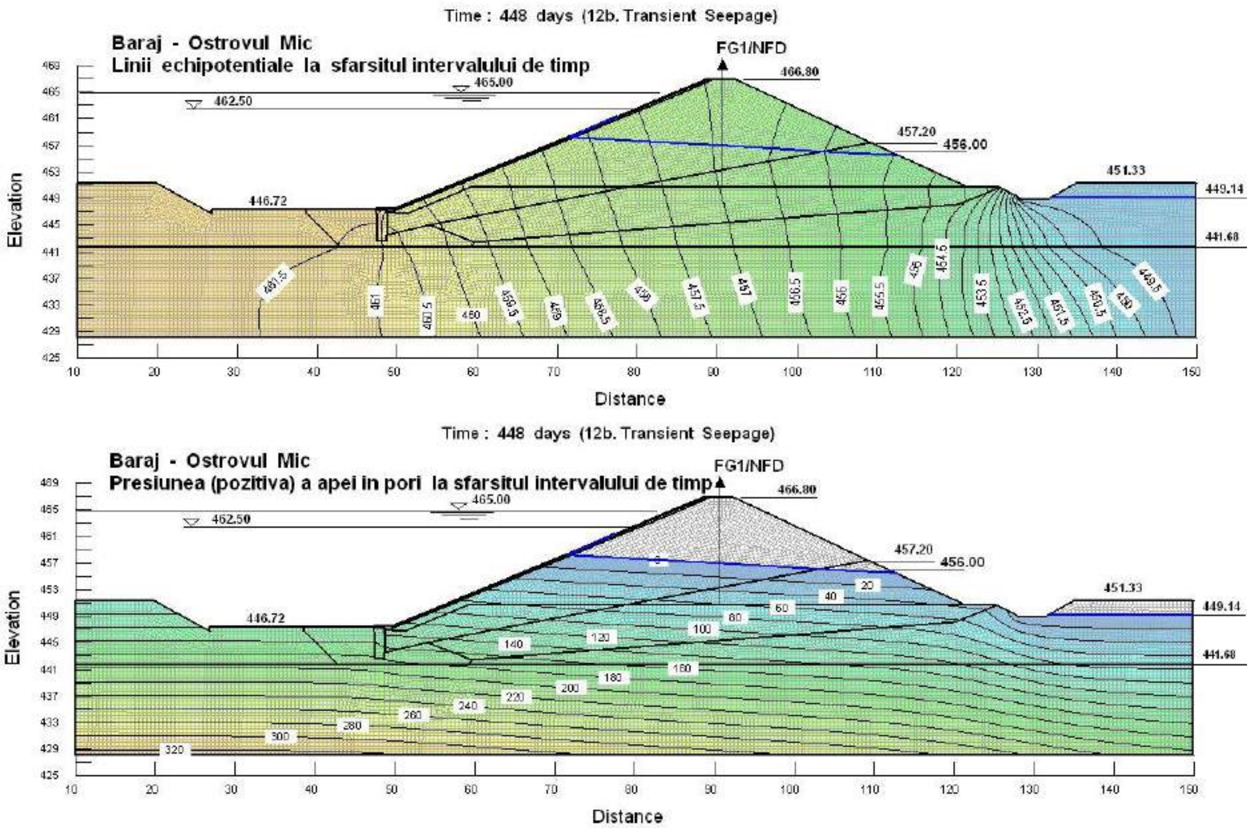

Fig. 5. Equipotential lines and pore water pressure at the end of the transitory phenomenon time interval 24.10.2013 - 18.03.2015

The following figure 6 shows the correlated water levels in the reservoir and observation well FG1/NFD along the given monitoring time interval.

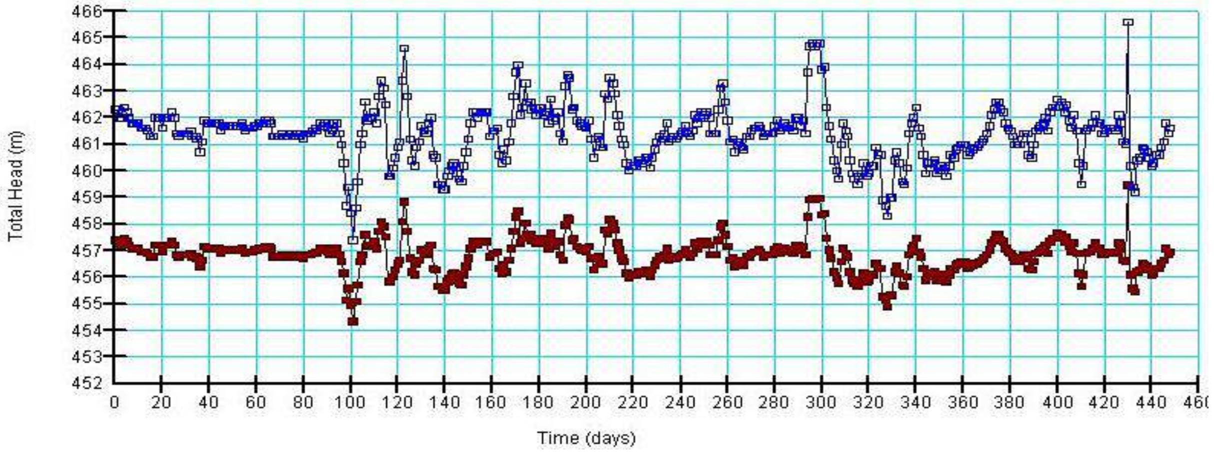

Fig. 6. Reservoir water level development with time and corresponding level in the monitoring well FG1/NFD along the given time interval 24.10.2013 - 18.03.2015

The figure 7 shows the comparative development of the reservoir water levels and the measured (supplied by the owner of the water arrangement) and model calculated water levels in the observation well for the mentioned monitoring (analysis) time interval.

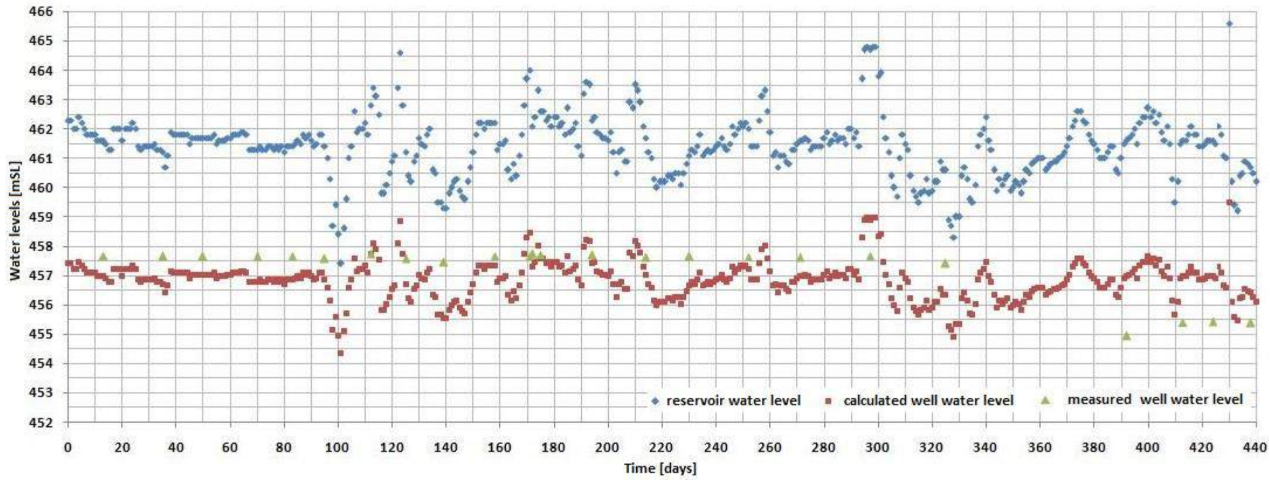

Fig. 7. Measured and calculated well water levels correlated with the reservoir water levels development along the monitoring time interval 24.10.2013 - 18.03.2015

3. Numerical modeling of the suggested solutions for turning around the embankment sealing deficiency

3.1 Downstream drain, without upstream intervention in the water reservoir

Looking to lower the infiltration curve, a side longitudinal drain (perforated pipe of 318mm in diameter) was considered with the 2D numerical model. By considering the stationary regime for the reservoir usual water level of 465.00 mSL, the model led to a decreased infiltration curve and an exfiltrated specific discharge of 3.828 l/s/m (figure 8, as to see with respect to basic data given by figure 4).

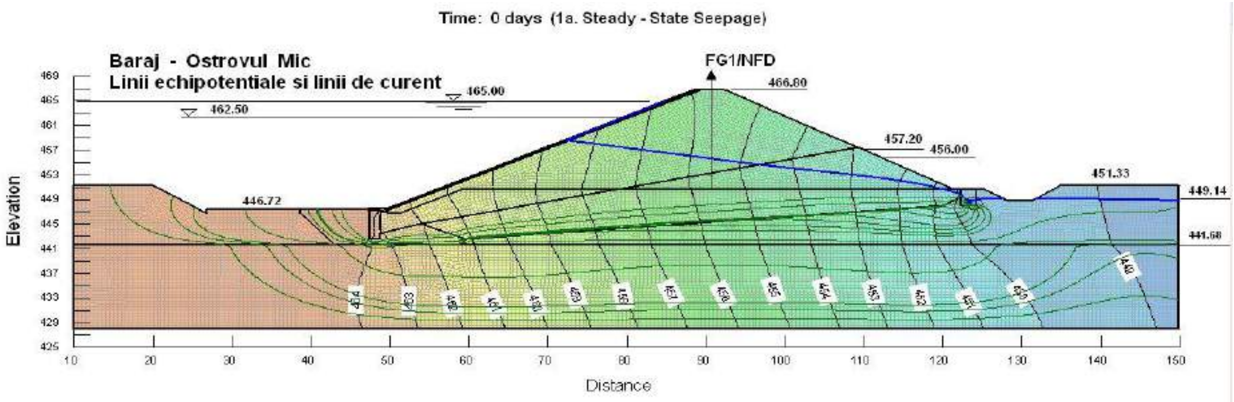

1		0 days						
2	Distance	Water Flux (m³/days)			Nivel lac NNR =		465	mdM
3	0	-699.885						
4	0.095273	-515.041			-57.875			
5	0.180976	-461.451			-41.8441			
6	0.271632	-423.757			-40.1248			
7	0.366623	-352.126			-36.8506			
8	0.466628	-241.276			-29.6716			
9	0.5598	-164.207			-18.8898			
10	0.658415	-151.134			-15.5487			
11	0.748042	-179.263			-14.8062			
12	0.829613	-248.644			-17.4525			
13	0.917009	-330.324			-25.2995			
14	1.000746	-444.411			-32.4373			
15			Qtotal_exfiltrat=		-330.8	mc/zi =	-3.828	l/s

Fig. 8. Equipotential and flow current lines corresponding to the upstream level of 465.00 mSL in case of lowering the infiltration curve by the help of a downstream drain

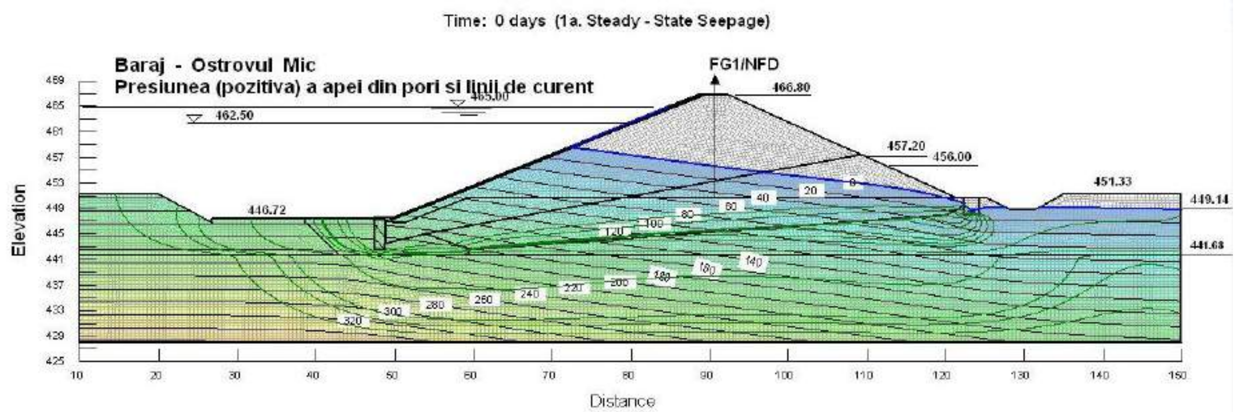

Fig. 9. Pore water pressure and flow lines by considering a downstream drain

3.2 Downstream drain and consequent upstream warping, without upstream intervention in the water reservoir

There is considered the warping effect given by the reduced flowing velocities in the funnel zone due to the lowered infiltration curve. Alluvia settlement is determined in time which concludes in permeability reduction (similar to warping produced by the fine material brought by high waters). This modeled phenomenon leads to an exfiltrated specific discharge of 2.836 l/s/m (figure 10).

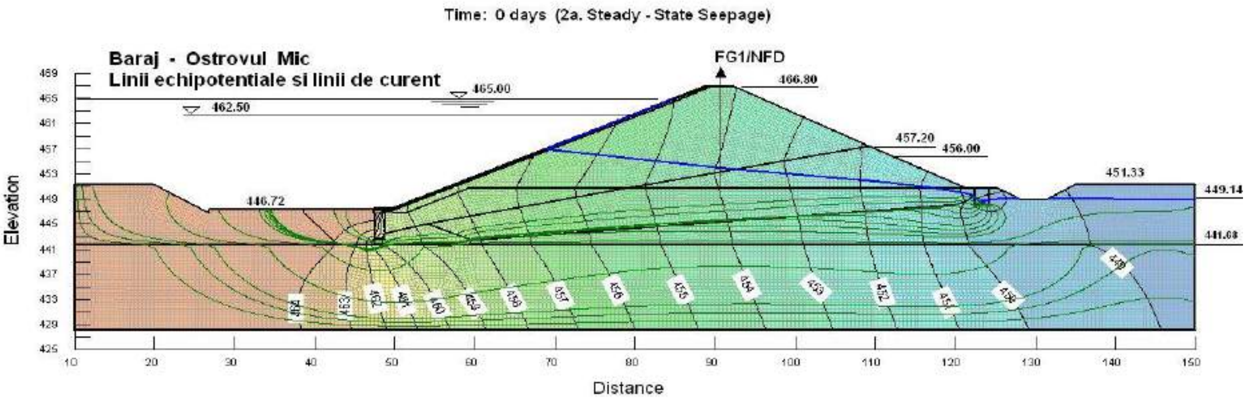

1		0 days					
2	Distance	Water Flux (m^3/days)		Nivel lac NNR=		465	mdM
3	0	-638.688			Kcolmatat=		
4	0.095273	-451.861		-51.9501			
5	0.180976	-384.647		-35.8456			
6	0.271632	-326.806		-32.2488			
7	0.366623	-233.451		-26.6095			
8	0.466628	-110.747		-17.2108			
9	0.5598	-40.6399		-7.0525			
10	0.658415	-54.6442		-4.69824			
11	0.748042	-113.573		-7.53841			
12	0.829613	-192.302		-12.4753			
13	0.917009	-283.174		-20.7771			
14	1.000746	-398.786		-28.5529			
15			Qtotal_exfiltrat=	-244.96	mc/zi=	-2.836	l/s

Fig. 10. Equipotential and flow current lines corresponding to the upstream level of 465.00 mSL in case of lowering the infiltration curve and assuming alluvia warping in the funnel

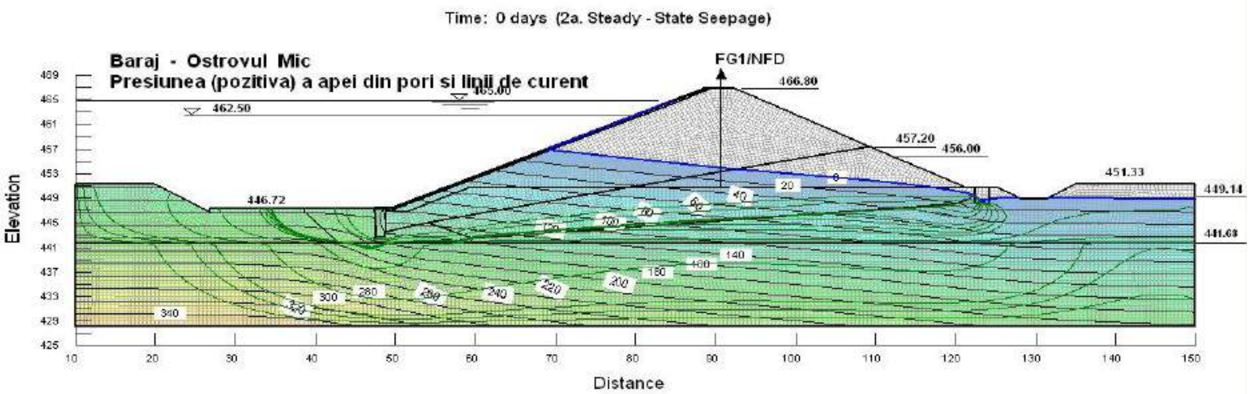

Fig. 11. Pore water pressure and flow lines by considering a downstream drain and the warping phenomenon

3.3 Downstream drain and superficial filling operation of the upstream funnel

Accompanying the drain accomplishment, in order to reduce the embankment seepage a mechanized filling of the existing exfiltration funnel is proposed. This operation can be developed either with or without emptying the reservoir, by adopting corresponding technologies.
By considering a compacted earthfill, the numerical modeling led to an exfiltrated specific discharge of 2.31 l/s/m (figure 12).

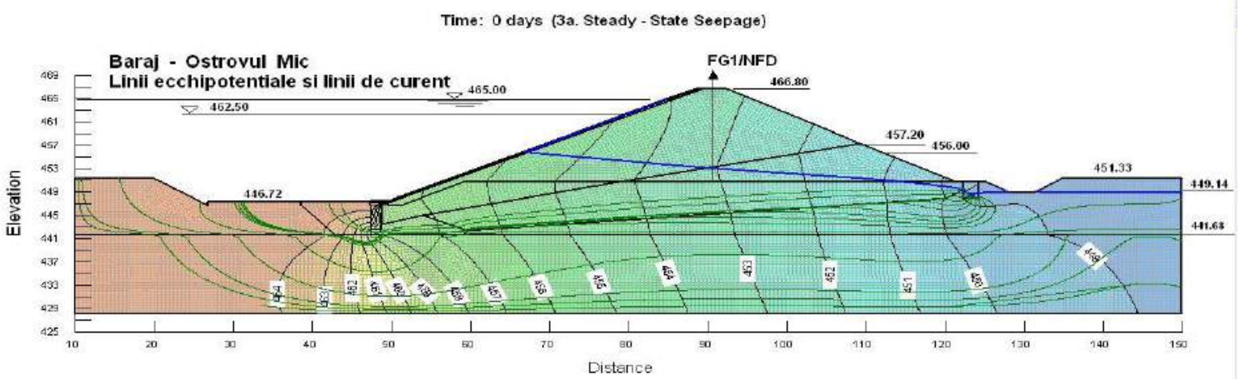

1		0 days					
2	Distance	Water Flux (m³/days)		Nivel lac NNR=		465	mdM
3	0	-606.341					
4	0.095273	-418.466		-48.8183			
5	0.180976	-344.05		-32.6749			
6	0.271632	-275.561		-28.0858			
7	0.366623	-170.722		-21.1963			
8	0.466628	-41.7522		-10.6243			
9	0.5598	24.67519		-0.79555			
10	0.658415	-3.64203		1.037097			
11	0.748042	-78.8509		-3.6968			
12	0.829613	-162.52		-9.8445			
13	0.917009	-258.252		-18.3867			
14	1.000746	-374.669		-26.4997			
15			Qtotal_exfiltrat=	-199.59	mc/zi =	-2.31	l/s

Fig. 12. Equipotential and flow current lines corresponding to the upstream level of 465.00 mSL in case of considering a downstream drain and upstream funnel filling

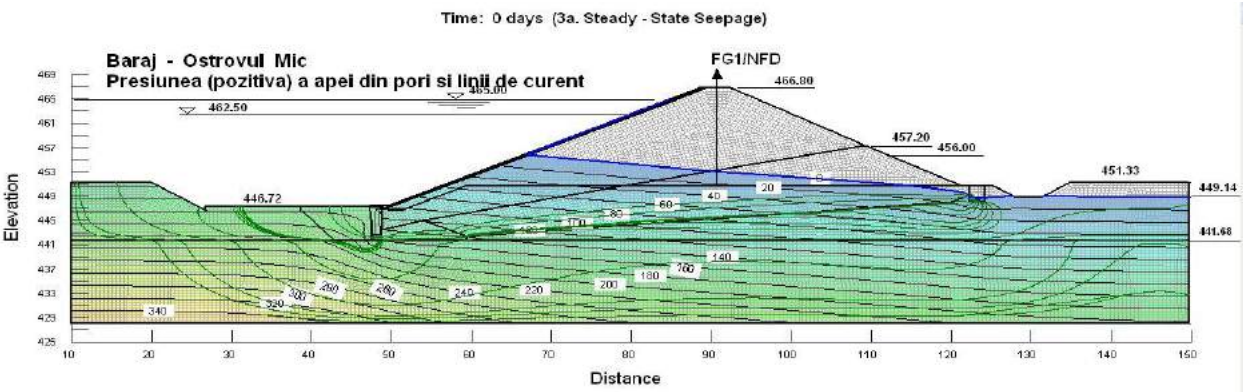

Fig. 13. Pore water pressure and flow lines by considering a downstream drain and the upstream funnel filling

3.4 Downstream drain and upstream bottom sealing structure

There is suggested a major intervention upon the upstream sealing solution by an extension with a bottom fore-raft structure, either as a concrete rigid one or an elastic one of gabions. The exfiltrated specific discharge was obtained in this case of 1.12 l/s/m (figure 14).

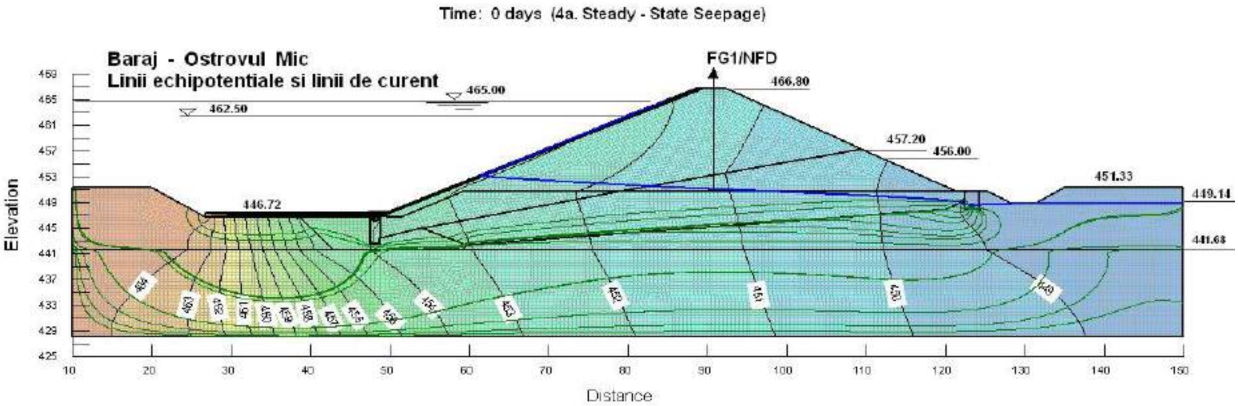

1		0 days						
2	Distance	Water Flux (m^3/days)			Nivel in lac =		465	mdM
3	0	-533.051						
4	0.095273	-342.801			-41.722623			
5	0.180976	-252.07			-25.491072			
6	0.271632	-159.453			-18.653511			
7	0.366623	-28.5965			-8.9314099			
8	0.466628	114.57			4.2988882			
9	0.5598	172.6606			13.380908			
10	0.658415	111.9145			14.031745			
11	0.748042	-0.18017			5.0072047			
12	0.829613	-95.0443			-3.8837995			
13	0.917009	-201.784			-12.970689			
14	1.000746	-320.028			-21.847673			
15			Qtotal_exfiltrat=		-96.782	mc/zi =	- 1.12	l/s

Fig. 14. Equipotential and flow current lines corresponding to the upstream level of 465.00 mSL in case of considering a downstream drain and an upstream bottom sealing structure

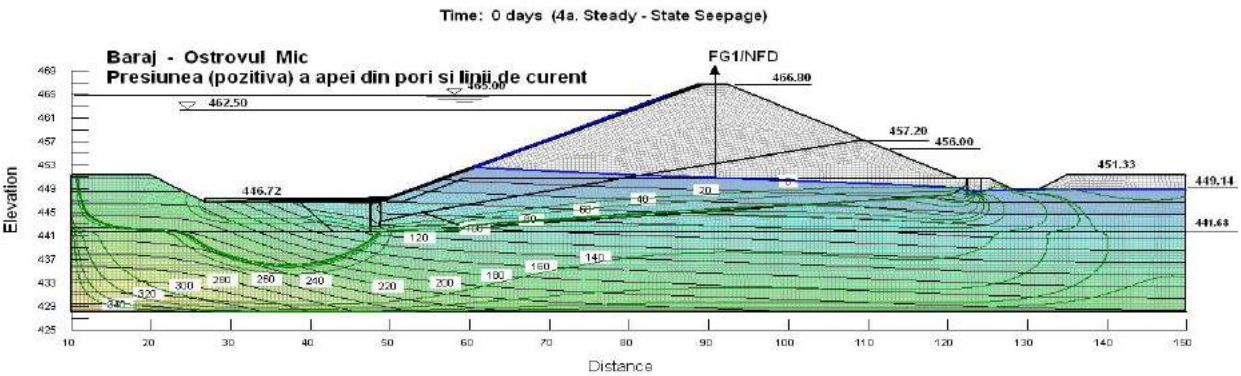

Fig. 15. Pore water pressure and flow lines by considering a downstream drain and an upstream bottom sealing structure

4. Conclusions

As the reached 2D model graphic representation show, the infiltration flow is lowered towards the downstream interception drain (perforated pipe). The modeled exfiltration from the funnel zone is considerably reduced, the situation being even more improved by the upstream accompanying works. As expected, the major upstream intervention by extending the sealing structure with a bottom fore-raft shows the most drastic reduction of the existing exfiltration problem, but the economic aspect should be also considered by a specific feasibility study in order to decide towards the optimum solution.

The 2D numerical modeling of the embankment infiltration phenomenon for the most radical structural intervention leads to a drop in the exfiltrated specific discharge from a value of 10.717 l/s/m to a value of 1.12 l/s/m, while the outgoing infiltration curve level reaches well in the alongside existing safety counter duct. As considering the reservoir usual water level of 465.00 mSL, the outgoing level actually below the downstream ground level would thus ensure the safety running of Ostrovul Mic water development.

References

[1] ***. *Lacul de acumulare Ostrovul Mic – Refacerea etanșării în zonele de risc maxim / Ostrovul Mic water reservoir – Sealing restoration in the zones of maximum risk*. ISPH SA, Bucharest, 2010.
[2] Chirică, A.. *Elemente constructive şi interpretarea rezultatelor lucrărilor geologico-geotehnice de teren privind digurile amenajării hidrotehnice Ostrovul Mic* / *Constructive elements and results interpretation of in situ geological and geotechnical works upon embankments of Ostrovul Mic water development*. Technical University of Civil Engineering Bucharest, Department of Geotechnics and Foundations, December 1998.
[3] Sârghiuţă, R., D. Stematiu, C. Popescu. *Studiu privind Lacul de acumulare Ostrovul Mic. Refacerea etanşării în zonele de risc maxim / Study regarding the Ostrovul Mic water reservoir. Sealing restoration in zones of maximum risk*. Faculty of Hydrotechnics, Department of Hydrotechnical Constructions, Bucharest, June 2010.
[4] Gaftoi, D.. "Refacerea sistemului de etanșare al amenajării Ostrovul Mic / Restoration of the sealing system of Ostrovul Mic water development". Paper presented at the 7th Conference of hydro-energy specialists from Romania - *Dorin Pavel*, Bucharest, 2012.
[5] Ion, M., Gh. Lazar. *Nota de comandă: Stabilirea soluției pentru stoparea exfiltrațiilor la diguri - barajul Ostrovul Mic / Order note: Establishing the solution for ceasing the embankment exfiltration - Ostrovul Mic dam*. SSH HIDROSERV SA, SUCURSALA HATEG, 2015.

UNIUNEA EUROPEANĂ

Instrumente Structurale 2014-2020

Comunicat de presă

București, septembrie 2018

ANUNȚ ÎNCEPERE PROIECT POC - Axa G

INSTITUTUL NAȚIONAL DE CERCETARE-DEZVOLTARE PENTRU OPTOELECTRONICĂ INOE 2000, cu sediul în localitatea Măgurele, Bucuresti-Ilfov, str. Atomiştilor, C.P. 077125, nr. 409, judeţul Ilfov, România, telefon 0214574522, fax 0314056397, derulează, începând cu data de 25.06.2018, proiectul ***“ELABORAREA DE TEHNOLOGII EFICIENTE ENERGETIC ÎN APLICAŢIILE DE NIŞĂ ALE FABRICAŢIEI SUBANSAMBLELOR MECANOHIDRAULICE LA CERERE ŞI MENTENANŢEI ECHIPAMENTELOR HIDRAULICE MOBILE“*****, cod P_40_415, cod SMIS 2014+ 119809,** cofinanţat prin **Fondul European de Dezvoltare Regională,** în baza contractului de finanţare nr. 6/25.06.2018, încheiat între **MCI** în calitate de **Organism Intermediar (OI)** pentru Programul Operaţional Competitivitate (POC), în numele și pentru **Ministerul Fondurilor Europene (MFE)** în calitate de **Autoritate de Management (AM)** pentru Programul Operaţional Competitivitate (POC) și **INSTITUTUL NATIONAL DE CERCETARE DEZVOLTARE PENTRU OPTOELECTRONICĂ INOE 2000.**
Valoarea totală a proiectului este de 8.301.282 lei, din care asistenţa financiară nerambursabilă este de 6.348.984 lei.
Proiectul se implementează de către beneficiarul INOE 2000 prin filiala Institutul de Cercetări pentru Hidraulică și Pneumatică (INOE 2000 Filiala IHP).
Obiectivul general al proiectului îl constituie dezvoltarea interacţiunii INOE 2000 cu IMM-urile specializate în producţia şi mentenanţa de echipamente hidraulice pentru **transferul de cunoştinţe** în subdomeniul aplicaţiilor de nişă privind tehnologiile destinate producţiei de subansamble mecanohidraulice şi sisteme pentru utilaje complexe la cerere, şi al mentenanţei echipamentelor şi instalaţiilor hidraulice (întreţinere, reparaţii, verificări şi control).
Beneficiar proiect: INOE 2000
Potenţiali beneficiari ai rezultatelor proiectului sunt firmele producătoare de subansambluri mecano-hidraulice la cerere (netipizate sau cu destinații speciale), firmele producătoare sau care se ocupă cu repararea de aparatură, echipamente și instalații hidraulice, firme care se ocupă de vânzarea, montarea, întreţinerea şi exploatarea unor astfel de produse.
Durata contractului: 54 de luni de la semnarea contractului între INOE 2000 şi Autoritatea Contractantă.
Rezultate prevăzute: cursuri de instruire, acces la facilităţile institutului, studii de soluții, proiecte, realizare de modele experimentale şi prototipuri pentru diverse echipamente /instalaţii, metodologii de testare şi tehnologii de mentenanţă, brevete, articole, simpozioane etc.

Proiect cofinanțat din Fondul European de Dezvoltare Regională prin Programul Operaţional Competitivitate 2014-2020

Date de contact:
INOE 2000 Filiala IHP, cu sediul în București, sector 4, str. Cuțitul de Argint nr. 14, cod postal: 040558
Tel.: 0213363991, Fax: 0213373040, e-mail: dumitrescu.ihp@fluidas.ro
www.ihp.ro

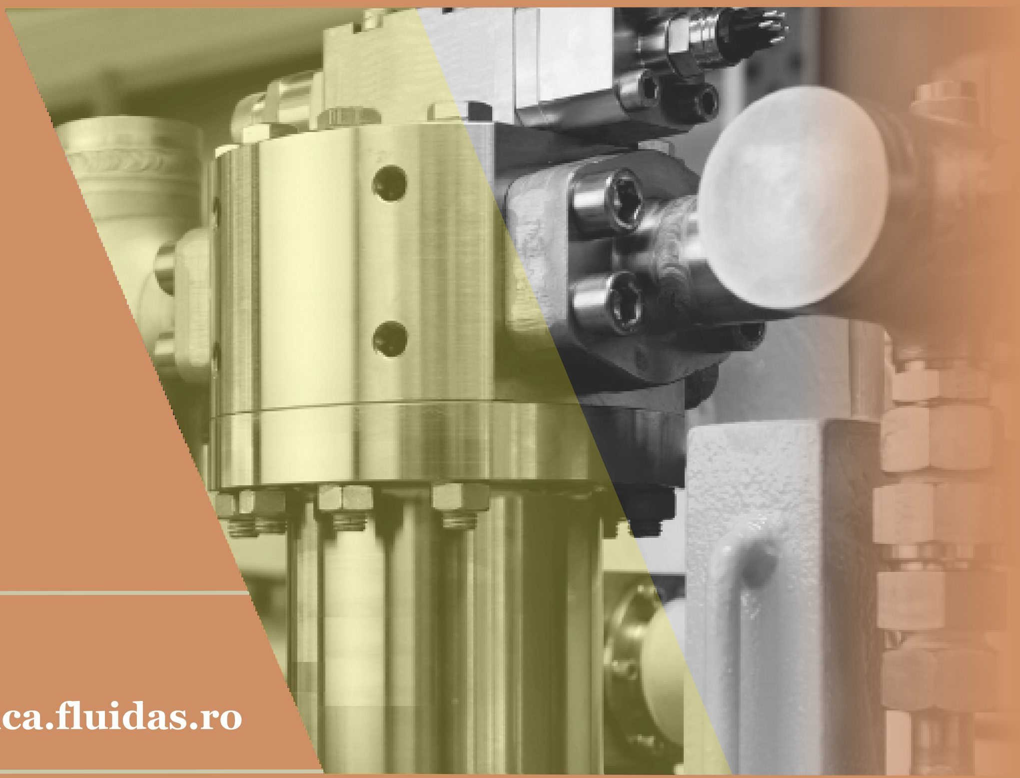

http://hidraulica.fluidas.ro